1966

An analytical treatment of ionization efficiency data for xenon from a pulsed retarding-potential ion source

Gene Rodell Sparrow
Iowa State University

SPARROW, Gene Rodell, 1939-

AN ANALYTICAL TREATMENT OF IONIZATION EFFICIENCY DATA FOR XENON FROM A PULSED RETARDING-POTENTIAL ION SOURCE.

Iowa State University of Science and Technology, Ph.D., 1966
Chemistry, physical

AN ANALYTICAL TREATMENT OF IONIZATION EFFICIENCY DATA FOR XENON FROM A PULSED RETARDING-POTENTIAL ION SOURCE

by

Gene Rodell Sparrow

A Dissertation Submitted to the
Graduate Faculty in Partial Fulfillment of
The Requirements for the Degree of
DOCTOR OF PHILOSOPHY

Major Subject: Physical Chemistry

Approved:

Signature was redacted for privacy.

In Charge of Major Work

Signature was redacted for privacy.

Head of Major Department

Signature was redacted for privacy.

Dean of Graduate College

Iowa State University
Of Science and Technology
Ames, Iowa

1966

TABLE OF CONTENTS

I. INTRODUCTION

The ionization of gases due to interactions of low energy electrons with atoms or molecules has been studied for many years. In these "ionization efficiency" studies the procedure is to measure ion intensity of a specific ionic species at varying electron energies while the pressure and ionizing current are held constant. Field and Franklin (1) have reviewed the early applications of mass spectrometry to studies of the ionization of gases by electron bombardment. However, several similar books (2, 3, 4) have been published recently which include new techniques, developments, and theories of ionization. The IIIrd International Conference on the Physics of Electronic and Atomic Collisions resulted in a recently published book, Atomic Collisions (5), edited by McDowell, which presents detailed coverage of work dealing with most aspects of electron and atom or molecule interactions. Besides ionization processes, excitation and scattering processes are included.

Each of the above references contains comprehensive reviews of the historical development of electron bombardment technology and its application to ionization studies. Therefore, much of the initial work which lead to the present state of this field need not be discussed here.

All of the above general references indicate the diversified applications of ionization efficiency studies. Most of these studies were made using the mass spectrometer

because it permits accurate identification of the ion under investigation. In the last two decades many improvements in ionization efficiency studies have been realized. Most of these improvements were in the instrumentation of mass spectrometers, especially that which is used for controlling the electron beam and reading the ion current intensities. Some of these improvements and their effects will be discussed below.

The results of ionization efficiency studies have already furnished a wealth of thermodynamic data for physicists and chemists, however, these data would be more accurate, and more information could be obtained from them if the ionization processes in the ion source were better understood. Only in the last few years have any significant analytical techniques been applied to ionization efficiency data. Previously, rare gases were used to calibrate each ionization efficiency curve. In this work it will be shown that the instrument can first be calibrated by using the rare gases and then appearance potentials can be obtained at various conditions without the further use of a calibrating gas.

Ionization efficiency data that are obtained by use of a retarding potential in the electron beam will be analyzed in detail. An attempt will be made to demonstrate that the retarding-potential-difference method gives only slightly better results than an appropriate analytical treatment.

Before presenting the exact techniques used for trying to establish the above ideas, it will be advantageous to explain in detail ionization efficiency curves, and factors which affect their accuracy. Actual experimental verification of how some of these factors influence the ionization efficiency data will be presented later.

II. IONIZATION EFFICIENCY CURVES

A. General Characteristics

If the measures of the ion current intensity of a specific ionic species are plotted against the energy of the bombarding electrons, a curve is obtained which is normally termed the ionization efficiency curve for that ionic species. A typical ionization efficiency curve for Xe^+ is shown in Fig. 1. Several important characteristics of this curve which also occur in the ionization efficiency curves of many other ionic species are described below. These characteristics are also cited by Field and Franklin (1).

1. An initial rapid increase of the slope of the curve may be observed over the first 0.5 to 3.0 volt range above the ionization onset. This is commonly referred to as the tail of the curve and it is this tail that can greatly reduce the accuracy and precision of much ionization efficiency work.
2. The following portion of the curve has a steep but nearly constant slope over a range of from 1 to 10 volts above onset. Since this part of the curve is often linearly extrapolated to zero ion current in order to obtain the ion appearance potential, it is frequently referred to as the linear part of the curve.

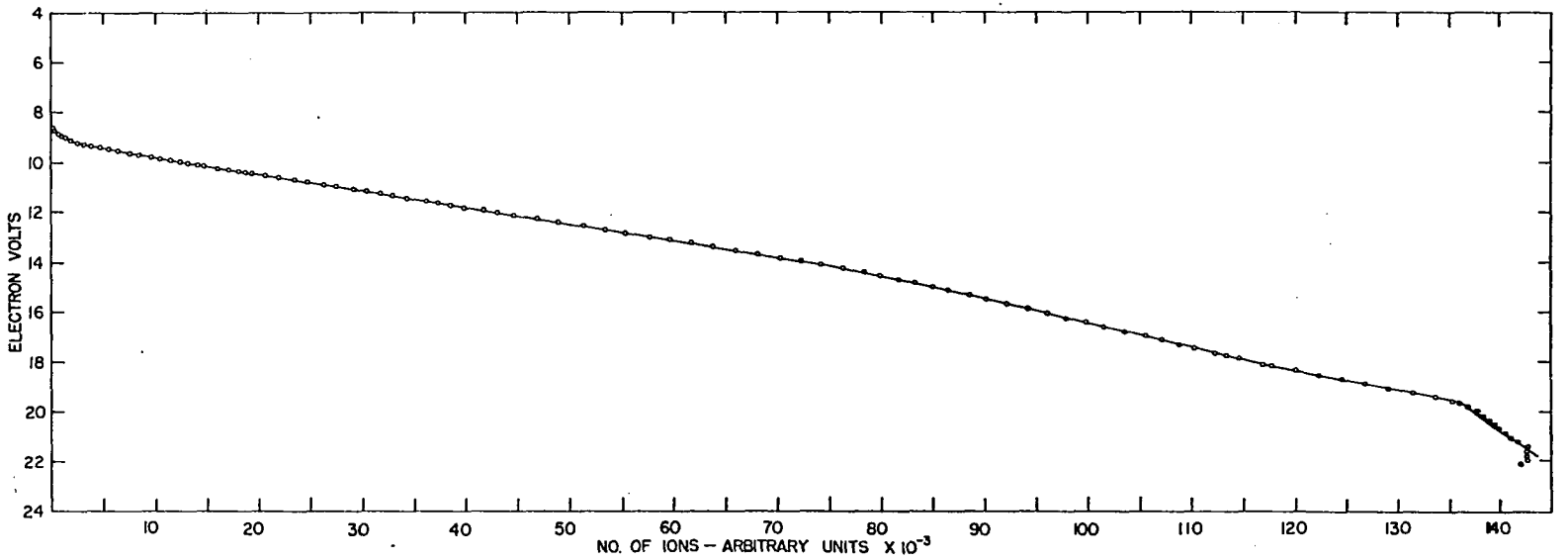

Fig. 1. Typical ionization efficiency curve for Xe^{+}.

3. If the ionization efficiency curve is investigated over a large enough voltage range, an absolute maximum is usually observed.
4. After reaching this maximum, the slope of the curve usually decreases much more slowly than it increased prior to reaching the maximum.
5. In addition to the characteristics described above, other details are often observed. For example, several near-linear areas, breaks or relative maxima often appear, depending upon the instrument that is used and the type of ion that is investigated. It will be shown later that all of the above characteristics are dependent upon both the physical properties of the electrom beam and the instrumental conditions. In fact, apparent relative maxima and inflection points have been observed[1] by using incorrectly aligned source magnets (2, p. 428, 6a, 6b).

B. Physical Properties Effecting Ionization Efficiency Curves

Since the ionization efficiency curve is dependent upon the energy of the bombarding electrons, the distribution of energies within the electron beam is of primary concern. It has been commonly accepted that the major portion of the initial tail or curvature of an ionization efficiency curve

---

[1]G. Junk, Iowa State University, Ames, Iowa, Information on electron beams, private communication, 1965.

is due to the spread of energies that occurs in the electron beam emitted from a hot filament. If dN_e represents the number of electrons emitted per unit volume with energies between U and U + dU, the <u>energy distribution</u> for the electrons within the entire electron beam is (7);

$$dN_e = \frac{4\pi mAUe}{h^3} - \frac{\Phi+U}{kT} \, dU \qquad 1$$

where; m = the mass of the electron

A = the area of the emitting surface

T = the temperature of the emitter

Φ = the work function of the emitter

h = Planck's constant

k = Boltzmann's constant.

The above distribution is not the same as a true Maxwellian distribution which is shown below for the velocity components, v, of the electrons in the beam;

$$dN_e = \frac{4\pi mAve}{2kT} - \frac{\Phi+mv^2}{2kT} \, dv \qquad 2$$

Thus the electron energy distribution is termed a pseudo-Maxwellian distribution rather than a Maxwellian distribution.

Eq. 1 was used in calculating the energy distribution of electrons emitted from a 0.001 inch x 0.025 inch tungsten ribbon at several temperatures. For these calculations N_e was set equal to the number of electrons emitted with energies from 0 to a, and N_{tot} was set equal to the total number of electrons emitted. The percentage of electrons having

energies between 0 and a is then given by;

$$\%N_a = \frac{N_a}{N_{tot}} \times 100, \qquad 3$$

where;

$$N_a = \int_0^a \frac{4\pi mAU}{h^3} e^{-\frac{U+\Phi}{kT}} dU \qquad 4$$

$$N_{tot} = \int_0^\infty \frac{4\pi mAU}{h^3} e^{-\frac{U+\Phi}{kT}} dU. \qquad 5$$

Solution of Eq. 5 gives Richardson's (8) equation for total emission,

$$N_{tot} = \frac{4mAe}{h^3} e^{-\frac{\Phi}{kT}} (kT)^2 \qquad 6$$

Curves of the energy distribution for several temperatures in the range 2240°k to 2420°k, plotted at 20° intervals are shown in Fig. 2. Chart 1-a lists typical results for a single temperature. It can be shown that the average energy of the electrons in a given direction is kT. These average energies are also indicated on the curves in Fig. 2 by vertical lines. Note that the average energy is very nearly equal to the most probable energy, and this average increases only slightly at higher temperatures. Chart 1-b lists the total emission current, number of emitted electrons and average energy for each temperature. The calculations were made using an IBM-7074 computer which was also equipped with

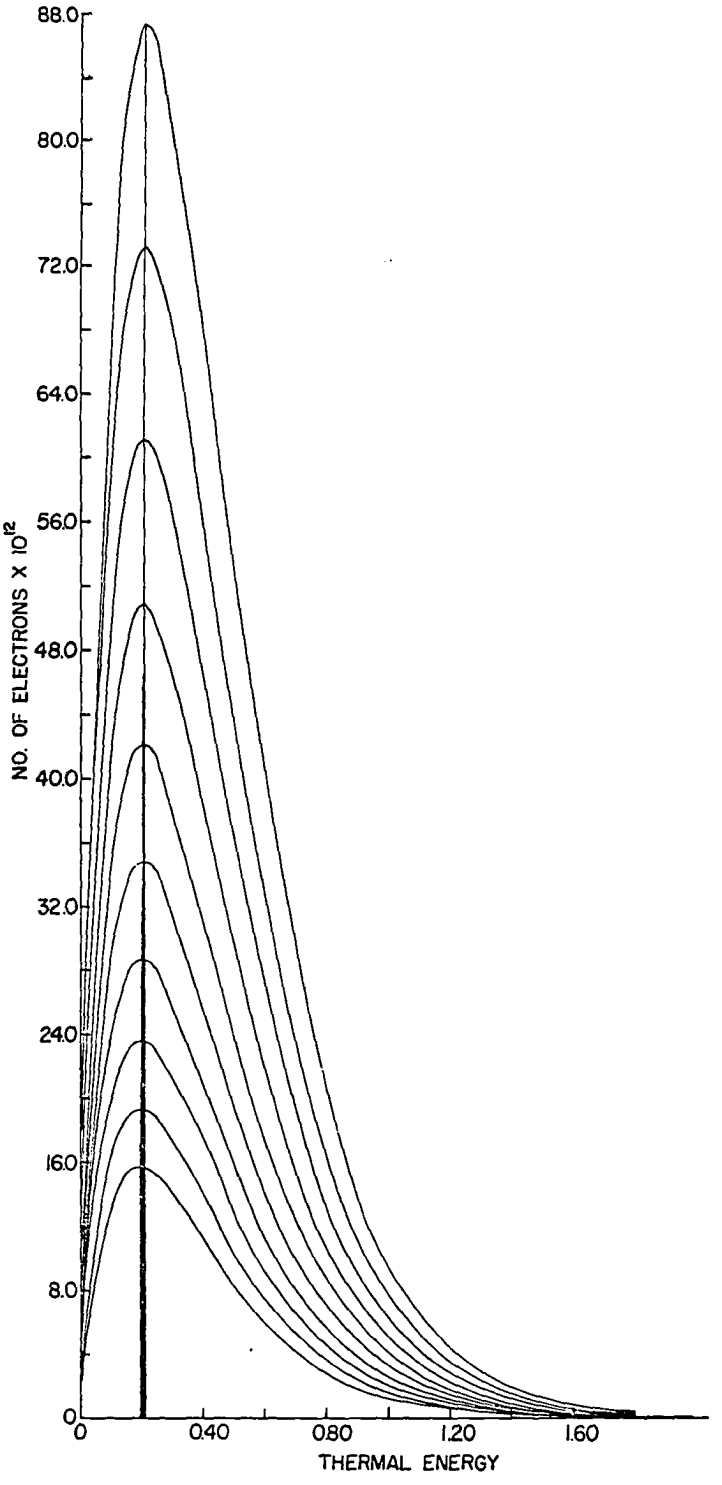

Fig. 2. Electron thermal energy distributions for several temperatures.

10-14-65

TEMPERATURE= 2390.00 NO.ELECTRONS= 0.1870E 17 AVERAGE ENERGY= 0.2058 TOTAL EMISSION CURRENT = 0.29773E 01

THERMAL ENERGY	NO.ELECTRONS 0 TO A	CURRENT	PERCENT OF TOT	NO.AT U(J)	DIFFERENTIAL NO.
0.000	0.000000E 00	0.000000E 00	0.0000	0.8768E 12	0.0000E 00
0.020	0.827290E 14	0.131709E-01	0.4424	0.1673E 14	0.1601E 14
0.040	0.3104C5E 15	0.494182E-01	1.6598	0.2964E 14	0.2906E 14
0.060	0.655485E 15	0.104357E 00	3.5051	0.4002E 14	0.3956E 14
0.080	0.109428E 16	0.174216E 00	5.8515	0.4823E 14	0.4786E 14
0.100	0.160648E 16	0.255761E 00	8.5904	0.5457E 14	0.5429E 14
0.120	0.217474E 16	0.346231E 00	11.6291	0.5932E 14	0.5912E 14
0.140	0.278428E 16	0.443273E 00	14.8886	0.6273E 14	0.6258E 14
0.160	0.342260E 16	0.544897E 00	18.3019	0.6499E 14	0.6490E 14
0.180	0.407914E 16	0.649422E 00	21.8126	0.6630E 14	0.6626E 14
0.200	0.474505E 16	0.755439E 00	25.3735	0.6681E 14	0.6680E 14
0.220	0.541298E 16	0.861777E 00	28.9452	0.6666E 14	0.6668E 14
0.240	0.607685E 16	0.967468E 00	32.4951	0.6596E 14	0.6601E 14
0.260	0.673168E 16	0.107172E 01	35.9967	0.6482E 14	0.6489E 14
0.280	0.737345E 16	0.117389E 01	39.4285	0.6333E 14	0.6341E 14
0.300	0.799898E 16	0.127348E 01	42.7734	0.6156E 14	0.6165E 14
0.320	0.860577E 16	0.137009E 01	46.0181	0.5957E 14	0.5967E 14
0.340	0.919192E 16	0.146341E 01	49.1525	0.5742E 14	0.5753E 14
0.360	0.975607E 16	0.155322E 01	52.1652	0.5516E 14	0.5528E 14
0.380	0.102973E 17	0.163938E 01	55.0631	0.5283E 14	0.5295E 14
0.400	0.108149E 17	0.172179E 01	57.8312	0.5046E 14	0.5058E 14
0.420	0.113087E 17	0.180041E 01	60.4718	0.4807E 14	0.4819E 14
0.440	0.117787E 17	0.187523E 01	62.9849	0.4569E 14	0.4581E 14
0.460	0.122250E 17	0.194629E 01	65.3715	0.4334E 14	0.4346E 14
0.480	0.126480E 17	0.201363E 01	67.6334	0.4104E 14	0.4115E 14
0.500	0.130482E 17	0.207734E 01	69.7733	0.3878E 14	0.3890E 14
0.520	0.134261E 17	0.213752E 01	71.7944	0.3660E 14	0.3671E 14
0.540	0.137826E 17	0.219426E 01	73.7003	0.3449E 14	0.3459E 14
0.560	0.141182E 17	0.224770E 01	75.4951	0.3245E 14	0.3255E 14
0.580	0.144338E 17	0.229795E 01	77.1829	0.3050E 14	0.3059E 14
0.600	0.147303E 17	0.234515E 01	78.7683	0.2863E 14	0.2872E 14
0.620	0.150085E 17	0.238943E 01	80.2557	0.2684E 14	0.2693E 14
0.640	0.152691E 17	0.243093E 01	81.6496	0.2514E 14	0.2522E 14
0.660	0.155132E 17	0.246979E 01	82.9547	0.2352E 14	0.2360E 14
0.680	0.157415E 17	0.250613E 01	84.1754	0.2199E 14	0.2207E 14
0.700	0.159548E 17	0.254010E 01	85.3161	0.2054E 14	0.2061E 14
0.720	0.161540E 17	0.257181E 01	86.3813	0.1917E 14	0.1924E 14
0.740	0.163399E 17	0.260140E 01	87.3751	0.1788E 14	0.1794E 14
0.760	0.165131E 17	0.262898E 01	88.3016	0.1666E 14	0.1672E 14
0.780	0.166745E 17	0.265468E 01	89.1648	0.1552E 14	0.1557E 14
0.800	0.168248E 17	0.267861E 01	89.9684	0.1444E 14	0.1449E 14
0.820	0.169646E 17	0.270087E 01	90.7161	0.1343E 14	0.1348E 14
0.840	0.170947E 17	0.272156E 01	91.4113	0.1249E 14	0.1253E 14
0.860	0.172155E 17	0.274080E 01	92.0573	0.1160E 14	0.1164E 14
0.880	0.173277E 17	0.275866E 01	92.6574	0.1077E 14	0.1081E 14
0.900	0.174319E 17	0.277525E 01	93.2144	0.9995E 13	0.1003E 14
0.920	0.175285E 17	0.279064E 01	93.7312	0.9271E 13	0.9306E 13
0.940	0.176181E 17	0.280491E 01	94.2105	0.8595E 13	0.8628E 13
0.960	0.177012E 17	0.281813E 01	94.6548	0.7965E 13	0.7996E 13
0.980	0.177782E 17	0.283039E 01	95.0664	0.7378E 13	0.7407E 13
1.000	0.178495E 17	0.284174E 01	95.4476	0.6832E 13	0.6858E 13
1.020	0.179155E 17	0.285225E 01	95.8005	0.6323E 13	0.6348E 13
1.040	0.179766E 17	0.286197E 01	96.1271	0.5850E 13	0.5873E 13
1.060	0.180331E 17	0.287096E 01	96.4292	0.5411E 13	0.5432E 13
1.080	0.180853E 17	0.287928E 01	96.7086	0.5002E 13	0.5022E 13
1.100	0.181336E 17	0.288697E 01	96.9669	0.4623E 13	0.4641E 13
1.120	0.181782E 17	0.289407E 01	97.2055	0.4271E 13	0.4288E 13
1.140	0.182194E 17	0.290064E 01	97.4259	0.3945E 13	0.3961E 13

Chart 1-a. Electron emission data for 2390°K.

Filament Temperature	No. of Electrons Total Emission	Total Emission Current, MA	Average Energy, eV
2200.00°K	0.26647E 16	0.42423E 00	0.1895
2210.00	0.29761E 16	0.47382E 00	0.1944
2220.00	0.33208E 16	0.52870E 00	0.1912
2230.00	0.37020E 16	0.58938E 00	0.1921
2240.00	0.41230E 16	0.65641E 00	0.1929
2250.00	0.45877E 16	0.73039E 00	0.1938
2260.00	0.51002E 16	0.81198E 00	0.1947
2270.00	0.56648E 16	0.90187E 00	0.1955
2280.00	0.62864E 16	0.10008E 01	0.1964
2290.00	0.69702E 16	0.11097E 01	0.1922
2300.00	0.77216E 16	0.12293E 01	0.1931
2310.00	0.85469E 16	0.13607E 01	0.1989
2320.00	0.94523E 16	0.15049E 01	0.1999
2330.00	0.10445E 17	0.16629E 01	0.2007
2340.00	0.11533E 17	0.18361E 01	0.2016
2350.00	0.12723E 17	0.20256E 01	0.2024
2360.00	0.14026E 17	0.22330E 01	0.2033
2370.00	0.15449E 17	0.24596E 01	0.2041
2380.00	0.17004E 17	0.27071E 01	0.2050
2390.00	0.18701E 17	0.29773E 01	0.2059

Chart 1-b. Electron emission at several temperatures.

a 1401 readout system. The 1401 computer was coordinated with a mechanical plotter which was incremented to 0.01 inch.

The cause of the tailing of ionization efficiency curves is evident from the data listed in Chart 1-a. More than 40 percent of the electron beam consists of electrons whose thermal energy is greater than the average thermal energy. Since this energy distribution extends to infinity as a limit, theoretically one should be able to observe the formation of ions even when the electron accelerating voltage is at zero, if a sensitive enough ion detection system is used.

The accuracy of the above calculations depends upon how accurately Eq. 1 describes the situation involved in electron emission by a hot metal. Several assumptions are necessary to derive this energy distribution law which is based upon statistical thermodynamics. Since this derivation is not rigorously covered in recent literature, it is given in Appendix I. For a more detailed discussion of electron emission theory the reader is referred to Fowler and Guggenheim (9) and the original works listed therein (10, 11a, 11b).

The major assumptions necessary for the derivation are discussed here briefly.

1. The electron gas surrounding the emitter is assumed to be in equilibrium with the electrons in the emitter.
2. The electrons within the electron gas are assumed to follow a Maxwell-Boltzmann momentum distribution.

3. The electron specific heat is ignored.
4. The space charge caused by the electron gas cloud near the filament is also ignored. The nature of space charge and its effect upon electron emission is discussed more fully in Harman (12, p. 128) and Ryder (13, p. 116).
5. The external potential fields used for withdrawing the electrons are disregarded. The effect of penetrations of these external electric fields to the filament (Schottky effect) can change the resultint characteristics of the total energy barrier which the electrons encounter after leaving the emitter surface. A more detailed account of the Schottky effect is found in Ryder (13, p. 97) and Heemstra (14, p. 7).
6. The filament surface is assumed to be pure and uniform with a constant work function. Becker (15) described in detail the proper interpretation of the term "work function" and its dependence upon temperature, external electric fields, and the condition of the emitting surface.
7. Other substances within the vacuum system are ignored.

Many of the above assumptions do not introduce significant errors in the results although neglecting space charge and the "effective work function" may result in small errors.

It is important to recognize that this energy distribution function is not necessarily the same as that for the electrons which finally pass through the ionizing region of an ion source (16, 17).

Both the effective work function and the space charge surrounding the emitter depend upon the electron accelerating voltage, as does the focus of the electron beam on the collecting electrode, commonly designated as the "trap". The emitter temperature can be held constant by regulating the current which passes through the filament. Schottky and space charge effects can be held constant by maintaining a constant potential near the filament and applying the electron accelerating voltage only after the electron beam has been collimated.

During a qualitative test of the emission regulator circuit using the above conditions, several relative maxima and minima were observed in the trap current as the electron accelerating voltage was changed. Flesch and Svec (18) also observed this, as shown in Fig. 3, and investigated it in greater detail. They applied the general equation of motion for an electron within a magnetically confined beam, (19) and found that the relative maxima corresponded to integral numbers of helical revolutions of the electrons within the ion box. Furthermore, the relative <u>maxima</u> of the ion box current <u>vs</u> electron accelerating voltage, corresponded to the relative <u>minima</u> observed in the trap current.

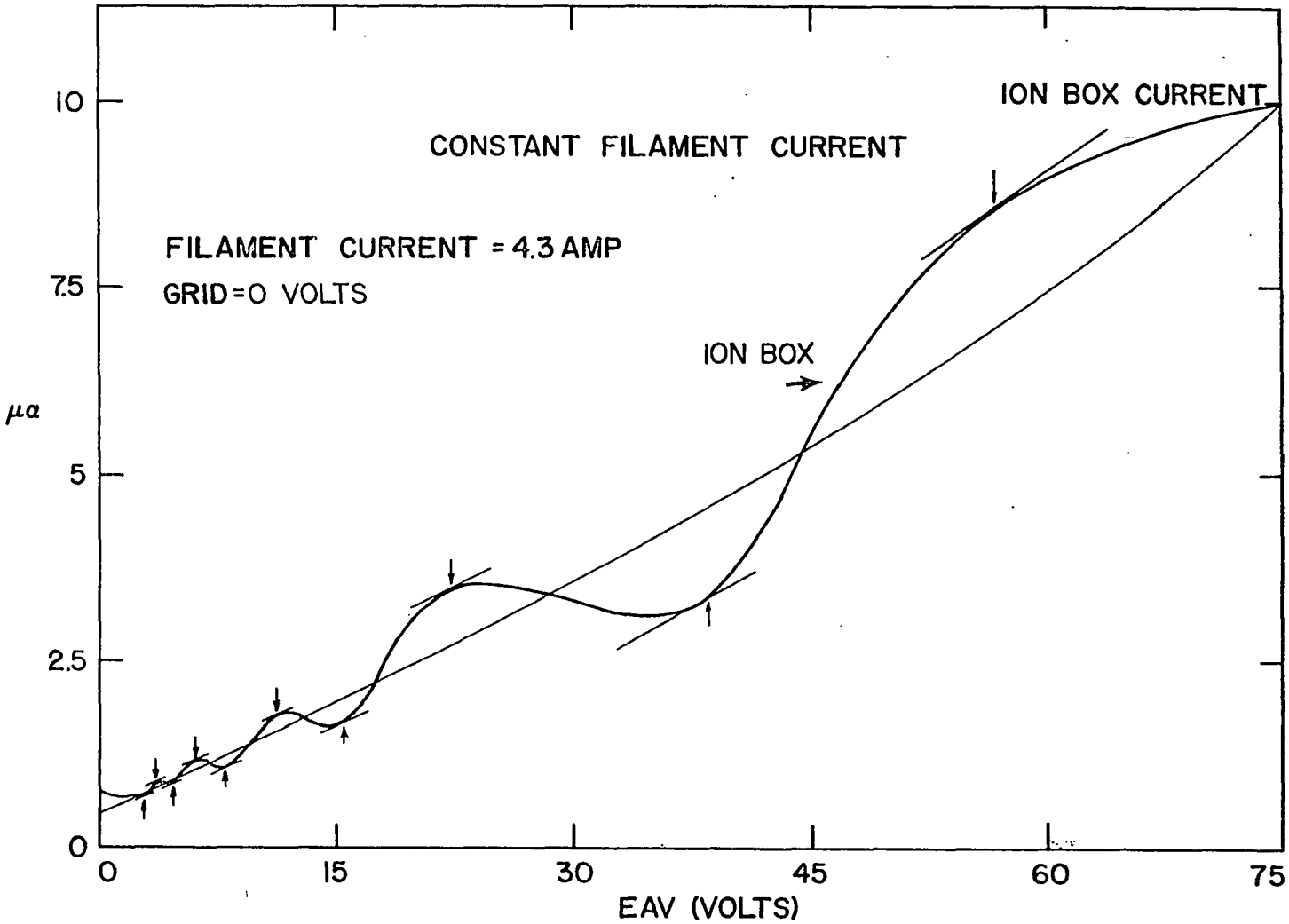

Fig. 3. Variation of trap current with electron accelerating voltage (Reprinted with permission of authors).

These studies strongly emphasize the fact that trap current is not a true measure of the actual number of electrons which can cause ionization within the ion box.

Electrons in the emitted electron beam can also have velocity components perpendicular to the desired direction of propagation. Cloutier (20) has determined these transverse velocity effects and he has described a method reducing their effect. Fox and Hickam (21) have also discussed transverse velocities of electrons. They concluded empirically that the effects of transverse velocities were negligible in their ionization efficiency studies.

The existence of numerous excited electronic, vibrational and rotational energy levels produces greater curvature and tailing effects in ionization efficiency curves than does any other physical factor. For complex fragments and ionization processes, this effect is usually more prominent than the effect of electron thermal energy. This is also the aspect of ionization efficiency studies which is the most difficult to understand and ascertain. A detailed discussion of the problems attending this will be given later.

In high intensity electron beams the electrons in the beam will diverge slightly due to space charge effects. For magnetically confined beams, this spreading is directly dependent upon the electron current and accelerating voltage, and inversely dependent upon the squares of the magnetic flux and initial electron beam diameter (22). Even at gas

sample pressures of 10^{-6} Torr or lower, it has been found that the positive ions which are found in the electron beam cause a reduction in space charge dispersion (22, p. 164). Thus, for a mass spectrometer ion source where pressures approach 10^{-5} Torr and magnetic collimation fields are used to define the electron beam, the space charge spreading will be small and the contribution of space charge spreading to the energy distribution of the electrons will be negligible. Previous workers have used electron currents to the trap of less than 10 microamperes to obviate space charge effects. The present work was carried out using electron trap currents ranging from 3 to 25 microamperes with the assumption that possible energy spread caused by space charge spreading was negligible. It should be clarified, however, that although space charge spreading does not influence the electron energy distribution, space charge does affect the actual energy of the entire electron beam. Within an ion source, high electron currents reduce the potential gradients near the electron beam. Because of this, the actual potential through which the electron beam passes, is dependent upon the intensity of the electron beam. In this way the energy of the electrons is also dependent upon the electron current intensity. The present work considers this effect in an attempt to calibrate the instrument for ionization efficiency studies.

The space charge of the ion beam can also become significant if an intense ion beam (10^{-9}A) of low momentum is used, and if the ion beam must traverse a long path, after which it is collected using a small collector slit. During ionization efficiency studies using those conditions, the ion beam space charge decreases in proportion to the ion beam intensity. Since the ion beam intensity is dependent directly upon the electron accelerating voltage, a general positive curvature of the entire ionization efficiency curve will occur. Similar effects can be produced by poor focussing, excess ion kinetic energy, poor resolution, or instrumental instabilities.

Taubert (23) has shown that when ions are formed with excess kinetic energy, the ion beam is appreciably broadened after it has passed through the magnetic field. If the excess kinetic energy is not linearly dependent upon the electron energy, slight curvature or significant irregularities will be observed in the ionization efficiency curve. In fact, results shown later in this thesis indicate that processes involving excess kinetic energy may occur with ionization efficiency laws which are different from the law for the major portion of the ionization efficiency curve.

C. Instrumental Factors

Within any ion source, there always exist potential gradients of several types. Elbert (24) constructed a large

scale model of the ion source used in this work from 1/8 inch and 1/4 inch brass plates in order to experimentally measure these field gradients. This model ion source was placed into a large glass tray and partly immersed in distilled water. Low voltages, which were proportional to the actual ion source potentials were applied to the various plates. It was assumed that the potential gradients which were thus created throughout the distilled water within the model ion source, were similar to the potential gradients present in an actual ion source. The low voltage divider circuit which was designed to supply and control the plate voltages is shown in Fig. 4.

An accurate drawing of the model ion source was made on tracing paper and placed in juxta position to the model. The main axes of the model and the drawing were made parallel and the other axes were made to coincide. A pantograph was mounted in a fixed position so that when one of its contacts was placed at a given point within the model, the other contact was at the corresponding point on the drawing of the model. The contacts were made of thin but rigid wire which could be partly immersed in the distilled water within the model.

Lead 1 of an electrometer (Model 600A Electrometer Keithley Instruments Incorporated, Cleveland, Ohio) was attached to the pantograph contact which was positioned in the model. Lead 2 of the electrometer was placed at a fixed position

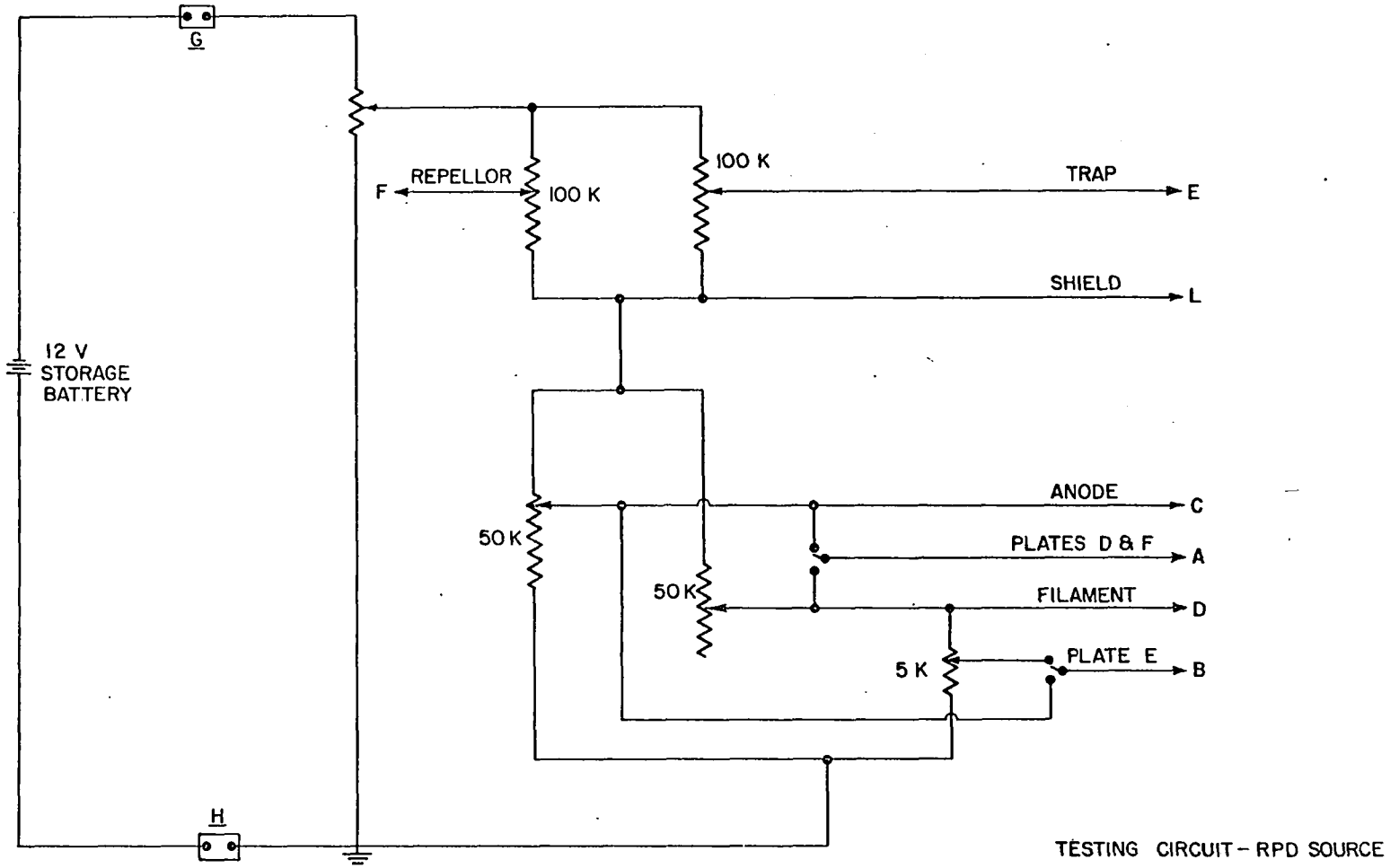

Fig. 4. Control circuit for model ion source voltages.

within the model ion source. For each fixed position of electrometer lead 2, a null on the electrometer was found by moving electrometer lead 1 through the water in the model ion source with the pantograph contact. This null indicated that both of the electrometer leads were at the same potential. The other pantograph contact indicated this null point at the corresponding point on the drawing, hence the point was marked. An equipotential line was established on the drawing by determining many similar null points for a fixed position of electrometer lead 2. Placing electrometer lead 2 in a new position and thus at a different potential, permitted a different equipotential line to be found. Fig. 5 illustrates the results of measurements which were made by Elbert. The results of similar tests with different potentials and positions for the various ion plates were used in designing the ion source for the present work.

In a conventional ion source, the penetrations of filament potential fields can become significant if large apertures are used to admit the electron beam into the ionizing region. Field penetrations from the filament potential are directly dependent upon the electron accelerating voltage, hence the effect upon ionization efficiency tailing can also become significant. Reduction of this effect can be accomplished by increasing the distance from the filament to the ion box. This is preferably done by inserting electron collimating plates between the filament and the ion box. Use

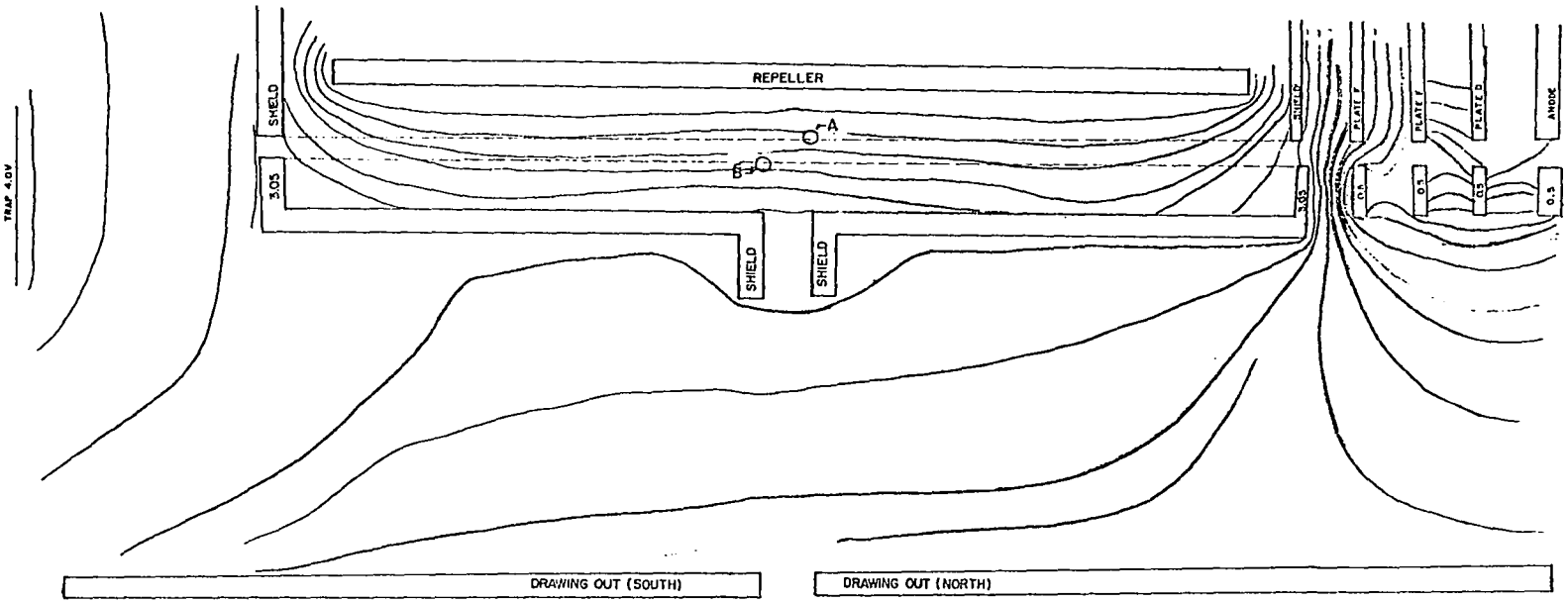

Fig. 5. Measured potential gradients within model ion source.

of small apertures for transmitting the electron beam is also desirable.

A similar effect will be encountered near the electron trap when high trap voltages are used. Here the effect can be reduced by increasing the distance from trap to ion box and by using lower trap potentials. The effect of these field penetrations are usually negligible because they remain constant throughout most ionization efficiency experiments.

The primary source of instrumental errors is due to field gradients which are necessary to remove the ions. Even when the field penetrations of the filament and trap are eliminated, the repeller or drawing out electrodes set up field gradients which affect the ionization efficiency data. The effect of these potential gradients can best be explained by reference to Fig. 5 in which the dashed lines represents the extent of the electron beam in the ion box. The ions formed near A are at a greater potential energy than those formed near B. Thus the electrons which cause ionization in the proximity of A have a greater energy than the electrons which cause ionization near B. For a particular ion source this energy spread depends upon the width of the electron beam, the strength of the collimating magnetic field, and the potential difference between the repeller and the shield. Robertson (25) has calculated that this effect contributes less than 0.11 V to the energy spread of an electron beam in a typical ion source. The effect is minimized by

using low repeller or drawing out potentials and strong collimating magnetic fields.

It is important to note that the electron energy is usually determined by measuring the potential difference between the filament and the shield. Fig. 5 shows that because of the potential gradients induced by the repeller, the electron beam is actually accelerated to a potential greater than the shield potential. A more accurate measure of the electron energy would be to approximate the effect of the repeller voltage on the electron energy and then to add this to the measured potential difference between the shield and filament. This was done in the present work in an attempt to determine appearance potentials without the direct use of calibrating gases.

Any slits through which an electron beam passes can be regarded as electrostatic lenses with focussing actions on the electron beam. Such focussing may have only a minor effect on the electron energy spread. Klemperer (26), Pierce (22), and Harman (12), are excellent references regarding electron optics and electron motion for conditions analogous to mass spectrometer conditions.

D. Miscellaneous Effects

The accuracy of results which are obtained from ionization efficiency studies depends largely upon the method of analysis and the absolute ion detection sensitivity of the

mass spectrometer. As previously stated, for perfect sensitivity one should be able to observe ions even at 0 electron accelerating voltage because of the electron thermal energy. The curve in Fig. 6 shows a possible ionization efficiency curve for the formation of ions within the ion source. Unless there is a 100 percent transmission of these ions to the collector and a 100 percent efficiency throughout the collector and amplifier system, one could observe the appearance potential at points 1, 2, or 3 depending upon the ion detection sensitivity of the instrument. Lines A, B, and C indicate these different sensitivities. Sensitivity is discussed in greater detail later, and an attempt is made to determine its absolute value for the present instrument.

It is obvious that the accuracy of ionization efficiency data is directly dependent upon the stabilities of the electron beam, the ion beam, the magnetic field, and the amplification-read-out system. The effect of any instabilities on the accuracy of the results depends upon whether the instability is relative to the intensity of the ion beam or if it is an absolute or constant instability. In the present work, magnet and ion source instabilities are considered to cause relative errors in ion intensity measurements, whereas amplification-read-out instabilities are considered to contribute both to relative and absolute errors. The effect of these instabilities should be

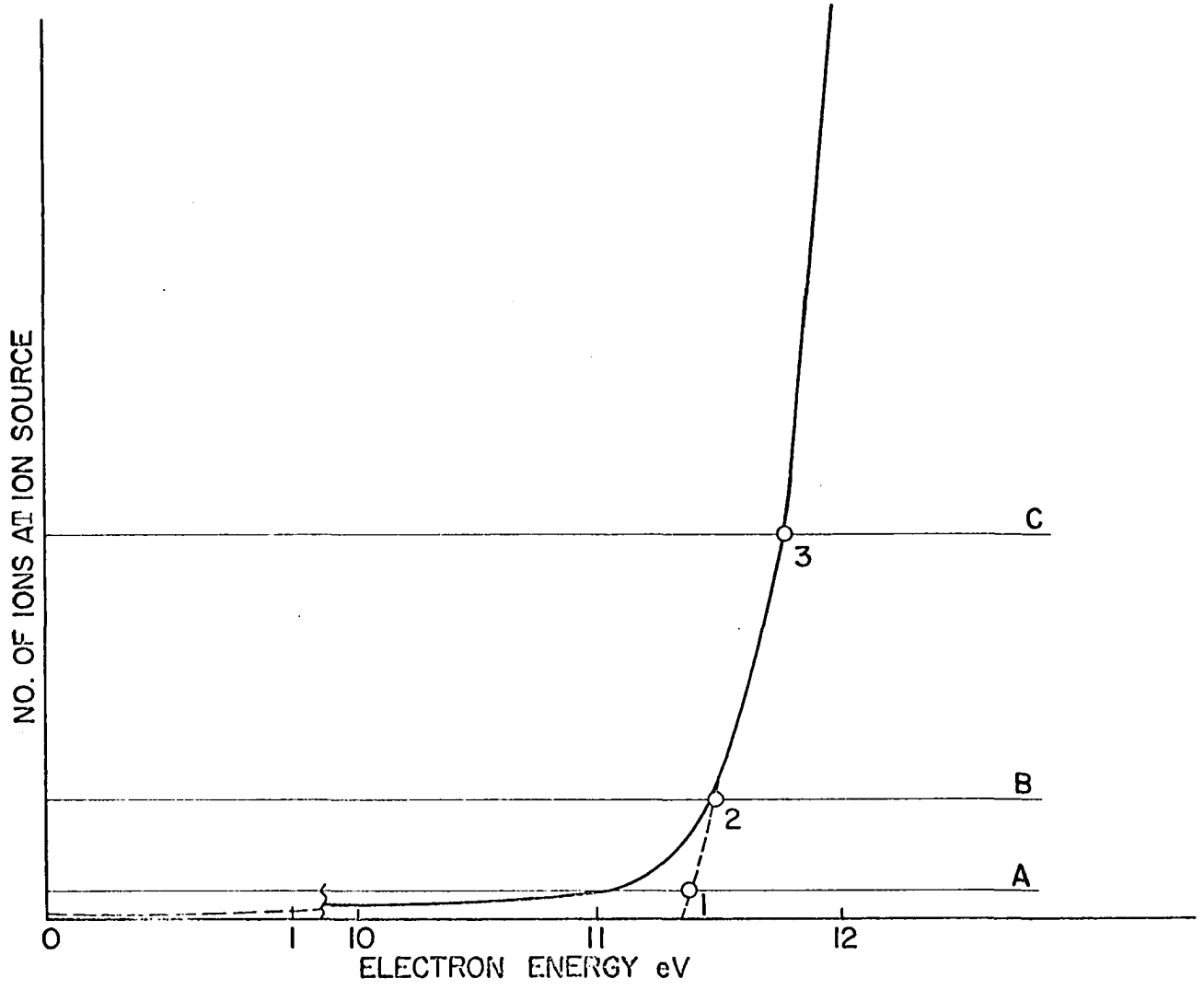

Fig. 6. Enlarged portion of possible ion efficiency curve.

considered in any analysis of the errors associated with ionization efficiency data.

Contact potentials have been mentioned as sources of error; however, only few attempts (27, 28, 19, p. 54) have been made to determine their exact values. In this work contact potentials are assumed to be constant and therefore not detrimental to the method of calibrating the instrument.

III. MASS SPECTROMETER ION SOURCE DESIGNS FOR IONIZATION EFFICIENCY STUDIES

A. Introduction

Many of the errors discussed above have been greatly reduced by appropriate instrument design and by careful adjustment of instrumental conditions. Factors which should be emphasized in trying to optimize results are the use of low repeller and trap voltages, strong electron collimating magnetic fields, substantial separation of the trap and filament from the shield, high ion accelerating voltages, and collector slits which are as large as the necessary resolution will permit.

Instrumental methods of eliminating the effects of electron thermal energy have been in use for the last decade. Some of these methods are discussed below. Refer to Fig. 7 for a comparison of the various types of electron collimating systems which are used for these methods.

B. Conventional Ion Sources

Most mass spectrometers have simple electron collimating systems which consist of a filament, repeller, ion box, and an electron trap. The inaccuracies of ionization efficiency studies using such conventional sources may be caused by any or all of the factors discussed previously. Several simple modifications of these sources can be made which improve the results. A single collimating plate placed between the filament and the ion box is sufficient to reduce the penetration

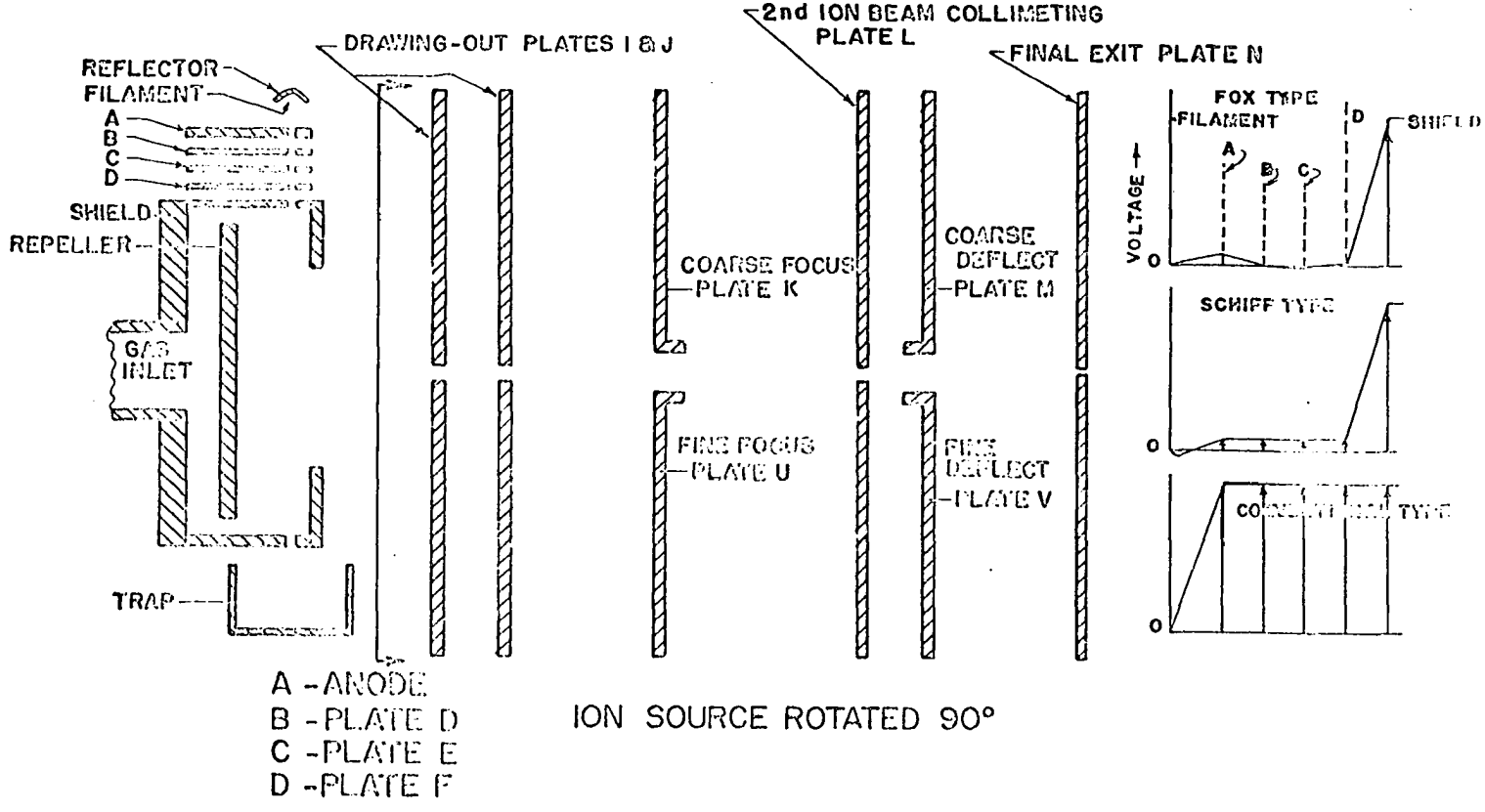

Fig. 7. Types of ion source modes of operation.

of filament potentials into the ionizing region and also to reduce the width of the ionizing electron beam. The net result is a decrease of the tail of the ionization efficiency curve. Furthermore, better emission characteristics are obtained if the potential of this collimating plate is fixed at 2 to 6 volts above the shield potential, rather than at shield potential. As previously explained, this creates a constant space charge because it maintains a constant potential gradient around the filament. Further improvements in the electron emission are obtained if more collimating plates are used. In the present work, four collimating plates are used.

C. Retarding - Potential Ion Sources

1. Fox and Hickam design

In 1953 Fox and Hickam (28) described an ion source that essentially eliminates the effects of electron thermal energy. The potentials of the various plates within the electron collimating system relative to the potential of the filament are indicated at the right in Fig. 7. The basic operating principle for this source is the use of a retarding potential electrode, plate E. Electrons cannot reach the ionizing region unless they have thermal energy which is sufficiently high to enable them to surmount the potential barrier created by the retarding potential that is applied to plate E. Electrons which have insufficient energy do not pass through the electron retarding plate E. The ion current intensity

is then due only to the electrons which do pass the potential barrier. Area A of Fig. 8 shows the electrons that can cause ionization for a retarding potential of 0.18 volts. If the total number of electrons emitted from the filament is held constant, and the retarding potential barrier is reduced by a small amount, for example, 0.02 volts, then the number of electrons which can reach the ionizing region increases slightly. Area B indicates this increase. The difference in the ion current intensity measured for these two retarding potentials is assumed to be caused by the electrons represented by Area B. The thermal energy spread of the electrons which produced this difference is indicated by the difference in the voltage of the two retarding potentials. In this example the thermal energy spread is only 0.02 volts. If the differences in ion current intensities are measured over a range of electron accelerating voltages near the ionization onset, an ionization efficiency curve is obtained with only slight tailing.

2. Cloutier and Schiff source

Cloutier and Schiff (20, 29) have described a retarding potential ion source which is a modification of the Fox and Hickam ion source. Their source is physically the same as that illustrated in Fig. 7 but instead of using the four electron collimating plates to retard the electron beam, they maintain these plates at a potential of +2 to +5 volts with respect to filament. Under these conditions the electron

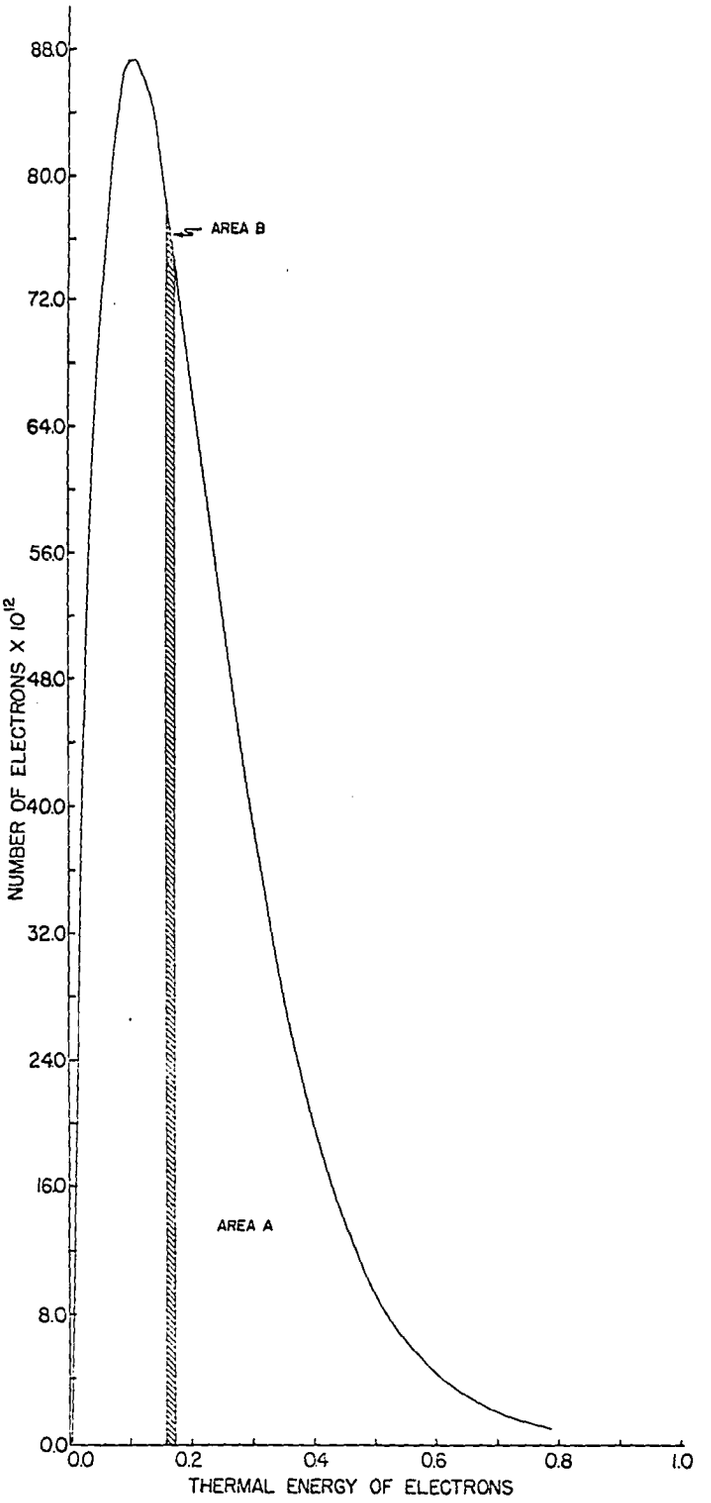

Fig. 8. Electron energy distribution and an RPD increment of 0.02 volts.

emission is very similar to the emission encountered in a simple space charge limited diode (13, p. 112). Due to the space charge surrounding the filament, electrons must pass through a negative or retarding potential field in order to leave the vicinity of the filament. The magnitude of this space charge retarding potential depends on the distance between the filament and the first electron collimating plate or "anode" (20, p. 20), on their voltage difference and on the filament temperature. The operation of the Cloutier and Schiff source is similar to that of the Fox and Hickam source in that the difference of ion current intensities is determined for two different retarding potentials. However, in the Cloutier and Schiff source, the retarding potential increment is produced by changing the potential of the anode. The space charge, or retarding potential changes only a fraction as much as does the anode potential change, hence it is much easier to control the retarding potential increment in this source than in the Fox and Hickam source.

D. Electron Velocity Selectors

The most accurate and most direct method of eliminating electron thermal energy is to pass the electron beam through an energy selector for which conditions can be chosen to pass only an electron beam with a narrow energy spread. This final electron beam is then accelerated and used to ionize the gas. Although several types of energy selectors have been described (30, 31, 32, 33) since the initial

designs of Nottingham (27) and Clarke (34), none of these are able to obtain electron currents above 10^{-6} amps and all of them encounter difficulties because of space charge, secondary electrons, and contaminations. The use of electron energy selectors is also discouraged by the complexity of the ion source and by their greatly reduced ion detection sensitivities. However, results of ionization efficiency studies made using electron energy selectors are superior to the results of other electron bombardment methods.

Results from photoionization are very similar to the results from electron energy selectors. Many of the advantages and disadvantages are similar (35, 36).

E. Pulsing Techniques

The effect of potential field gradients within the ionizing region can be reduced by using pulsing techniques (21, 29). In the usual pulsing procedures, potential gradients are eliminated by applying a negative pulse to the repeller plate while the electron beam is traversing the ion box. The amplitude of the negative pulse is just sufficient to equalize the repeller and shield d. c. voltages. This permits the ionization to occur in an ion source region which is free of potential field gradients from the repeller. Then the negative pulse is removed from the repeller and simultaneously a negative pulse is applied to the electron collimating plates. This prevents electrons from entering the ion

box to cause ionization while the repeller expels the ions that were formed during the previous pulse. The entire cycle is repeated at a frequency of 20 to 100 KCPS in order to reduce the effects of wall collisions within the ion box (21). Reduced tailing of the ionization curve is observed as a result of this pulsing technique (29).

F. Present Design

An attempt was made to incorporate all of the above designs, except the electron energy selectors, into the present ion source. Figs. 7 and 9 are diagrams of the present ion source. The electron collimating plates, D, E, F, and G are constructed of 0.025 inch thick (Nichrome V) metal. Plate G, the electron plate nearest the filament is called the anode in agreement with the usage of Cloutier and Schiff (20). The slits in plates D, E, F, and G for the electron transmission are 0.030 inch, 0.020 inch, 0.010 inch, 0.030 inch and 0.020 inch wide respectively. These sizes were chosen in order to obtain good electron transmission with a reduced transverse velocity spread. The slit in plate E is only 0.010 inch in order to produce more accurate retarding potentials. Previous work indicates that field penetrations affect the true potential in the center of this slit if it is too large. Such field penetration can reduce the "effective retarding potential" for the electrons. Field penetrations into the slit in plate E are further decreased

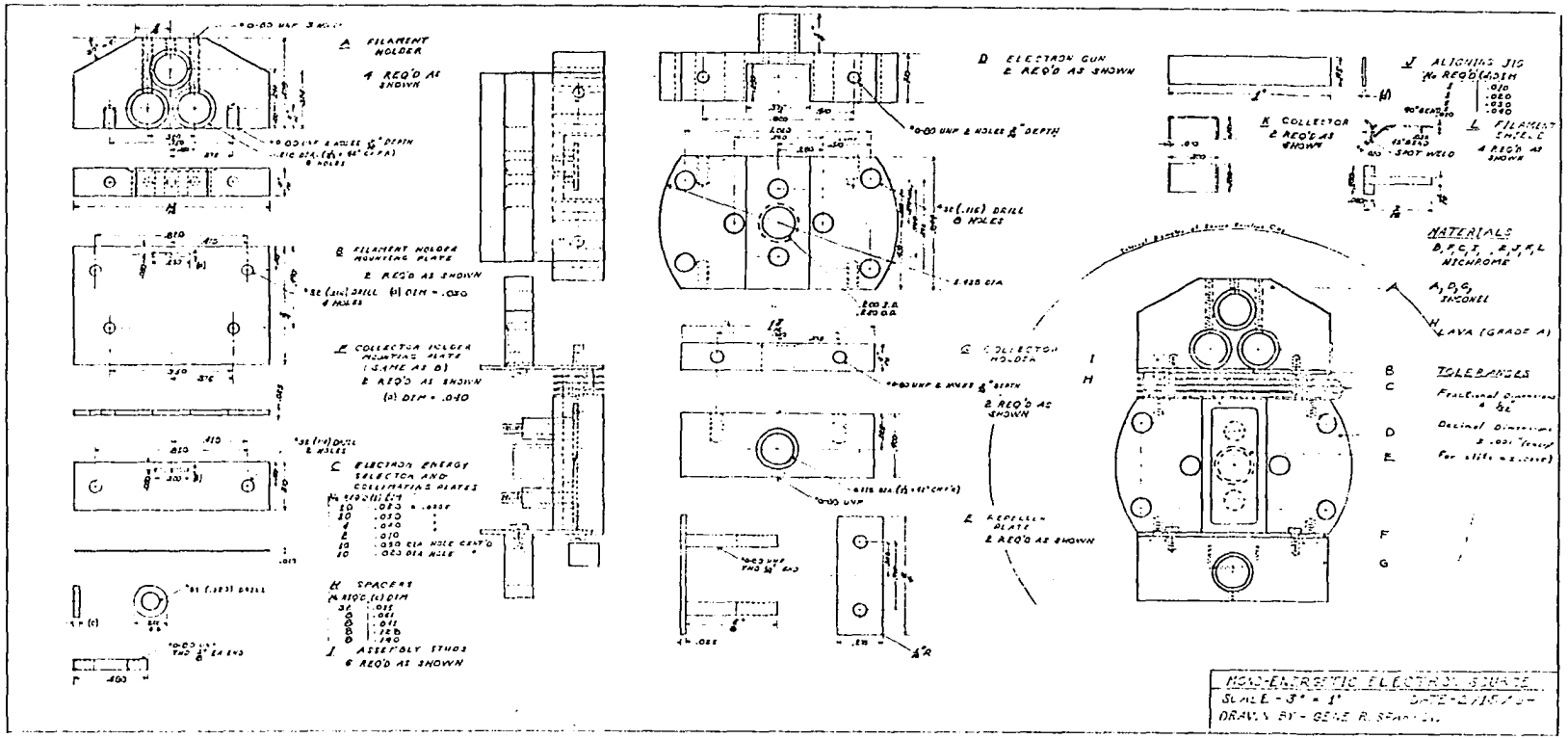

Fig. 9. Design of the electron gun.

by separating it from plates D and F, with 0.040 inch fired lava spacers. Plates D and F are separated from the shield and anode respectively, by 0.035 inch lava spacers.

The filament is a 0.032 inch x 0.001 inch tungsten ribbon heated by direct current, hence a voltage drop occurs over the length of the filament. For this reason care is taken to tie the small reflector behind the filament to the side of the filament which is at the lowest potential.

The entire electron collimating system is enclosed by a Nichrom V shield which is mounted directly on the anode plate holder. The electron trap is similarly enclosed with a shield which is maintained at the same potential as the ion box. The shields are used to prevent field penetrations to and from the electron collimating system and to confine to the filament region excess tunstic oxide distilled from the filament. Mounted in each shield is an iron button (Armco ingot iron, American Rolling Mill Co., Warren, Ohio) 1/4 inch D by 3/16 inch thick. One button is mounted directly behind the electron trap and the other button is mounted directly behind the filament. The electron collimating magnetic field is supplied by a small permanent magnet which is positioned immediately outside the ion source envelope.

Two improvements are realized by using the iron buttons.

1. They substantially increase the emission characteristics of the electron system by concentrating

the magnetic field between the filament and electron trap. A gaussmeter (Model 1890, Gaussmeter Radio Frequency Laboratory, Boonton, New Jersey) was used to measure the magnetic field in the center of the ionizing region. Before inserting the iron buttons, a magnetic field of 245 Gauss was obtained. After inserting the buttons, the magnetic field was increased to 288 Gauss. Without the buttons it was difficult to obtain 1 microampere of electron trap current when a current of about 5A was passed through the filament. After inserting the buttons and under similar conditions, trap currents of 10 to 15 microamperes are obtained using only 4.2A of filament current.

2. The iron buttons also reduce the effect of the source magnet position on the electron transmission. Because of this, optimum electron transmission can be obtained by less precise adjustment of the source magnet position.

The voltage of the anode; (plate G) is continuously variable from 0 to +8 volts with respect to the shield potential. The voltages of plates D, E, and F are independently and continuously variable from -1 to +16 volts with respect to either the filament or shield potential.

The voltages at either the anode or plate E can be incremented slightly by selecting one of two different

potentials by means of a switch. This produces either a Schiff or a Fox type of retarding potential increment.

The repeller plate is located as far away from the electron beam path as space permits. This prevents electrons from striking it, and produces more uniform potential field gradients within the ionizing region. This also reduces the effect of wall collisions and permits better adjustment of the potential field gradients.

Efforts were made to reduce the flow of sample gas out of the ion box through the slits in the electron collimating plates and through the slit for the electron trap. Four holes were drilled in the repeller plate to allow the flow of sample gas directly through the repeller instead of around it.

The electron beam is allowed to pass as close as is practicable to the ion box exit slit. This further reduces the effect of wall collisions, permits a shorter average exit time for the ions, increases ion detection sensitivity, and produces ionization in a region of more uniform potential gradients. In the present ion source the slits in the electron collimating plates place the axis of the electron beam 0.045 inch from the ion box exit slit. The potentials from the repeller plate cause a general sideward displacement of the electron beam. This displacement, which is dependent upon the strength of the magnetic collimating field and repeller potential, is calculated to be less than 0.005 inch in this ion source at nominal operating conditions.

The electron collector slit is 0.040 inch wide. This is large enough to compensate for electron beam space charge spreading, electron beam divergences due to focussing effects of the electron collimating plates, and to partially reduce the focussing effects caused by the electron accelerating voltage. The electron trap voltage is normally about 8 to 30 volts greater than the shield voltage. A negative square wave pulse with an amplitude of 0 to 54 volts can be applied to the anode at frequencies from 1 cps to 1 Mcps. The repeller plate can be similarly pulsed from 0 to 7 volts and 180° out of phase with the anode pulse. The symmetry of the two pulses can be varied to produce exactly symmetrical square wave forms at each plate.

The versatility of the present ion source is easily recognizable. Not only is it possible to operate it as a Fox or Schiff type ion source, but it can also be used in a convential type of operation. Many other modifications and combinations of these three types of source are also possible and pulsed or continuous modes can be used in either the normal or retarding potential methods for ionization efficiency studies.

IV. THE DESIGN OF THE MASS SPECTROMETER

A. General Description

The mass spectrometer which was used in the present work was initially designed by Svec (37) and also used by Saalfeld (6a, 6b). All of the components originally used by Svec have been modified or replaced, and since the description given by Saalfeld, the ion source, electromagnet, and most of the electronic circuits have been replaced or modified. Many additions have also been made.

The design of the present instrument is still essentially a Bleakney-Nier single focus mass spectrometer of the 60° sector type with a 15 cm deflection radius. The instrument is shown in Fig. 10.

B. Physical Components

1. Inlet system

The inlet system is similar to the one described by Saalfeld (6a), thus only a brief discussion is necessary. It consists of two separate and independently variable viscous leaks which allow two different gaseous samples to be simultaneously introduced into the ion source through a 1/4 inch o.d. copper tube 18 inches long. A 1/8 inch o.d. borosilicate glass tubing at the top of the ion source delivers the gas to the ionizing region and isolates the copper inlet tube from ion accelerating voltages. The copper tubing and the inlet valves can be baked out using a one

Fig. 10. Mass spectrometer.

inch by 8 feet, 768 watt (BIH-41, Briscoe Manufacturing Company, Columbus, Ohio) heating tape. An oil diffusion pump which is backed by a mechanical fore pump may be used to evacuate either inlet independent of the other.

2. Mass analyzer

The mass analyzer tube is the same as the one described by Saalfeld, and it is similarly mounted. It is a one inch o.d. copper tube 71.8 cm. long. It is bent at its center to 120° in a 15 cm radius, and it is flattened to approximately 1/2 inch. Collimation of the analyzer tube with the permanently positioned magnet is achieved by moving the entire aluminum frame which holds the analyzer tube, ion source, and collector. The motion is accomplished in a vertical direction by means of three screw adjustments and in a horizontal direction by means of two additional screw adjustments.

3. Ion source

The electron collimating system has already been described. Figs. 11 and 12 are photographs of the present ion source both assembled and disassembled, and it was illustrated in Figs. 7 and 9.

All of the ion plates were constructed from 0.025 inch thick Nichrome V metal or of Chromel-A which was cut into discs 1.437 inch in diameter. The spacers which are used

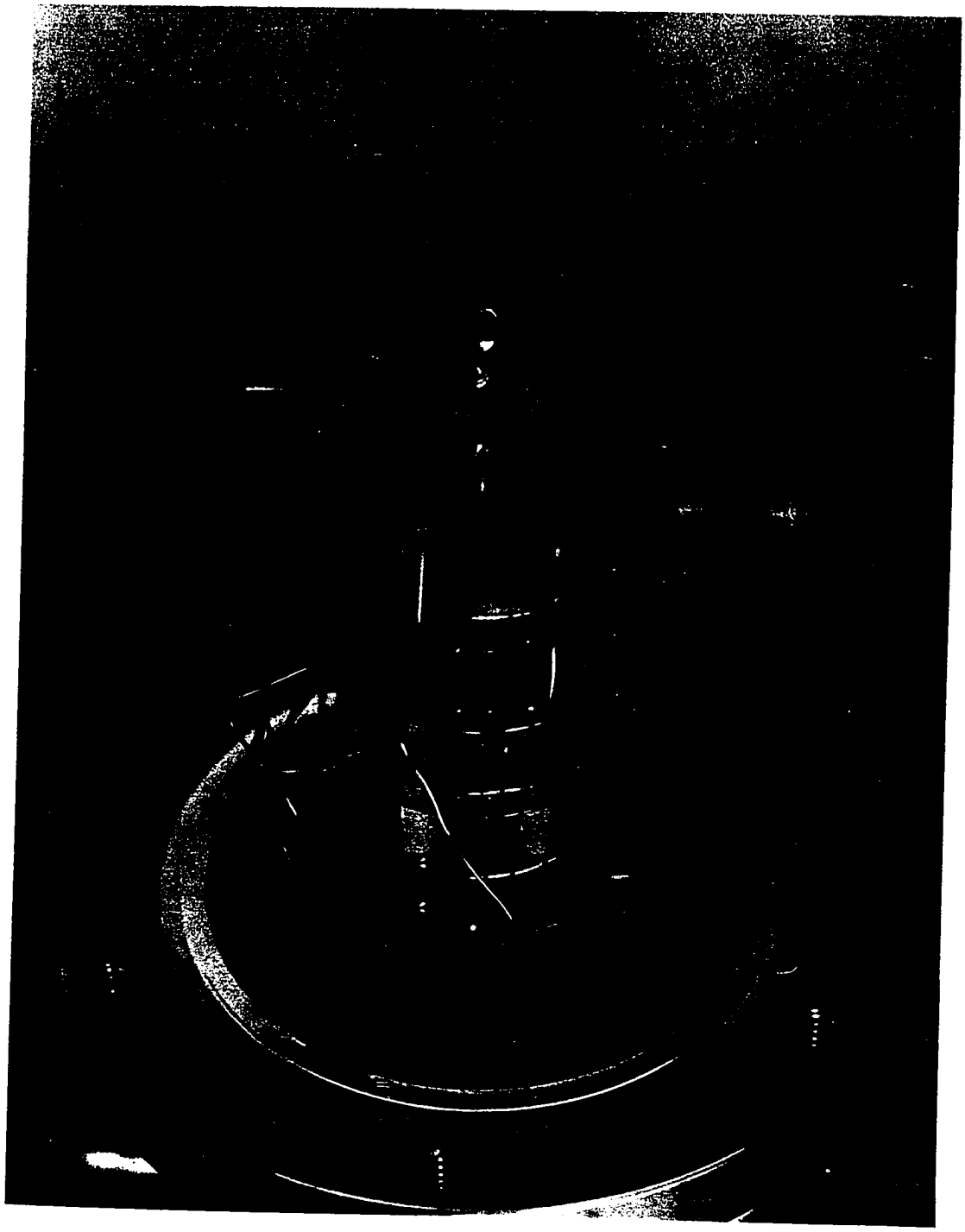

Fig. 11. Assembled ion source.

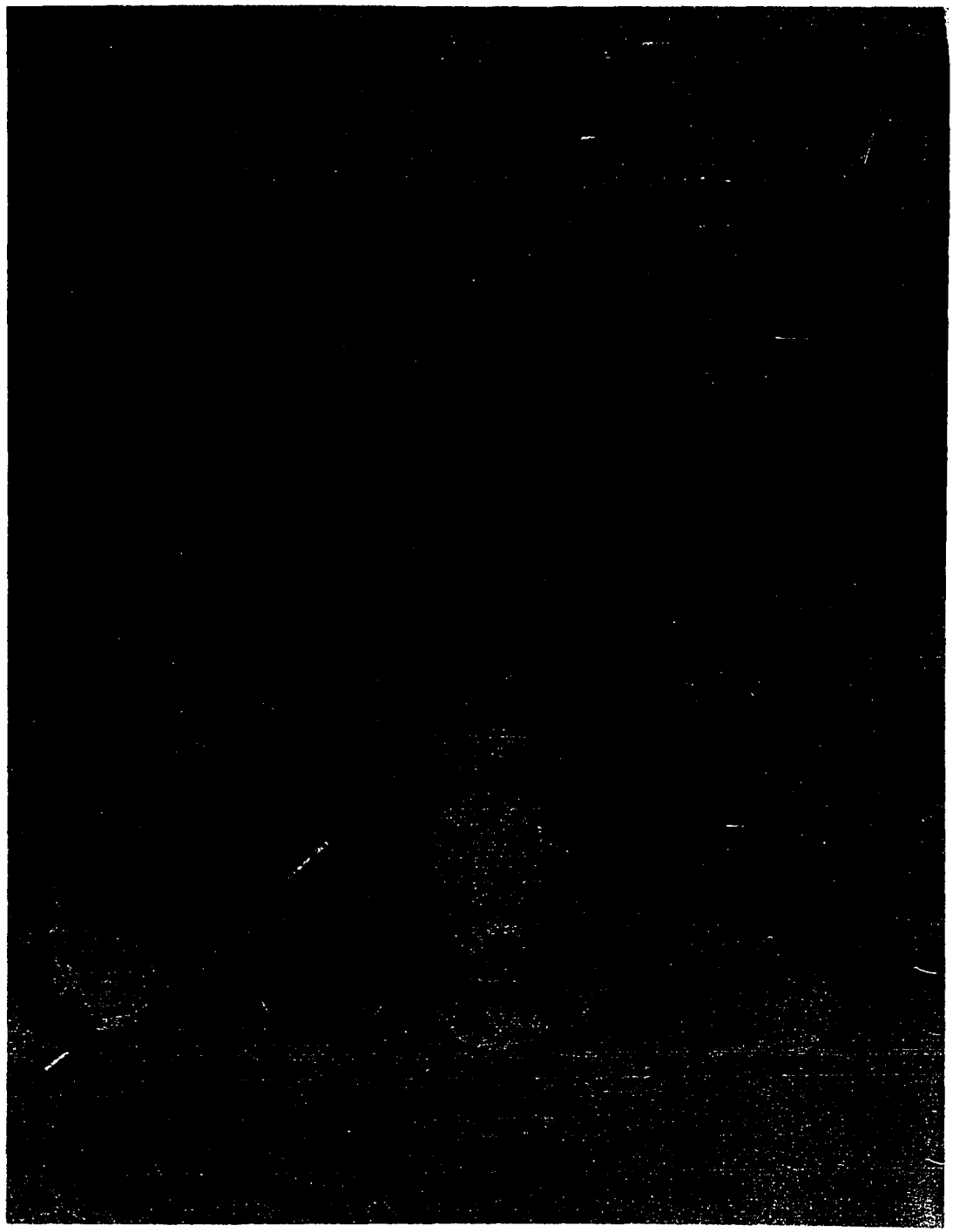

Fig. 12. Disassembled ion source.

to provide electrical isolation and to separate the plates are either glass, lava, or porcelain and are cut and ground to ± 0.001 inch tolerances.

The ion box potential which is normally 2000 volts, is variable from 0 to 3111 volts.

The initial ion exit slit is 0.015 inches wide and 0.500 inches long with short lips to reduce field penetrations into the ion source. The slit in the ion drawing out plate is 0.080 inches wide and 0.500 inches long with lips placed at its edges. The potential of this plate is normally about 20 volts below shield potential, however, it can be varied from +5 to -300 volts. It is spaced 0.313 inches from the initial ion exit slit. This is far enough to significantly reduce field penetrations into the ionizing region.

In a typical ion collimating system, the ion beam is passed through a slit formed by two half plates. These two plates are used to either focus or decrease ion beam displacements which are caused by misalignments in the ion source. Recently, Conzemius and Svec (38) described a method of improving the ion transmission of a mass spectrometer without significantly affecting the resolution. The present ion source also uses his technique which involves placing a second set of focus plates between the two grounded final collimating plates. The first set of focus plates, K and U in Fig. 7, is used at a potential of about 1800 volts. This potential can be varied from 0 to 400 volts below shield

potential. The second set of focus plates, M and V, is placed between two grounded collimating plates L and N. The potential of this second set of focus plates is normally about 400 volts at optimum focus, however, it is variable from 0 to shield voltage. The two collimating plates contain 0.011 inch slits which determine the minimum ion beam width.

All of the above plates are mounted on four stainless steel studs which are threaded at each end for 0 - 80 nuts. These four studs are screwed into a 0.025 inch thick ion base plate. Thin borosilicate glass capillary tubing provides electrical insulation between the ion source plates and the mounting studs. Hexagonal 0 - 80 nuts and small Nichrome washers are used at the top of the mounting studs to tighten the ion source assembly.

The entire ion source assembly is mounted on a slit alignment adapter which allows small rotations of the ion source about the main ion beam axis. This permits alignment of the ion source slits with the collector slit. The slit alignment adapter consists of three parts constructed of stainless steel. See Fig. 13 and the photographs shown in Figs. 11 and 12.

1. The <u>analyzer tube plate</u> is a disc 0.875 inch in diameter and 0.285 inch thick with a concentric cut 0.720 inch in diameter and 0.225 inch deep. It is attached directly to the end of the 1 inch copper analyzer tube by means of two 2 - 56 screws.

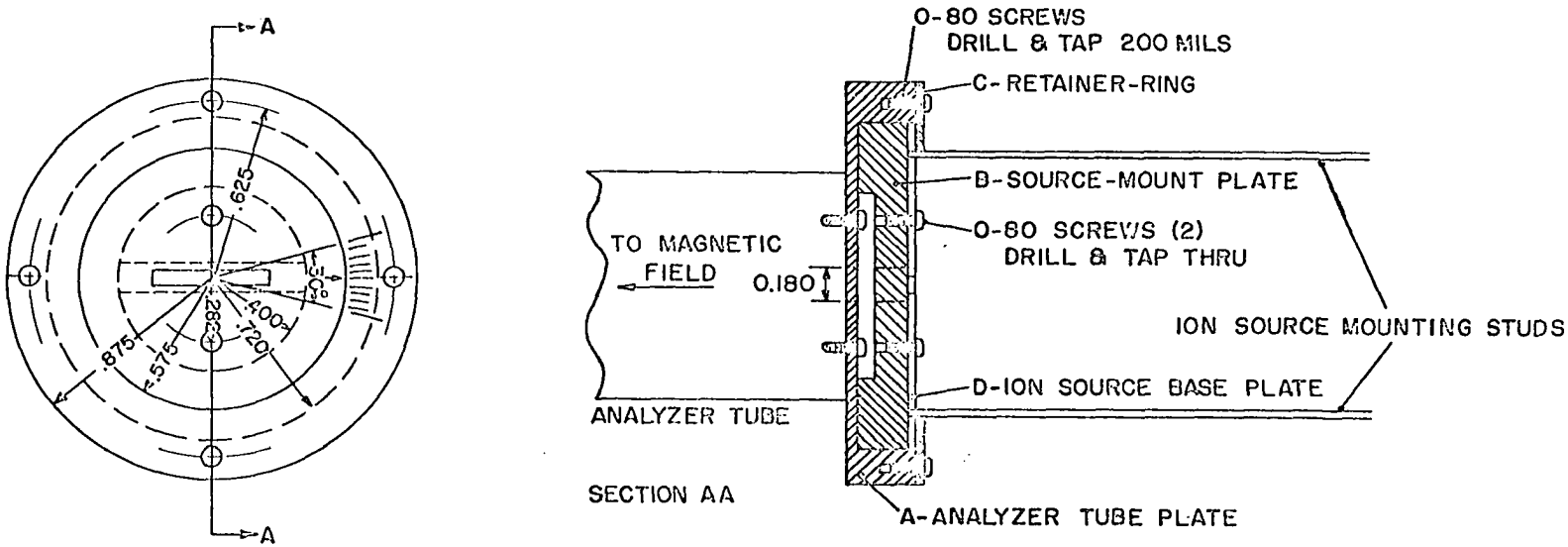

Fig. 13. Slit alignment adaptor.

2. A source mount plate 0.720 inch in diameter and 0.200 inch thick fits snugly into the cut of the analyzer tube plate. The base plate of the ion source is attached to this source mount plate by means of two 0 - 80 screws. The entire ion source assembly is connected to the source mount plate in this manner to allow smooth rotation of the ion source within the analyzer tube plate.
3. A 0.025 inch thick retaining ring holds the ion source base plate and the source mount plate within the analyzer tube plate. This retaining ring is attached to the analyzer tube plate with four 0 - 80 screws.

The entire ion source is mounted in a vacuum housing which has a removable cap in order to expose it completely for maintenance (See Fig. 11). The electrical potentials are supplied to the ion source by passing leads through two seven-lead bulkheads (Fusite Series 9-700, Fusite Corporation, Cincinnati, Ohio) which are vacuum sealed to the envelope with aluminum gaskets. Saalfeld (6a, p. 3) describes the envelope in detail.

4. Magnet

The magnetic field is produced by a permanently positioned electromagnet which is mounted on a steel base to elevate the entire mass spectrometer analyzer frame above the floor. Only the coils of the magnet are the same as the

magnet described by Saalfeld. Briefly, each coil consists of 20,000 turns of Heavy Formvar insulated copper wire (A.W.G. 22, Anaconda Wire and Cable Company, Chicago, Illinois) with a resistance to 500 Ω. The maximum magnetic field of the original magnet was 6300 Gauss.

Extensive calculations were made from basic equations for magnetic circuits, (39, 40a, p. 372) and the results of these calculations were used in redesigning the magnet. These calculations are discussed below.

Magnetomotive force, mmf, is given by the product of the current, I, and N, the number of coil turns through which it passes; or by the product of the reluctance, R, and the magnetic flux, Φ ;

$$\text{mmf} = R\ \Phi = NI. \qquad 7$$

The reluctance of a material with magnetic permeability, μ , length, ℓ , and cross section, A, is given by;

$$R = \frac{\ell}{\mu A} \qquad 8$$

and the magnetic flux within this reluctance is;

$$\Phi = H\mu A. \qquad 9$$

Combining Eqs. 7, 8, and 9 gives the magnetomotive force;

$$\text{mmf} = NI = \frac{\ell}{\mu A} \times H\mu A = \ell H \qquad 10$$

as the product of the length of the reluctance path, ℓ, and the magnetic field strength, H.

The magnetic flux, Φ, must be equal for each of several reluctances which are in series. Thus Eq. 9 can be used to determine the mmf for each reluctance, providing that the magnetic field is known for at least one of them. In the following calculations for an air gap in series with a steel bar, the variables with subscript "a" refer to the air gap, and those with a subscript "s" refer to the steel bar.

$$\Phi_a = H_a \mu_a A_a \qquad 11a$$

$$\Phi_s = H_s \mu_s A_s \qquad 11b$$

But Φ_a must equal Φ_s

Hence;

$$H_a \mu_a A_a = \Phi_a = \Phi_s = H_s \mu_s A_s \qquad 12$$

or;

$$H_s = \frac{H_a \mu_a A_a}{\mu_s A_s} . \qquad 13$$

Once the magnetic field within each reluctance has been determined, Eq. 10 can be used to calculate the mmf for each reluctance. For the above example, from Eqs. 10 and 13;

$$NI_s = \ell_s \times H_s \qquad 14$$

$$= \frac{\ell_s H_a \mu_a A_a}{\mu_s A_s}$$

Before the original magnet was redesigned, calculations were made to determine dimensions which would produce optimum

magnet characteristics. Because several dimensions of the original magnet could not be modified, the design was restricted. In these calculations the magnet coil currents which are necessary to produce various magnetic fields within the magnet air gap are calculated. A plot of the magnet coil current vs the magnetic field within the air gap was made from the results of each set of calculations.

First the values of $\frac{H\mu}{\mu_a}$ were calculated from Eq. 13 for each reluctance in the magnet circuit. This was done for each of a large number of values of magnetic fields within the air gap. The $\frac{H\mu}{\mu_a}$ values were assumed to be nearly equal to the intrinsic flux, β. Fig. 14 shows the "DC Magnetization Curves for Various Metals" which are used to relate the β values to the magnetizing forces. These magnetizing forces are then used in Eq. 14 to calculate the mmf for each reluctance of the circuit. The total mmf is then given as the sum of all the series magnetomotive forces and this total mmf is used to calculate the total magnet coil current that is necessary to produce the various magnetic fields within the air gap.

The magnet considered in these calculations consisted of four reluctances in series.

1. The reluctance of the air gap of the magnet is computed on the basis of dry air. The area of the gap is calculated by assuming that fringe fields increase all of the effective dimensions by one

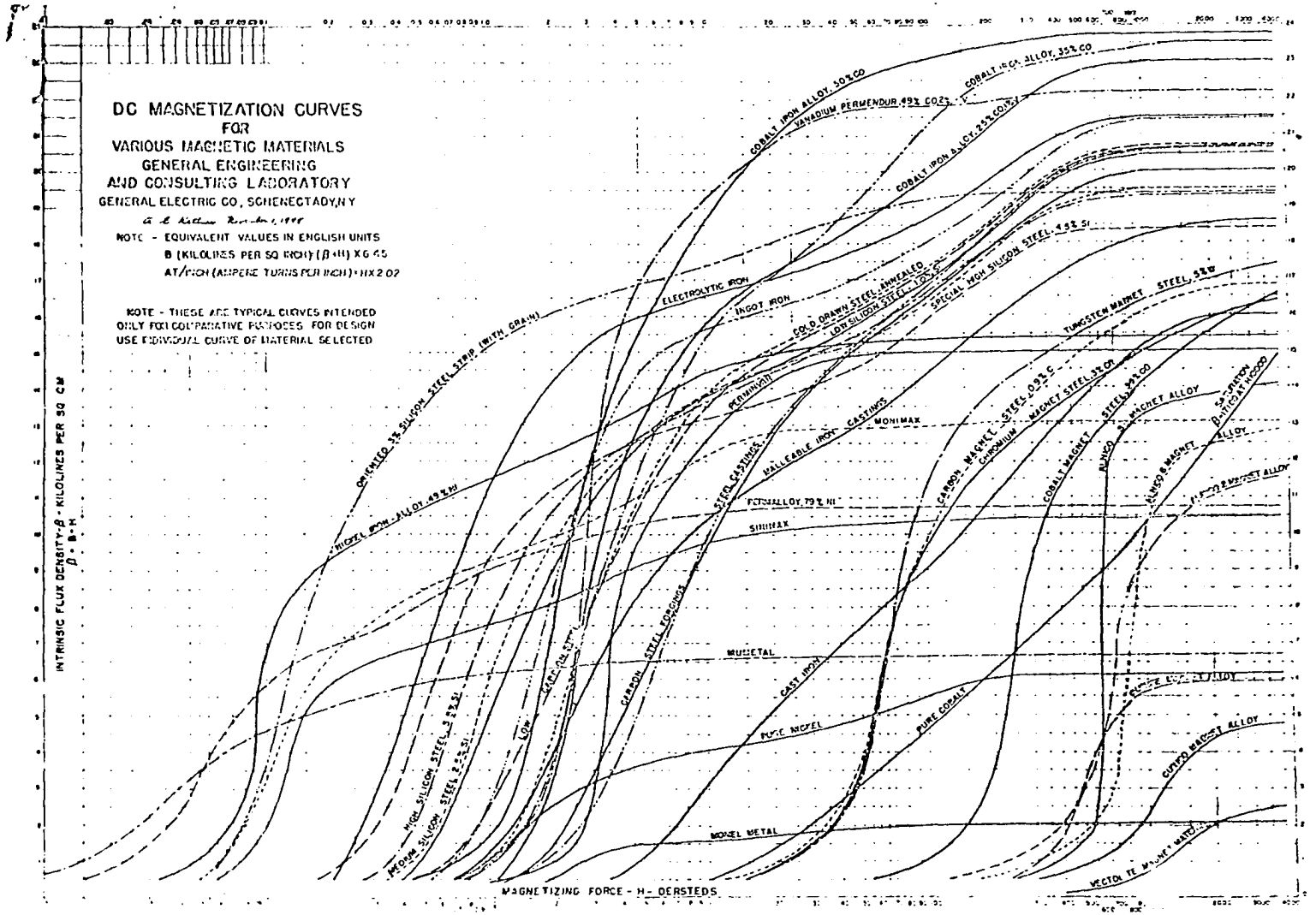

Fig. 14. Magnetization curves.

gap width (40b, p. 26). The air gap width is 9/16 inches.

2. The reluctance of both magnet core pieces is calculated as a single value.
3. The reluctance of the magnet yoke is included.
4. The reluctance of the magnet pole pieces is calculated as a single value.

First the calculations were made for the original magnet. Then the theoretical results of several proposed changes to this magnet were calculated in order to ascertain the feasibility of such changes. The plots in Fig. 15 show the results which are described below.

Curve A is a plot of the results for the calculations of magnet field strength vs magnet coil current for the original magnet which consisted of the iron pole pieces shown in Fig. 16a, and the magnet core pieces and yoke fabricated from mild steel, SAE 1020.

Curve B is a plot of these results for similar components but core pieces constructed from Armco Ingot Iron.

Curve C is a plot which indicates the calculated improvements which would result if the cross sectional area of the Armco core pieces were increased from 10.03 inches^2 to 12.29 inches^2.

Curve D illustrates the theoretical improvements cited above as well as the improvement expected by fabricating the

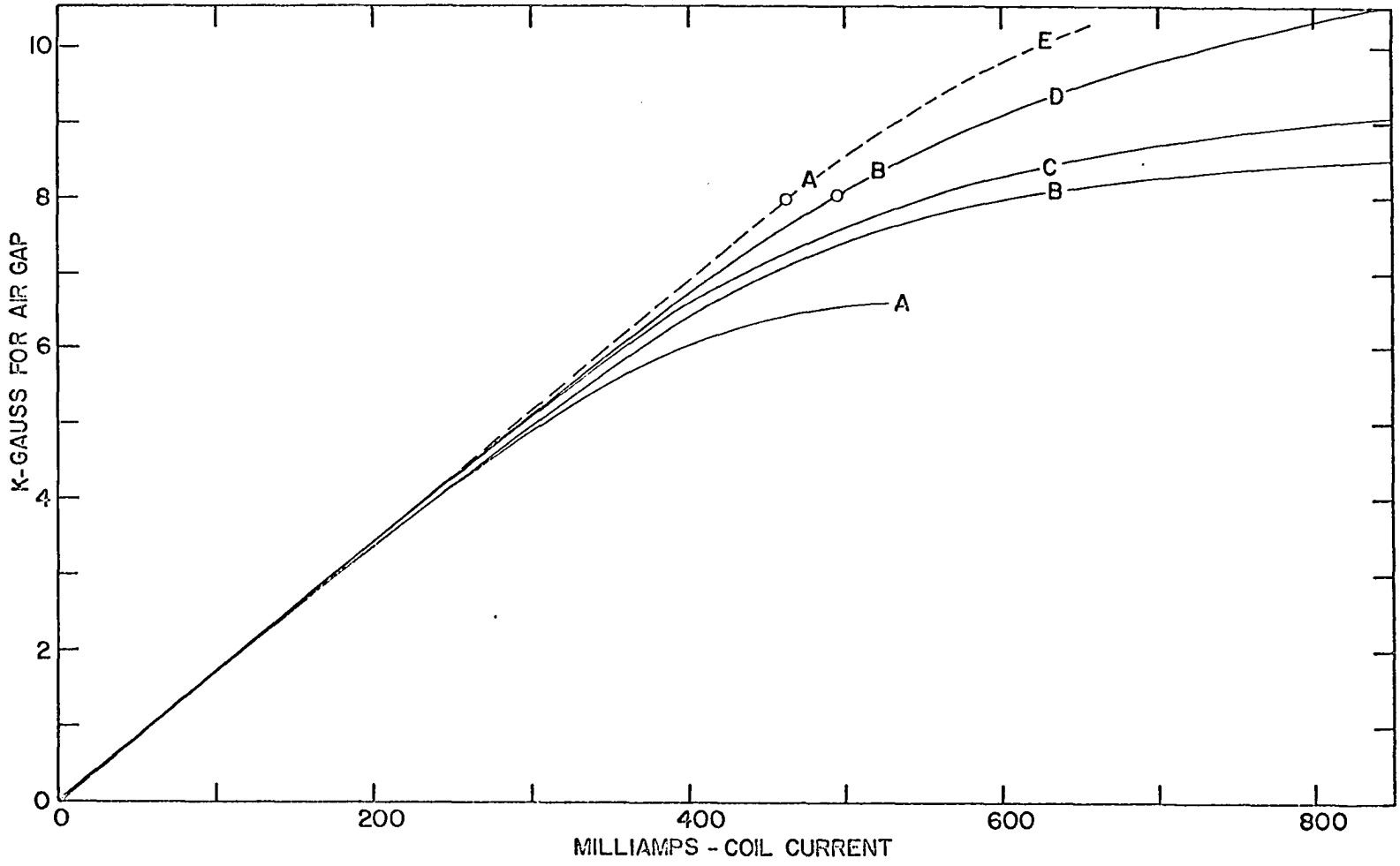

Fig. 15. Calculated magnetization curves.

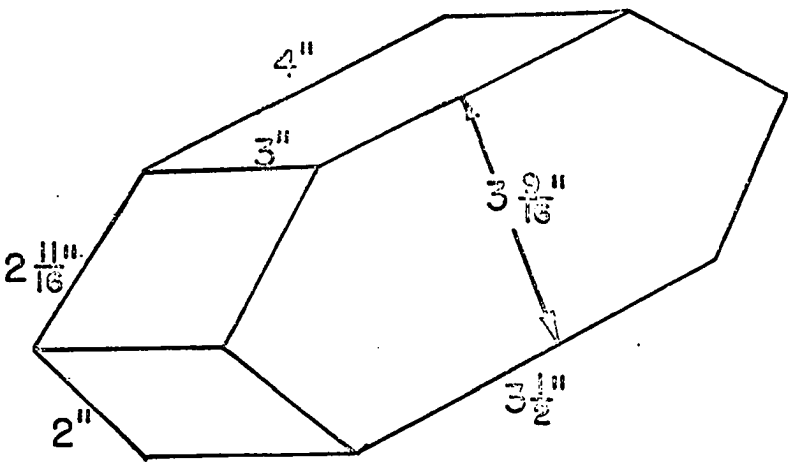

a.

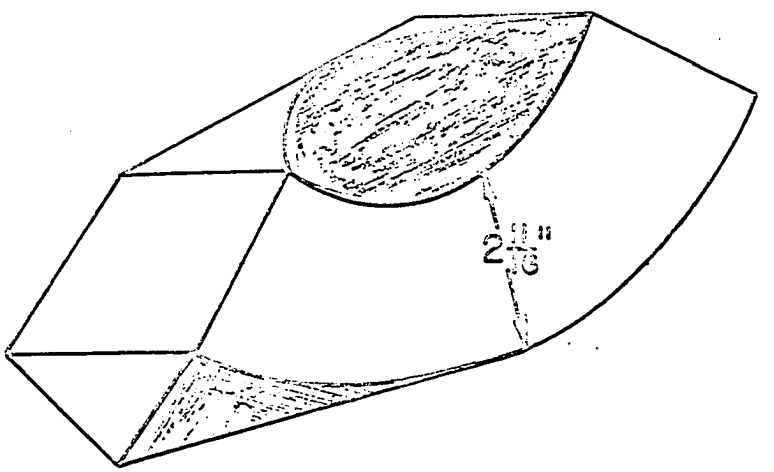

b.

Fig. 16. Magnet pole pieces.

yoke from Armco Ingot Iron and increasing its cross sectional area from 12 inches^2 to 20 inches^2

Curve E indicates all of the above changes plus the calculated improvement which would result from decreasing the effective area of the air gap by cutting the magnet pole pieces as shown in Fig. 16b. To prevent significantly decreasing the average cross sectional area of the pole pieces themselves, the cuts are tapered so that the area of only one side of the pole piece is decreased. The effective area of the air gap is thus decreased from 24.5 inches^2 to 19.8 inches^2. The cuts also result in pole faces which are more symmetrical to the ion beam path than are the original faces.

The results of the theoretical calculations strongly suggested that the proposed modifications of the original magnet would result in an improvement in the maximum obtainable field from 6300 Gauss maximum to over 8000 Gauss.

The modifications were made as described, and the magnet performance was then tested by two methods.

Method 1 involved the application of the general equation of motion in single focussing magnetic mass spectrometer to an ion of known mass focussed at a known ion accelerating voltage with the magnet coil current near its maximum. The parent ion of silicon tetrabromide, $SiBr_4^+$, mass 358, was focussed with an ion accelerating voltage of 2000 volts. Svec (37) has evaluated the various constants and simplified

the general equation of mass spectroscopy which relates these variables;

$$\frac{m}{e} = \frac{H^2R^2}{2Vc^2} = \frac{4.82 \times 10^{-5} H^2R^2}{V} \qquad 16$$

where m = atomic weight units

e = number of electronic charges

H = magnetic field strength in Gauss

R = radius of curvature of the ion beam in cm.

V = ion accelerating voltage in volts.

From this equation the maximum magnetic field strength for the present magnet is calculated to be 8150 Gauss.

Method 2 involved inserting a Hall Crystal (BH200 Transverse Field Hall Effect Device, Bell Inc., 1356 Norton Ave., Columbus 12, Ohio) into the magnet air gap and measuring its output voltage with a potentiometer or recorder. The output voltage is linearly dependent upon the magnetic field and this can be used as a measure of it. The Hall-Crystal circuits will be discussed below.

The Hall crystal measurements indicated that the maximum magnetic field is approximately 8000 Gauss which agrees well with the results in method 1.

In a comparison of the theoretical and actual magnetization curves, the output of the Hall Crystal was recorded while the magnet coil current was increased from 0 to 500 ma at a constant rate. The resulting curves shown in Fig. 17 are direct representations of the magnetization curves.

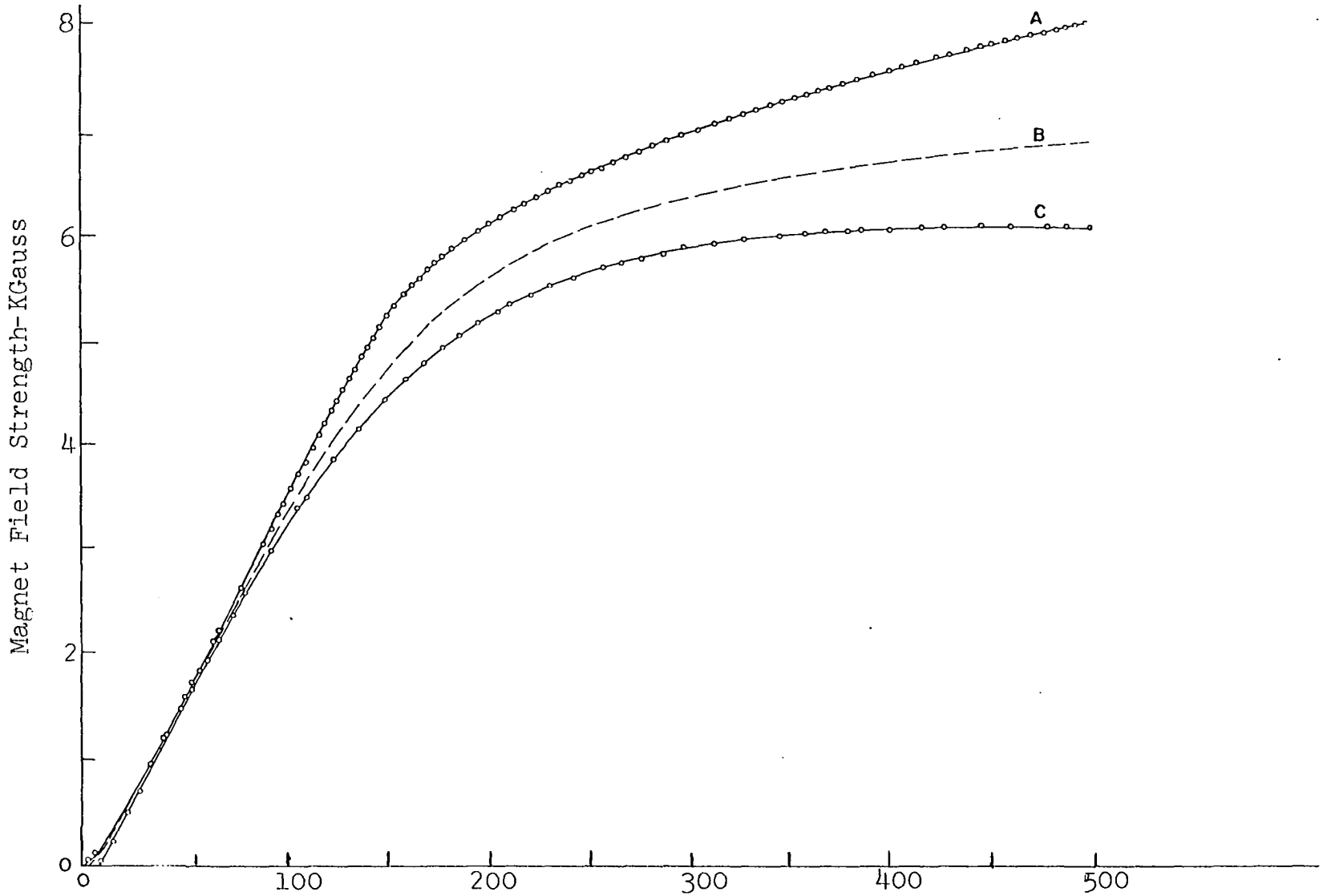

Fig. 17. Measured magnetization curves.

These curves compare well with the curves shown in Fig. 15 which were calculated theoretically.

Curve A of Fig. 17 and curve E of Fig. 15 correspond to the experimental and the calculated magnetization curves for the present magnet.

Curve B of Fig. 17 and curve D of Fig. 15 represent these curves for the present magnet before the pole pieces were modified.

Curve B of Fig. 17 and Curve A of Fig. 15 represent the curves for the original magnet.

5. Collector assembly

The Faraday Cup, secondary electron suppressor plate, collector mounting plate, and the variable slit are the same ones described by Saalfeld, however three modifications were made. A plate with a 0.040 inch slit was mounted in front of the 0.0 to 0.025 inch variable slit to serve as a means for measuring kinetic energy of fragment ions. The potential of this electrode is variable from -10 to +200 volts with respect to shield potential but it is grounded during normal operations. All the collector plates are assembled on two studs which are attached to the collector mounting plate. The whole collector assembly is mounted inside a cylindrical, Chromel-A shield which is used to prevent excess interference from stray potential fields. The electrical leads are introduced by high voltage terminals which are vacuum sealed with lead solder to three separate ports in the collector envelope.

This collector envelope is structurally similar to the ion source envelope.

6. Vacuum system

A metal mercury diffusion pump (MAG-40, Consolidated Vacuum Corporation, Rochester, New York), backed by a mechanical fore pump, evacuates the ion source, and the collector and analyzer tube regions. The diffusion pump is connected to the ion source envelope in series with a glass liquid nitrogen cold trap which was designed according to suggestions given in Dushman (41). A glass cold-cathode ion gauge (Miller Laboratories, Latham, New York) is mounted directly above the nitrogen cold trap to monitor the pressure within the ion source envelope.

An 11-liter per second ion pump (VacIon high vacuum pump, Model 96-0011, Varian Associates, Palo Alto, California) is connected to the collector envelope by means of a 2 inch diameter copper tube. A baffle constructed of 4 split, Chromel-A plates is mounted inside this copper tube in order to prevent diffusion of ions from the VacIon pump into the collector region.

Most of the ion source envelope, collector envelope, and analyzer tube is wound with a 1 inch flexible heating tape, 768 watts, (BIH-41, Briscoe Manufacturing Company, Columbus, Ohio) which permits bakeout. With the bakeout at approximately 80°C, a background pressure of 1×10^{-8} Torr is indicated at the cold cathode ion gauge and the VacIon pump.

C. Electronic Components

1. High voltage divider circuit

Refer to Fig. 18 for the complete circuit diagram. The high voltage divider circuit is composed of four strings of resistors connected in parallel between the input and ground leads of the high voltage power supply. The divider circuit is designed to supply and control 12 potentials within the ion source, the potential of the kinetic energy plate at the collector, the electron accelerating voltage, and the high voltage for an isolation transformer in the emission regulator.

Listed in Table 1 are the ion source plates that are controlled, their normal voltage, and their range of control for a nominal high voltage of 2200 volts.

The potentials of these plates are dependent upon the high voltage input. If the high voltage is changed, some of the relative potential differences will also change. The control of the potentials of plates D, E, F, and G is accomplished by using several groups of mercury dry cells in order to maintain potential differences which are absolute rather than relative. The potentials which are critical to the stability of operation are all controlled by 10 turn helical potentiometers (Helipot, Model AR Series, Beckman Instruments, Incorporated, Fullerton, California) to provide more precise voltage adjustments.

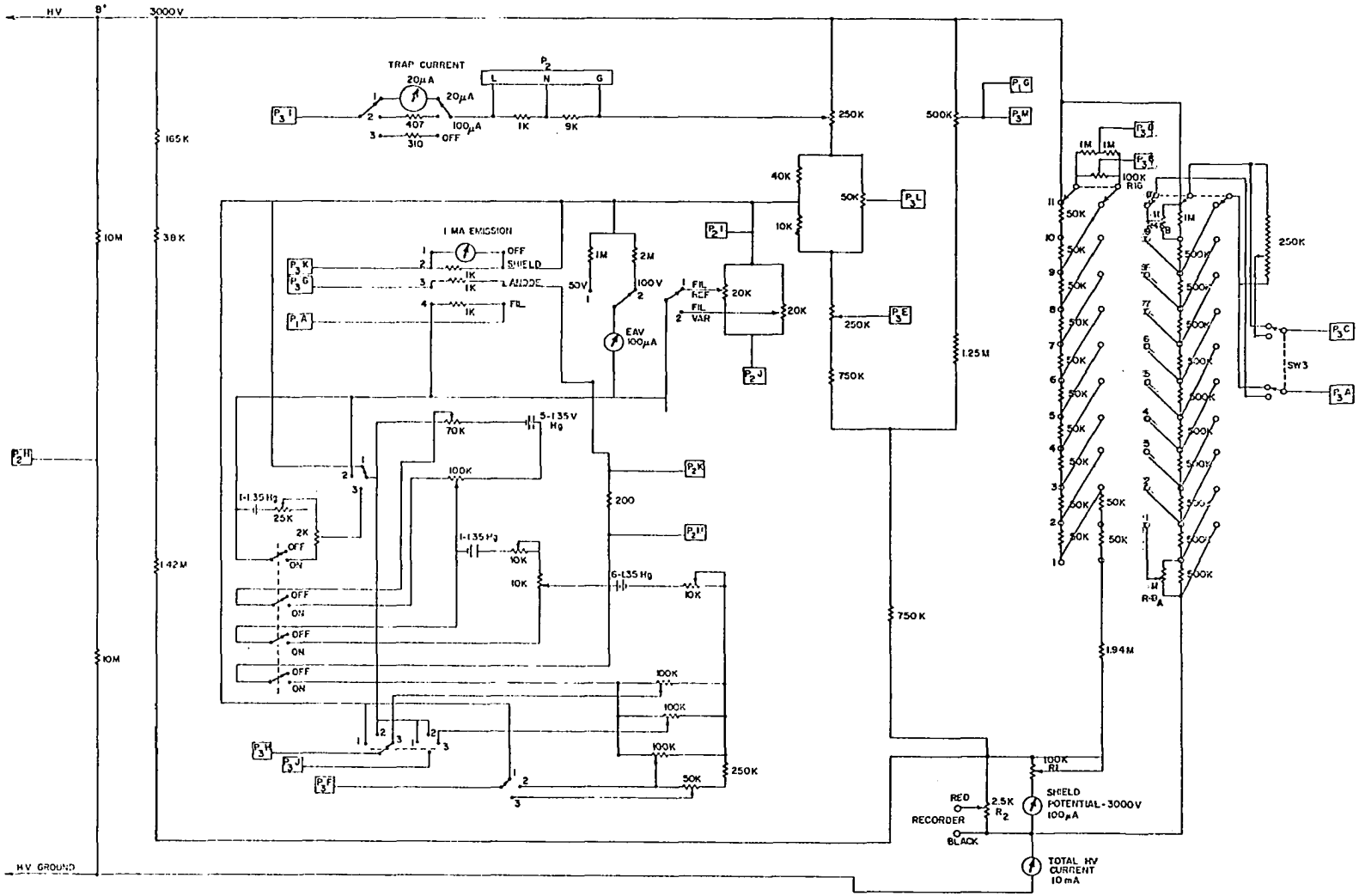

Fig. 18. High voltage divider circuit.

Table 1. Ion Source Voltages

Plates	Control and Range	Voltage relative to shield potential	Normal Potential
2-Focus	variable with high voltage stepwise plus fine focus	0 to -400 V	+2000 +1700 V
2-Deflect	stepwise plus fine focus plus beam deflect switch	0 to -2000	+300
Drawing Out	Continuous 10 turn helipot		+1980
Repellor	Continuous 10 turn helipot	-5 to +20	+2003
Trap	Continuous 1 turn helipot	-5 to +200	+2030
Filament	Continuous either of two - 10 turn helipots	-5 to +200	varies
K.E.	Continuous 10 turn helipot	150 to +200 voltage relative to filament	0
Anode, G	Continuous 10 turn helipot	0 to +8	varies
D, E, and F	Continuous 10 turn helipot for each	-7 to +16	varies
K.E. plate	Continuous 10 turn helipot	0 to -2200 V	varies

Additional control features include a switch to permit the application of a 0 to 1 volt increment to plate E, and a similar switch for adding a 0 to 1 volt increment to plate G. The filament voltage can be set with either of two 10K helical potentiometers in order to compare various measurements during an ionization efficiency study. The ion current intensity reading which results from a reference electron accelerating voltage, can be compared to ion current intensity readings at various other electron accelerating voltages which are determined by the second helical potentiometer. The design of the divider circuit incorporates minimum resistance between the shield, repeller, drawing out electrode and trap in order to reduce the instabilities of their potential differences.

Five appropriately calibrated meters are used to monitor the source conditions that are controlled by the high voltage divider circuit.

Total high voltage current for the divider circuit is indicated directly by a 0 - 10 milliampere meter.

Shield potential is indicated by a 0 - 100 microampere meter which represents 3000 volts full scale.

Electron accelerating voltage is indicated by a 0 - 100 microampere meter which when used in either of two positions represents 50 or 100 volts full scale.

Total emission from the filament is read directly from a 0 - 1 milliampere meter used in any of three positions.

The emission of electrons from the filament to either the anode, or the shield, can be monitored, or the total emission of electrons from the filament can be monitored.

Trap current is monitored by a 0 - 20 microampere meter used in either of two positions to read 0 - 20 or 0 - 100 microamperes full scale.

2. High voltage power supply

Refer to Figs. 19a and 19b for the circuit diagram.

The high voltage to the divider circuit is supplied by a commercial high voltage power supply (Model 413D, John Fluke Manufacturing Company, Incorporated, Seattle 33, Washington) which has a 0 to ±3111 volt dc output with a regulation of ±0.001 percent +2 millivolts for currents of 0 to 20 milliamperes. It is variable in five 500-volt steps, five 100-volts steps, ten 10-volt steps, one 0 to 11 volt vernier and a 0 to 200 mv vernier. The calibration accuracy is 0.25 percent of the dial readings.

3. Emission regulator

The circuit diagram is shown by Fig. 20.

The emission regulator is a solid state circuit designed and built at Iowa State University. The unit provides better than one percent regulation in any one of four modes for trap currents as low as one microampere. This is accomplished by the regulator, which automatically adjusts the filament current in order to maintain a preset constant voltage across sensor resistors which are in series with

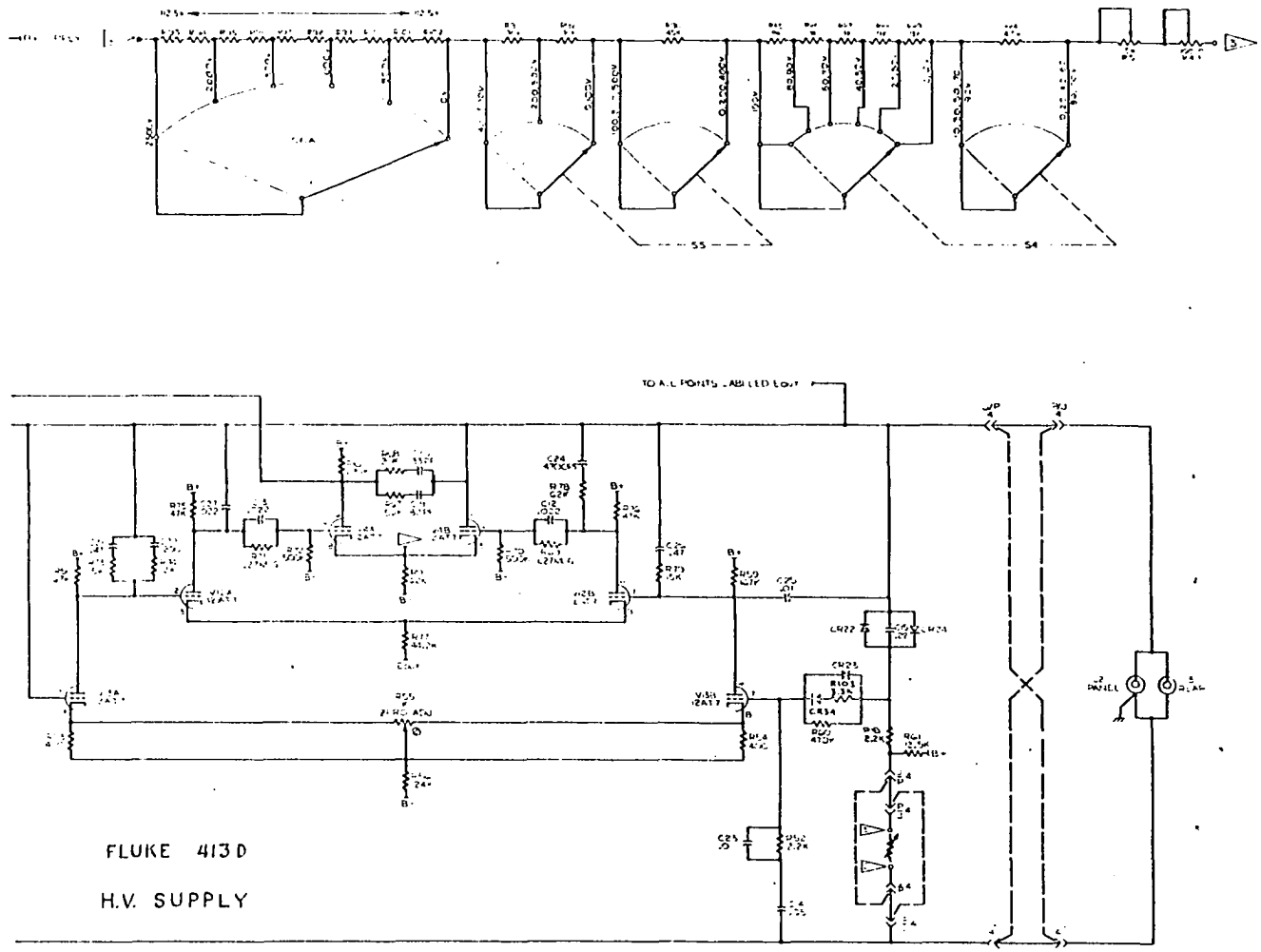

Fig. 19a. High voltage power supply.

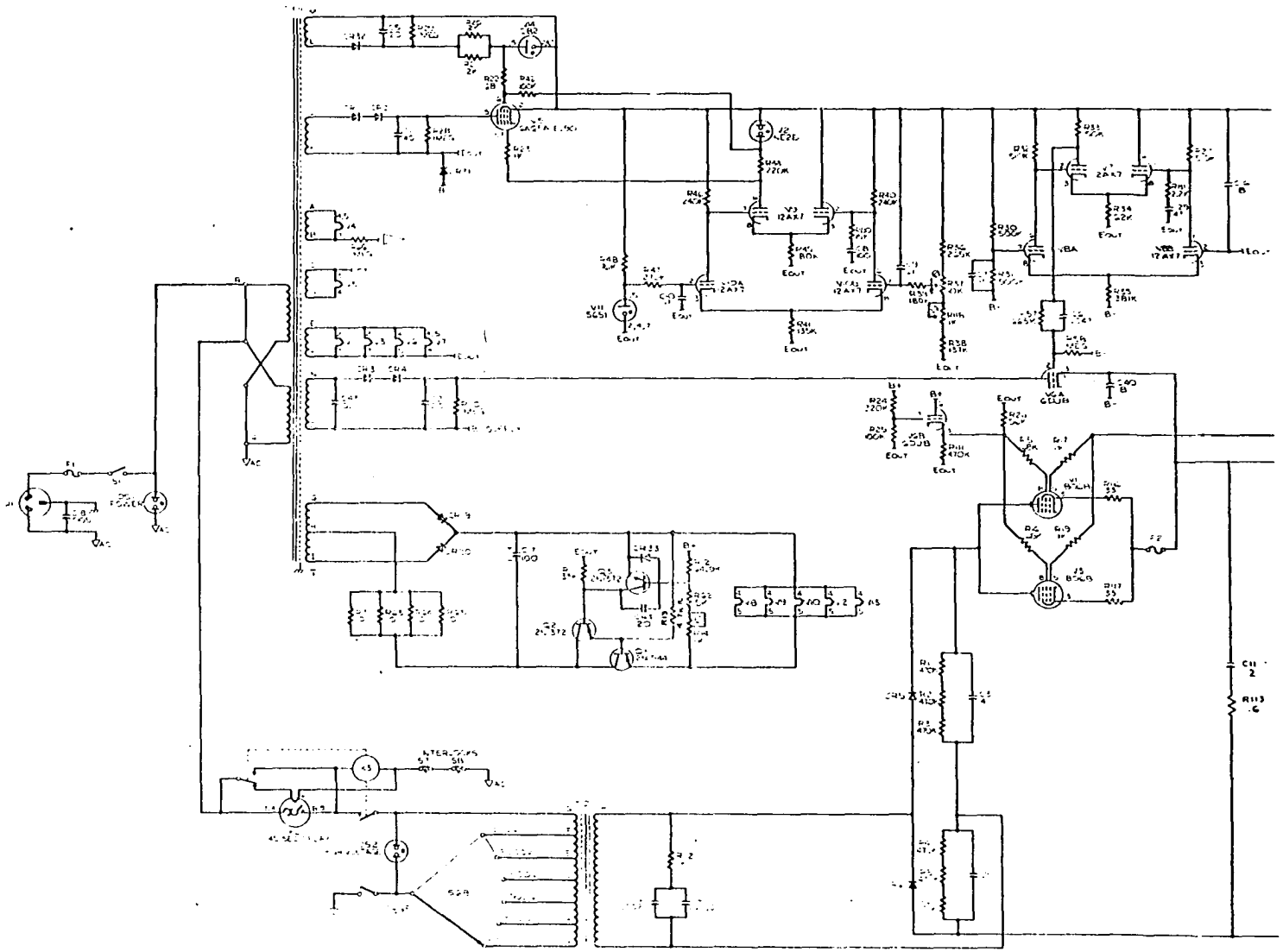

Fig. 19b. High voltage power supply.

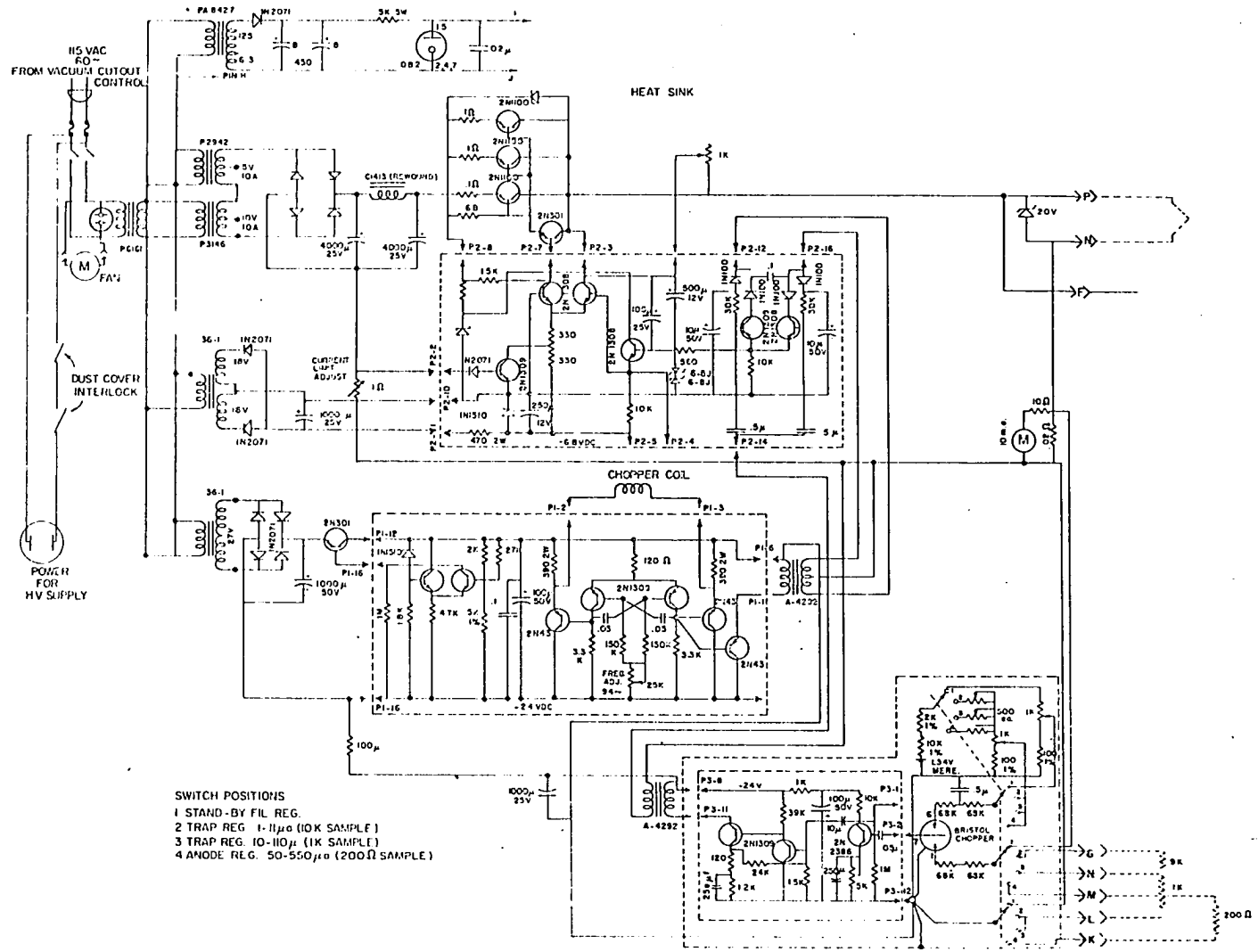

Fig. 20. Emission regulator.

either the anode or trap. The emission of electrons from the filament to these respective electrodes is directly dependent upon the voltage drop across these resistors, which are located in the high voltage divider circuit. Emission current to the anode can be regulated from 50 to 550 microamperes across a 50 resistor. The emission current to the trap is regulated either from one to 11 microamperes across a 10KΩ resistor or from 10 to 110 microamperes across a 1KΩ resistor. Both the trap and anode emission currents are adjusted by a 10-turn helical potentiometer. The current through the filament can be regulated up to 8 amperes across a 0.02Ω internal resistance in series with the filament.

Several other functions are performed by the emission regulator which is supplied by two isolation transformers so that it can float at shield potential. It provides a constant 107 volt, d.c. potential from an OB2 voltage regulator tube to two helical potentiometers in the high voltage divider. These are used to control the electron accelerating voltage. The input power to the high voltage power supply is supplied by the emission regulator also. A safety microswitch turns off the high voltage if there is a malfunction in the emission regulator or if its protective dust cover is removed.

4. Square wave generator

The circuit diagram for the square wave generator (Model 211A, Square Wave Generator, Hewlett-Packard Company, Palo Alto, California) is shown in Figs. 21a and 21b.

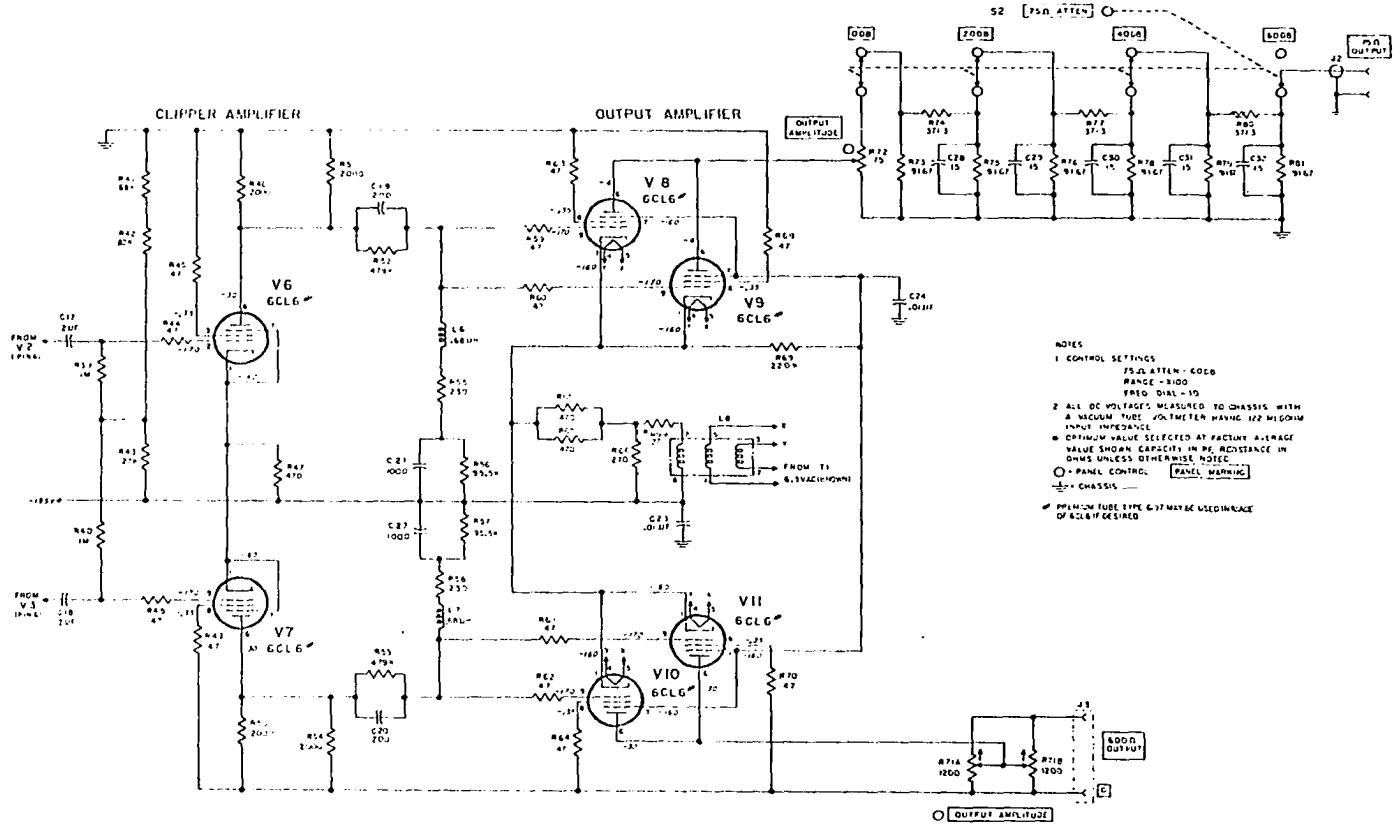

Fig. 21a. Square wave generator.

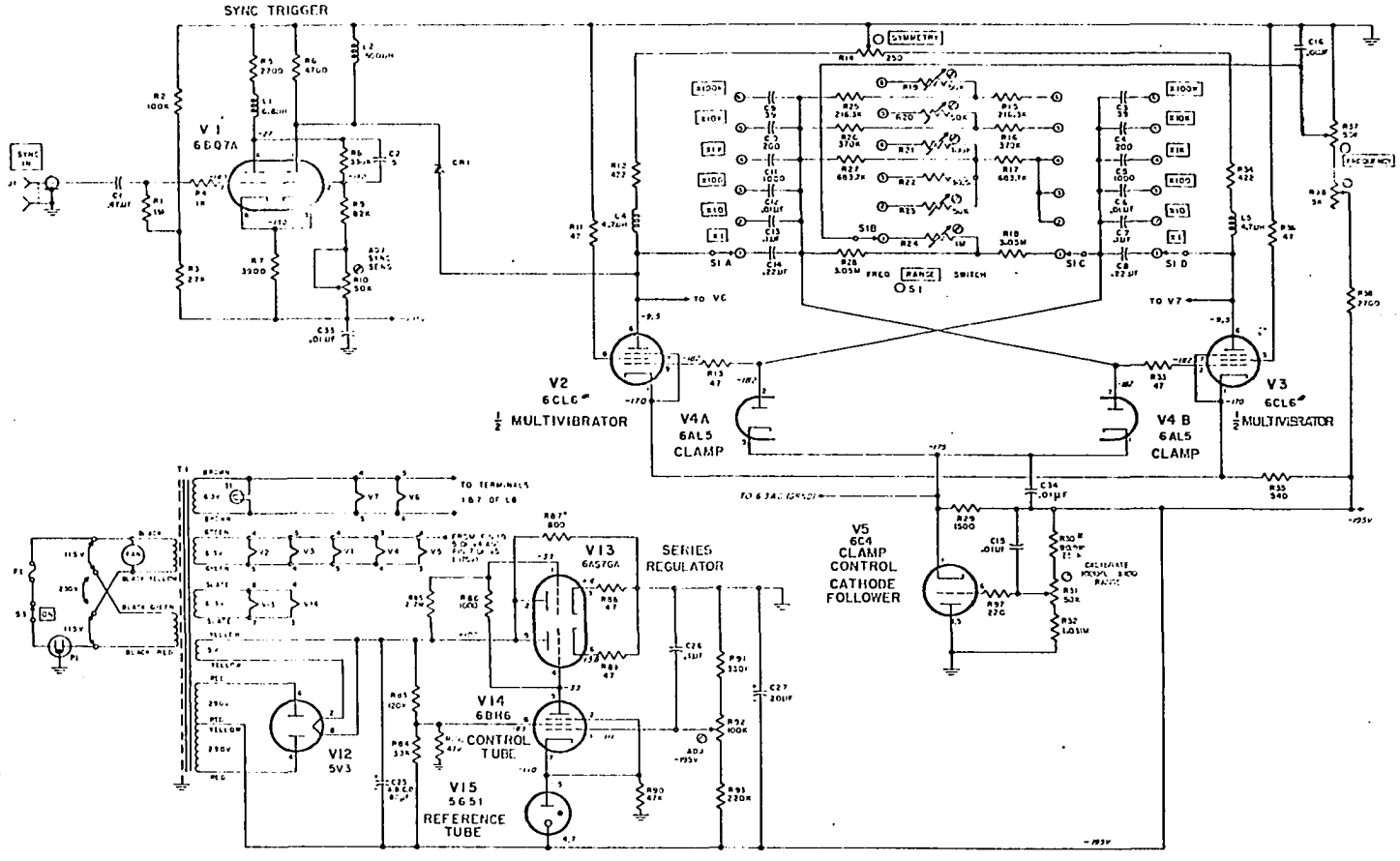

Fig. 21b. Square wave generator.

This generator can supply a negative 3.5 volt maximum square wave signal across a 75Ω load which is 180° out of phase with a negative 27 volt maximum square wave signal across a 600Ω load. The amplitude of each output is continuously and independently variable from one cps to one Mcps with controllable symmetry. The generator is mounted in the main instrument panel and the output is transmitted to the source region through two coaxial cables (no. 21-026).

5. Pulse filter circuit

Fig. 22 is a circuit diagram illustrating the ion source and the filter system which is used to prevent the square wave signals from influencing the voltages of any source electrodes other than the repeller and anode. The outputs of the square wave generator pass through the primaries of two 2:1 pulse transformers T_1 and T_2, (P/N EM-785, Raytheon Company, Waltham 54, Massachusetts) before they reach the ion source. T_1 is the anode pulse transformer. One of the leads from its secondary winding connects directly to the filament and the other lead is connected to the anode via a 0.01 microfarad capacitor. The repeller pulse is supplied by pulse transformer T_2. One of the leads from its secondary connects directly to the repeller and the other lead is connected to the shield via a 0.01 microfarad capacitor.

This filter circuit not only prevents interference of the pulses with other source and circuit components, but it

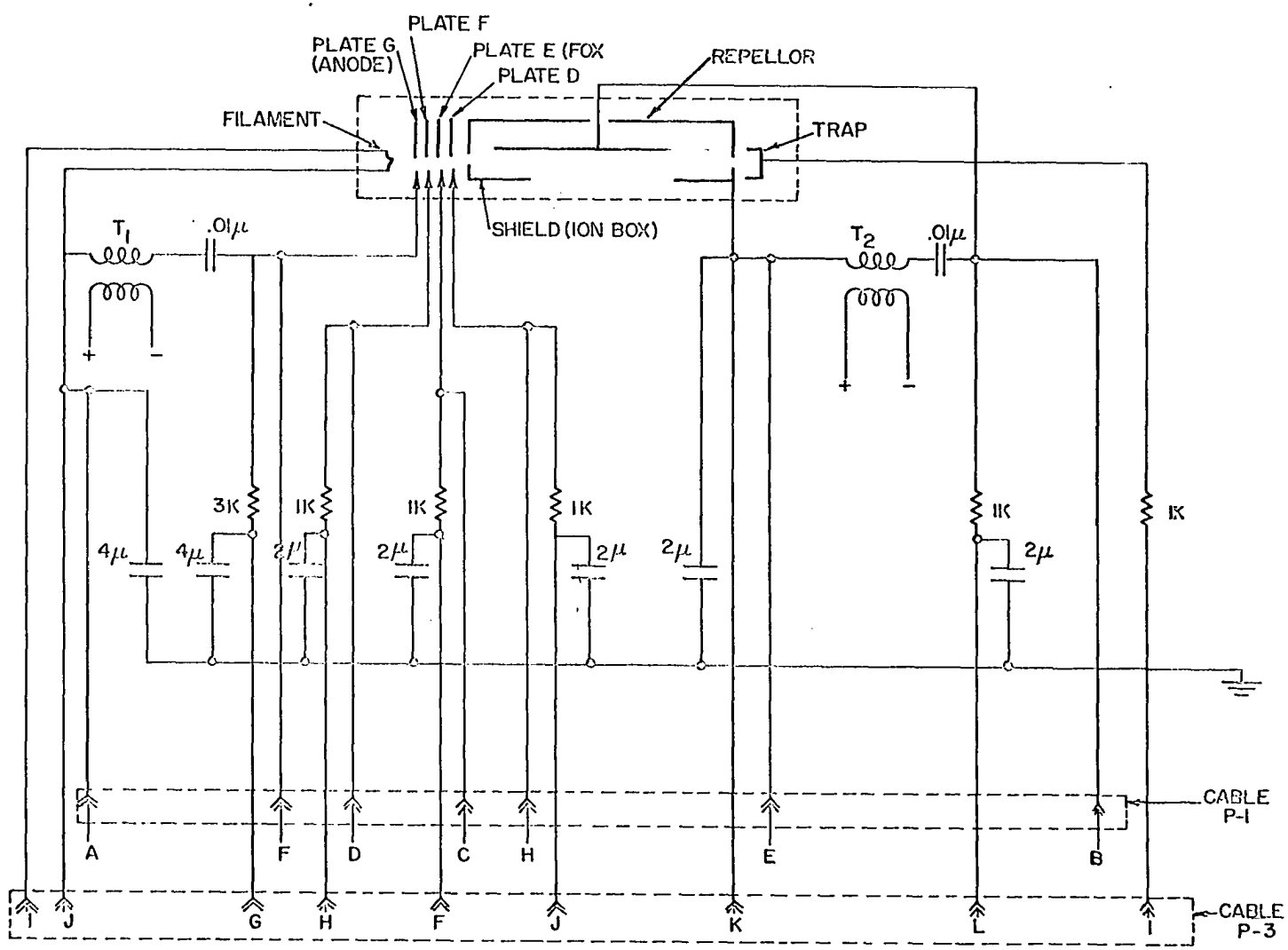

Fig. 22. Pulse filter circuit.

also increases the stability of the ion source. All of the potentials to the ion source electrodes are supplied by 18 inch coaxial cables from the filter system which is mounted on the mass analyzer frame as close to the ion source as possible.

6. Differential voltmeter

A differential voltmeter (Model 881AB Differential Voltmeter, John Fluke Manufacturing Company, Incorporated, Seattle 33, Washington) is used to measure the potential differences between the electrodes within the ion source. It is a commercial d.c. voltmeter which may be operated from either the 110V AC line or from internal batteries. A $\pm$.01 percent accuracy is guaranteed for the input ranges 1, 10, 100 or 1000 V. Each input range is covered by four null positions in steps of increasing sensitivity to a maximum sensitivity of 0.01 percent of the input voltage. An input voltage is successively adjusted to zero in each of the four null positions and its value is read directly from five decade dials. The entire differential voltmeter is of high potential, thus it is encased in wood and plastic and operated only from the internal batteries.

Coaxial cable, P1, connects the source electrodes directly to an input switching arrangement near the differential voltmeter. This switching arrangement consists of two 12-position switches, one with its moving contact connected to the positive input terminal of the voltmeter, the other

with its moving contact connected to the negative input terminal of the voltmeter. The eleven inputs are common to both switches, hence the voltage difference of any two inputs can be measured by appropriate switching. The various input potentials which can be measured by the voltmeter are listed below.

Switch Position	Input
1	off
2	off
3	shield
4	Plate E
5	Plate D
6	Plate G (anode)
7	Filament
8	Repeller
9	K.E. plate, ground, or trap
10	Plate F
11	Hall Crystal output

7. Amplifers and recorder

For circuit diagrams of the components discussed below, refer to Saalfeld (6a) or to the original operating manuals.

The ion collector lead is attached to a $10^{12}\Omega$ input resistor of a vibrating reed electrometer (Model 36, Applied Physics Corporation, Pasadena 1, California) which affords gain of either 1×10^{8} or 1×10^{7}. The vibrating reed output can be further amplified by an impedance matching, direct

current amplifier (Model 111BF, KinTel, a division of Cohu Electronics Incorporated, San Diego, California) which has a gain continuously variable from 10 to 2000. The final amplified ion beam current is recorded on a 100 millivolt, continuous-drive recording potentiometer (Model 6701, Daystrom, Incorporated, Weston Instruments Division, Chicago, Illinois).

8. Attenuation

The final input potential to the recorder may be controlled in any one of five ways by means of an attenuation selector switch. Refer to Fig. 23 for a circuit diagram of the attenuating circuit. Listed below are the control positions:

Position 1, Bucking Scale A Bucking scale, connects the vibrating reed output directly to the recording potentiometer. In this position a 100 millivolt vibrating reed output will read full scale on the recorder, however, up to 10 volt inputs can be bucked out in 100 millivolt increments. The bucking is accomplished by means of a Kelvin-Varley voltage divider which supplies up to 10 volts in 100 millivolt increments with a polarity opposite to the input. This permits observation of the ion beam current within a 100 millivolt range of its maximum without decreasing the sensitivity of the recording system.

Position 2, Logarithmic Scale A logarithmic attenuator permits the scan of a mass spectra so that peaks due to

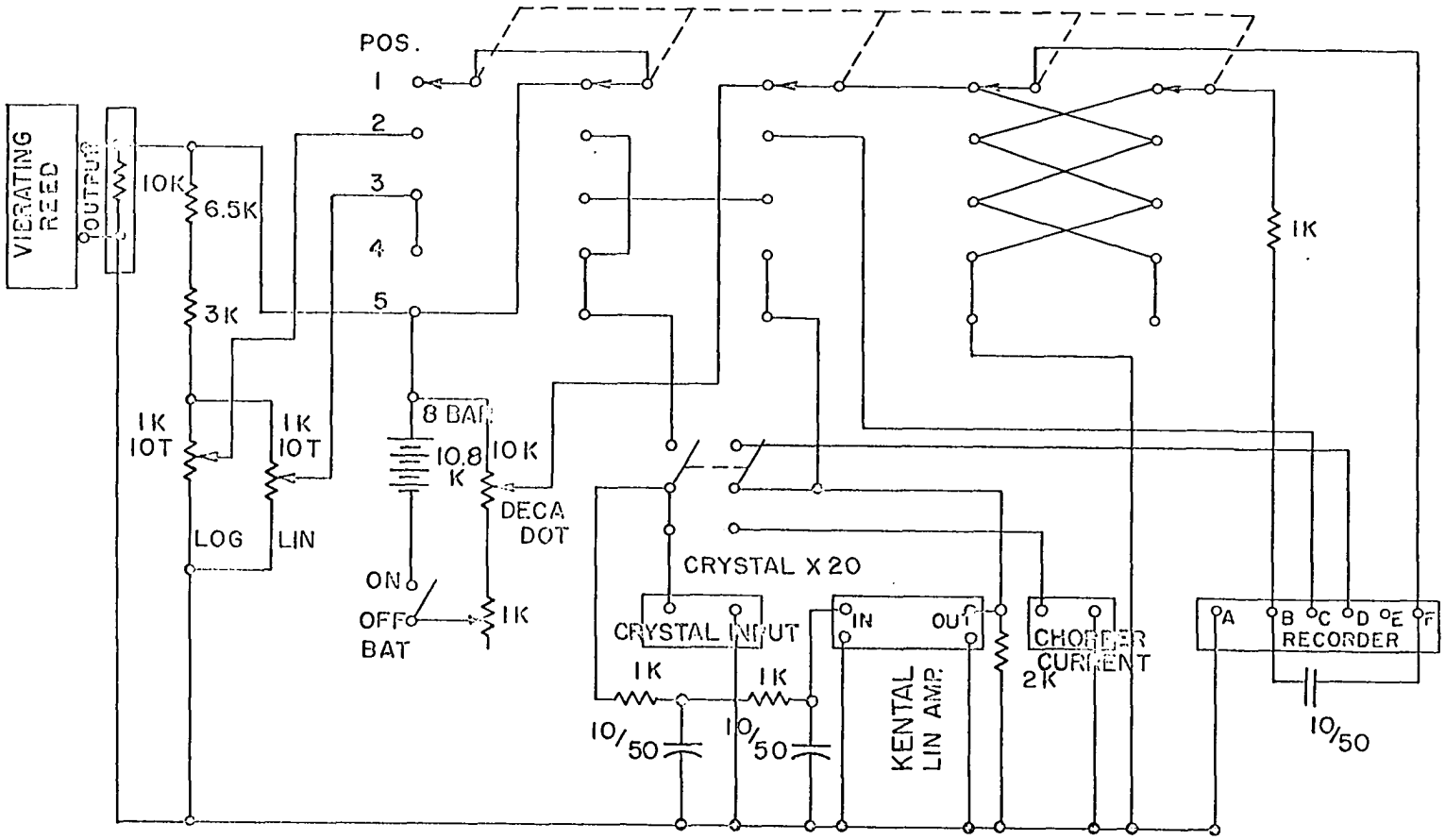

Fig. 23. Attenuating Circuit.

the less intense ion currents will not be excessively diminished, whereas the more intense ion currents can still be recorded. For this mode, the output from the vibrating reed is amplified by the KinTel amplifier before it is recorded. The KinTel gain can be changed in order to vary the sensitivity of the readout on the recorder but normally it is set at 100. A 10 turn helical potentiometer affords further continuous control of the logarithmic sensitivity to the extent that a 5V vibrating reed output can be made to read anywhere from 0 to full scale on the recorder.

Position 3, Linear Scale This scale permits a linear scan of a mass spectra so that all ion current intensities can be read directly from the recorder chart. Another 10 turn helical potentiometer allows variation of the sensitivity within the same limits for a 5V peak as for the Logarithmic scale. The KinTel amplifier is by-passed in this mode.

Position 4, Linear Amplified Scale A linear amplified scale, is similar to position 3 except that the vibrating reed output is amplified by the KinTel amplifier before it is recorded. For a normal gain of 100, a 0.5 millivolt vibrating reed output can be adjusted to read from 0 to full scale on the recorder chart.

Position 5, Bucking Amplified Scale On this scale the vibrating reed output is amplified by the KinTel amplifier and the resulting voltage is measured directly by the

recorder. Maximum sensitivity is obtained in this position. This is accomplished by amplifying the vibrating reed output with the maximum (2000) gain of the KinTel amplifier. This causes full scale deflection on the recording potentiometer for a vibrating reed signal of only 0.05 millivolt. However, noise levels and zero drift normally suppress any improvements of sensitivity for gains in excess of 500. Furthermore, in this mode the final amplified output cannot be read if it is greater than the 100 millivolt full scale recorder limit.

The sensitivities of all of the above positions can be decreased by a factor 10 by using the lower gain of the vibrating reed. This permits the reading of intense ion beam currents which result in amplifier outputs up to 100 volts which correspond to ion currents of 10^{-10} amps.

9. Hall crystal mass indicator and magnetometer

A few mass indicators have been reported for use with mass spectrometers for some time, however their operation is usually based on rotating coil magnetometers for which the accuracy is limited (42, 43). The magnetic response characteristics of semiconducting crystals suggested their potential use as mass indicators for mass spectrometers. Extensive studies were made to determine their capabilities for such a purpose, and a mass indicator circuit was designed and tested using commercially available semi-conductor crystals. Several other authors have employed these types of crystals

as sensing devices for magnetometers, (44, 45, 46, 47, 48, 49) and the theory of the Hall effect is discussed sufficently by them. However, they were not used for mass indicators.

The specific crystals used in these studies were indium-arsenide crystals 0.130 inch by 0.500 inch and 0.019 inch thick. For an input current, I, the output voltage, E_H, of the crystal is related to the magnetic field strength, H, normal to its surface by the approximate relationship,

$$E_H - KIH. \qquad 17$$

The constant in the above equation was evaluated using a CEC 21-201 Isotope Ratio Mass Spectrometer and the Hall crystal circuit shown in Fig. 24.

The Hall crystal input is supplied by a low voltage power supply (Model 4005R Universal Constant Voltage Current Power Supply, Power Designs Incorporated, Wesbury, New York) which produces 0.05 percent voltage regulation for 0 to 40 volts output or 0.02 percent current regulation for 25 to 500 milliamperes output. (See Fig. 25 for the circuit diagram). For calibration purposes, the Hall crystal output was measured using a manual potentiometer (Tpe K-3, Model 7553, Leeds and Northrup Company, Philadelphia 44, Pennsylvania) which had a low range sensitivity of 0.0161 volts $\pm$0.015 percent full scale. The potentiometer was balanced using a galvanometer (Rubicon Model 3414, Rubicon Division, Minneapolis Honeywell Corp., Philadelphia, Pennsylvania)

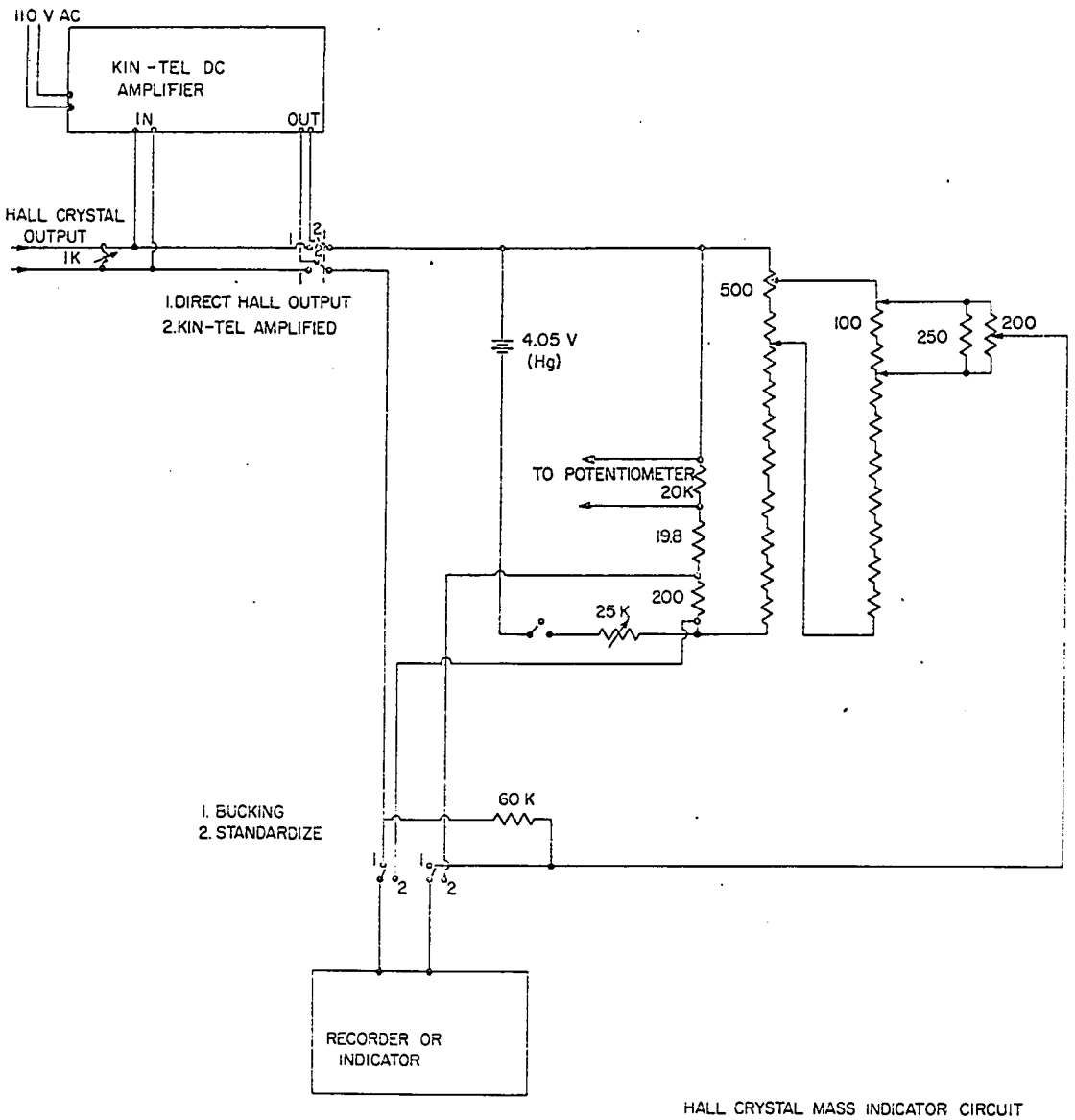

Fig. 24. Hall crystal mass indicator circuit.

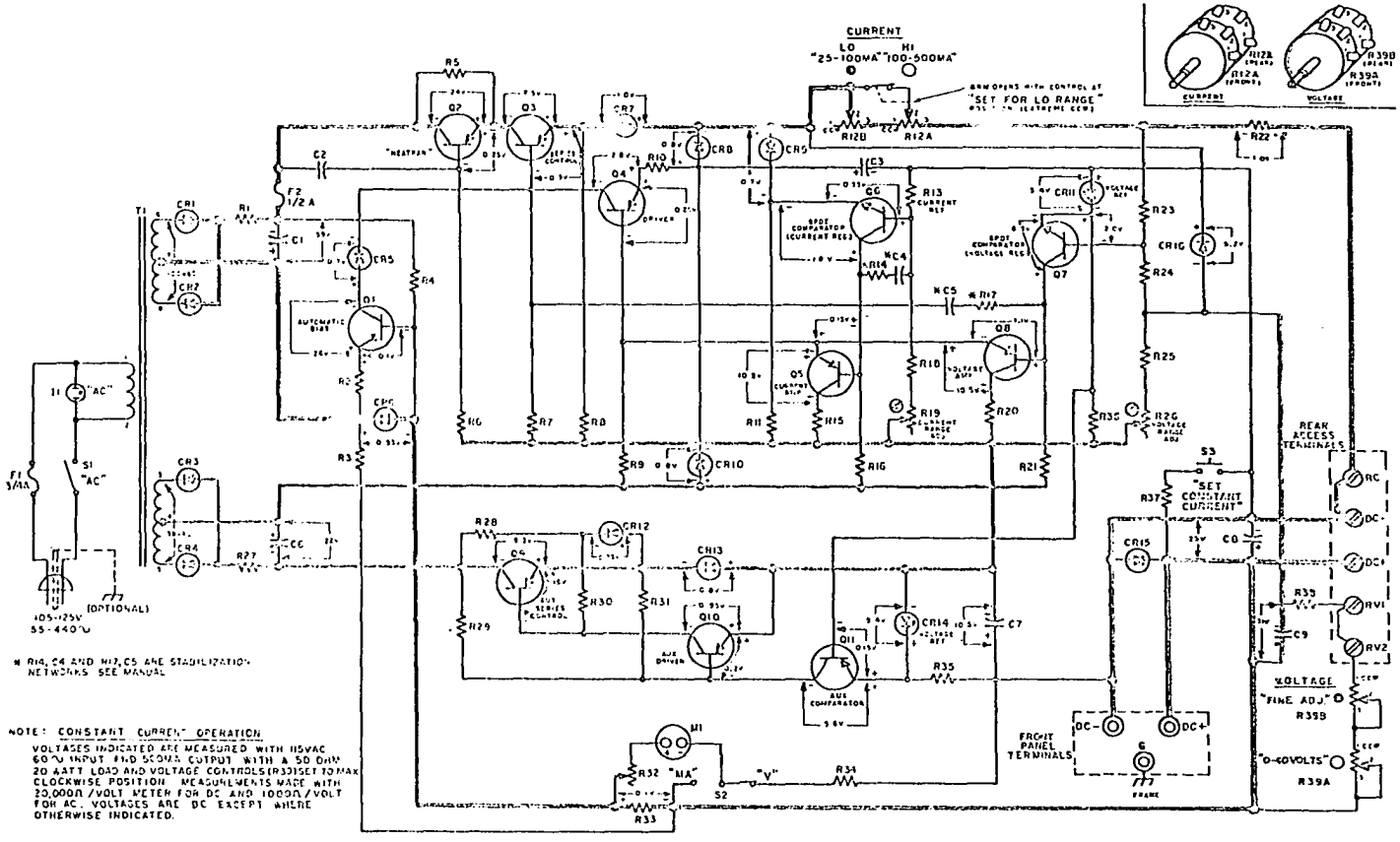

Fig. 25. Constant voltage/current supply for Hall crystal.

with a sensitivity of 0.0014 μ a/mm and an internal resistance of 518Ω . An attenuation circuit allows the operator to measure the Hall crystal output directly or to amplify it and then record it on a 20 millivolt full scale recording potentiometer. All but 20 millivolts of the Hall crystal output can be cancelled by the attenuation circuit. Twenty millivolt increments are used for measuring the Hall crystal output directly, and 2V increments are used when the amplified output is measured.

Each ion beam from the mass spectrum of butane was focussed magnetically and the focussing magnetic field was then calculated using Eq. 16 and the other known mass spectrometer conditions. At each ion peak the Hall crystal output was measured and the value of K in Eq. 17 was determined. It was found that the value of K was not constant but varied somewhat depending upon the values of the magnetic field, H, the Hall input current, I, and the load resistor, R_L. For I = 200 a, and R_L = 1KΩ, K was calculated to be $7.65 \times 10^{-5} \pm 0.12$ mv/ma-gauss with a uniform 3 percent increase over a magnetic field range of 1120 to 2370 gauss. This variation initiated a more vigorous analysis to determine optimum sensitivity of the crystal, and to find a more accurate relationship between E_H and H. The results are summarized below.

A. The output, E_H, was found to follow Eq. 18 or 19 more accurately for <u>all</u> conditions than it did Eq. 17.

$$E_H = (kH-b)I \qquad 18$$

and $E_H = H(kI + a) - cI + d$ 19

where a and b are constants depending upon the individual crystal properties and c, and d are constants depending upon the mass spectrometer characteristics.

B. It was calculated that a 194 Ω load resistor would yield maximum sensitivity, S, for an input of 200 milliamperes. The sensitivity, S, is defined as the percentage change of E_H for one mass unit

$$S = \frac{E_H \times 200}{M(E_1 + E_2)} . \qquad 20$$

C. A general equation was derived from the experimental data which relates the crystal output and M, the mass in focus.

$$[E_H - (aI + b)]^2 = \frac{deR^2H^2}{2Vc^2} - kM \qquad 21$$

where a, b, d, k are constants determined by the crystal, load resistor, and accelerating voltage. Using the CEC 21-201 mass spectrometer with 204 milliampere input to the Hall crystal and a 200 load resistor, the mass, M, in focus is calculated by the general equation,

$$M = \frac{(E_H - 1.42)^2}{(2.34 \times 10\text{-}2V - 1.44)} . \qquad 22$$

For verification of this relationship, a single mass focussed with 1000 volts ion accelerating

voltage gave a Hall output of 31.57 millivolts. The results of a calculation employing Eq. 22 predicted mass 41.2 whereas the true mass in focus was nominally 41. These results agree quite well considering that a single absolute result was calculated from a general equation.

D. Using specific conditions, the sensitivity of the Hall crystal was indicated in two ways. In the first measurement, the Hall output was sufficiently precise to permit measuring the difference in magnetic field strength which resulted in scanning across the N_2^+, mass 28, ion beam. The width of this ion beam was found to correspond to 0.038 mass units or 6.7 gauss. A second measurement was made to determine the magnetic field strength variations across the air gap. The Hall crystal output changed from 40.810 millivolts at the face of the pole piece, to 40.763 millivolts at the center of the air gap. For the total magnetic field of 2370 gauss the difference in these outputs represents approximately 3 gauss.

E. The reproducibility of the Hall output was very good for a series of measurements made on different days even when the Hall crystal circuit and the mass spectrometer were turned off between measurements. The Hall crystal output for one of these measurements

was 30.32 millivolts for a particular ion beam in focus at a corresponding magnetic field. The following day the mass spectrometer and the Hall crystal conditions were reset for the same ion beam, and, without further calibration, the Hall output was measured as 30.39 millivolts.

From the results of these studies, it was concluded that the Hall crystal mass indicator can easily obtain a mass resolution of 1 part in 400. The conditions for realizing this resolution are a 200 milliampere input regulated to 0.25 percent and an output read to within 25 microvolts. On the basis of a calibration curve from many E_H measurements, the mass resolution is much greater. A final check of the Hall mass indicator verifies its convenience as a mass indicator. In a magnetic mass spectral scan of UF_6, the Hall crystal output was recorded on a separate 20 millivolt recorder potentiometer while the mass spectrum was recorded on another potentiometer. At each ion peak the magnetic scan was momentarily stopped in order to focus the ion beam. This resulted in constant E_H outputs which were recorded as straight lines by the Hall output potentiometer. Thus each mass was indicated by a step or discontinuity on the Hall output recording. A similar recording is shown in Fig. 26 which is the actual recorded Hall crystal output during a magnetic scan of the Hg spectrum. A calibration curve representing E_H vs mass permits a fast reference for accurate mass identification.

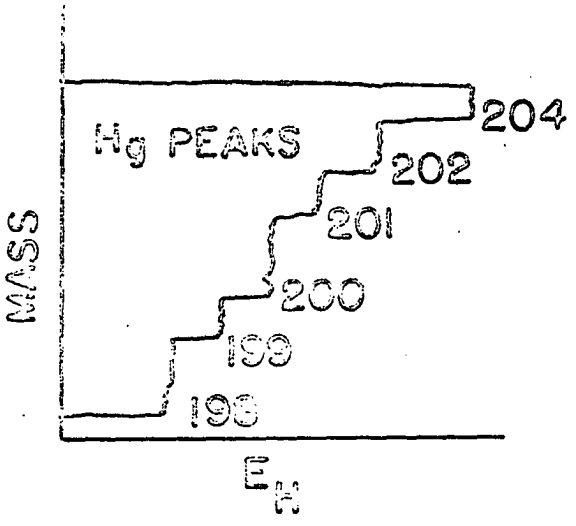

Fig. 26. Actual recording of Hall crystal output for mass marking.

10. Magnetic current regulator and power supply

The circuit diagrams of the magnet current regulator and magnet power supply are given in Figs. 27 and 28. The units were designed and built in these laboratories.

The magnet power supply provides 0 to 500 milliamperes through the magnet coils. The magnet current regulator normally is used to regulate the magnet coil current by comparing the voltage drop across the magnet coils with a reference voltage. This is accomplished with a 1000 cps Bristol Chopper which automatically adjusts the magnet coil current in order to maintain balance between the two voltages being compared. The reference voltage can be varied from 0 to 2 volts by means of a 20K Ω, 40 turn potentiometer. Since the 40 turn potentiometer can also be driven by a variable speed motor, the magnet coil current can also be increased at a constant rate. The 40 turn potentiometer is overlapped for greater sensitivity so that as it is turned from 0 to 40 turns the magnet coil current is increased from 0 to 250 milliamperes. A current selector switch is then manually turned. The variable speed motor is reversed and as the 40 turn potentiometer is turned back to zero the magnet coil current continues to increase to its maximum of 500 milliamperes. This type of magnetic scanning produces magnet field strength vs time curves as shown previously in Figs. 15 and 17. Note that although the magnet coil current is linearly increased, the curves are not linear because of

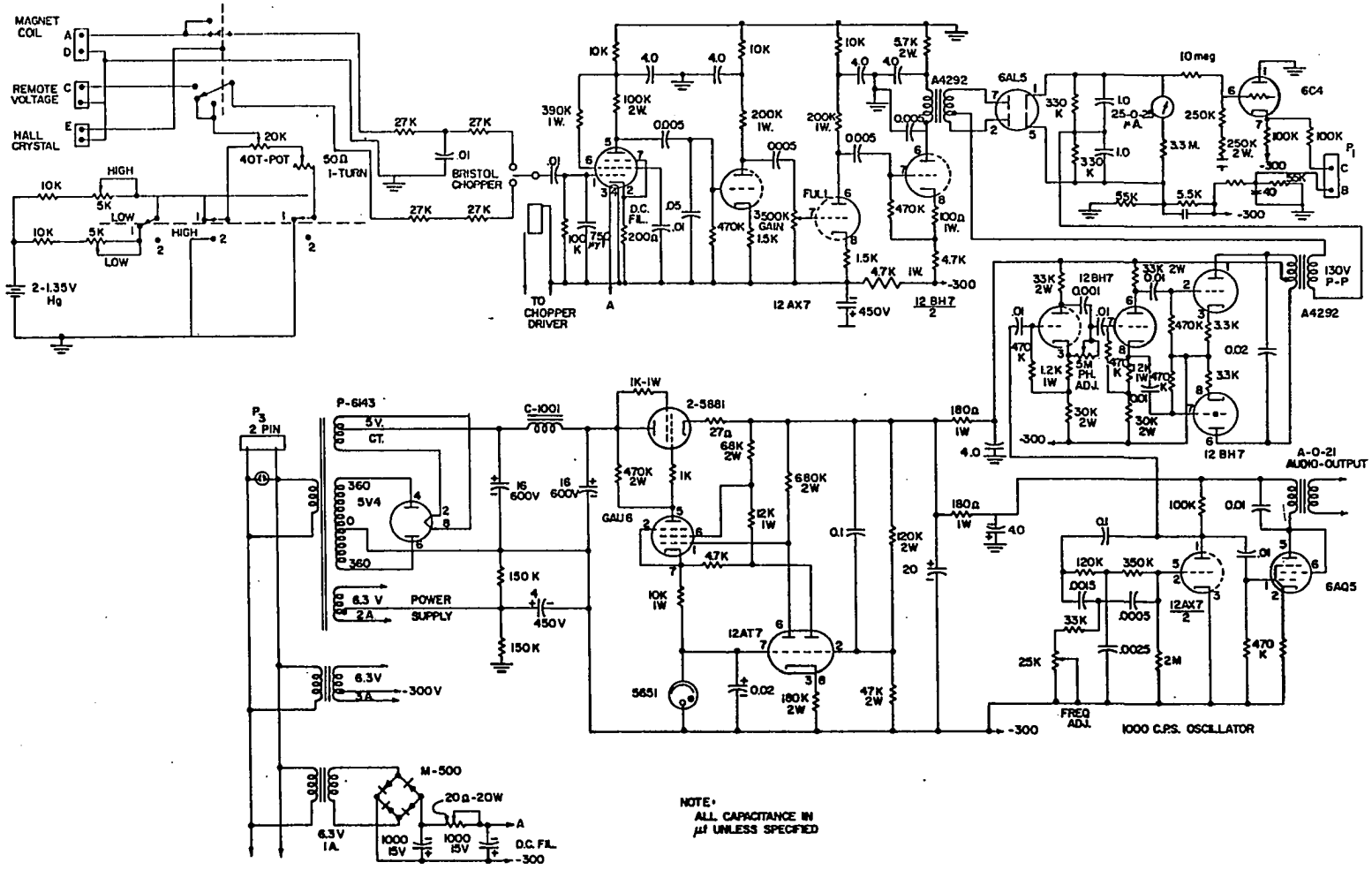

Fig. 27. Magnet current regulator.

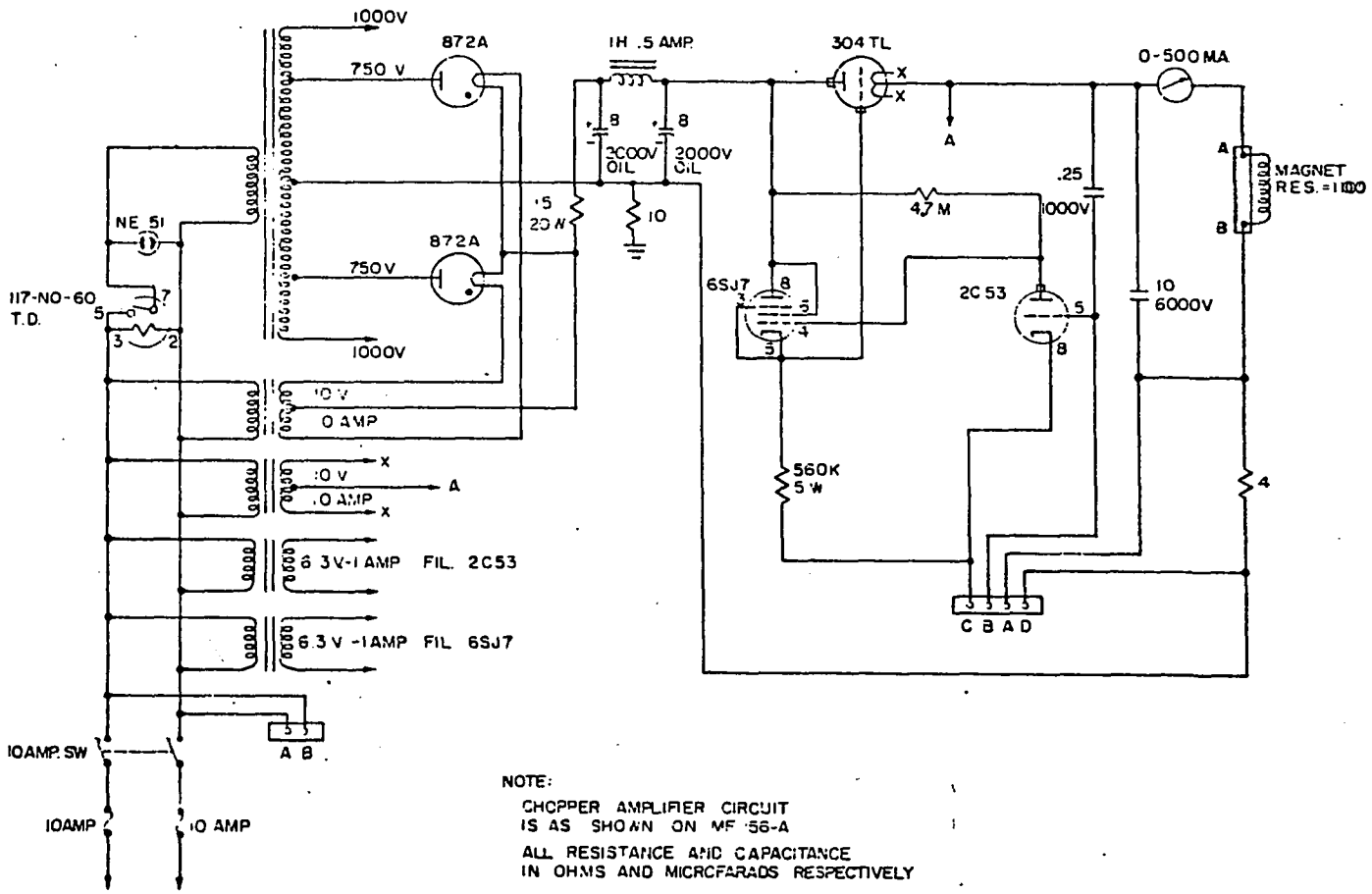

Fig. 28. Magnet power supply.

saturation effects and variations of the permeabilities within the magnet. Because of these effects the mass dispersion for a magnetic spectral scan does not hold to an inverse square root law with respect to mass. One would predict this law from Eq. 16 by assuming a linear increase of magnetic field strength. If the mass dispersion is defined as,

$$\frac{\Delta m}{m} \simeq \frac{dm}{m} \qquad 23$$

then for a magnetic scan of the mass spectra, during which time R and V are constant, the following relationships hold;

$$m = KH^2 \qquad 24$$

and

$$\frac{dm}{dt} = 2HK \frac{dH}{dt} . \qquad 25$$

If the magnetic field strength increases at a constant rate,

$$\frac{dH}{dt} = K' \qquad 26$$

and $\frac{dm}{dt} \sim \frac{\Delta m}{\Delta t} = 2KK'H = 2K^{1/2}K'm^{1/2}$

or $\frac{dm}{dt} = C' m^{1/2} .$ 27

For a constant time interval, the dispersion becomes,

$$\frac{\Delta m}{m} = \frac{C}{m^{1/2}} = \frac{K}{H} \qquad 28$$

The magnetic field strength certainly does not increase at a constant rate if the magnetic coil current is regulated,

hence the mass dispersion in such a scan would follow a much more complex function than Eq. 28 indicates.

The present magnet current regulator includes a modification of the Bristol Chopper circuit so that effectively the magnet field strength instead of the magnet coil current is regulated. Basically, in the Bristol Chopper circuit a reference voltage is compared with another voltage which is linearly dependent upon the magnetic field strength instead of linearly dependent upon the magnet coil current. The voltage which is linearly dependent upon the magnetic field strength is the output from a Hall crystal immersed in the gap of the magnet. The output of the Hall crystal is amplified by the KinTel amplifier and connected into the Bristol Chopper circuit in place of the voltage drop across the magnet coils. Before the regulation is switched to this mode, the magnet power supply is turned to the full 500 milliampere output and by varying the KinTel amplifier gain the Hall Crystal output is adjusted equal to the reference voltage. Starting at zero milliamperes again, the Hall crystal output voltage is regulated while the 40 turn reference potentiometer is driven at a constant rate. The magnetic field strength then increases linearly. A selector switch can be set to give a linear scan of the magnetic field to either 250 or 500 milliamperes coil current.

The block diagram in Fig. 29 illustrates the arrangement which enables the regulation of the magnetic field

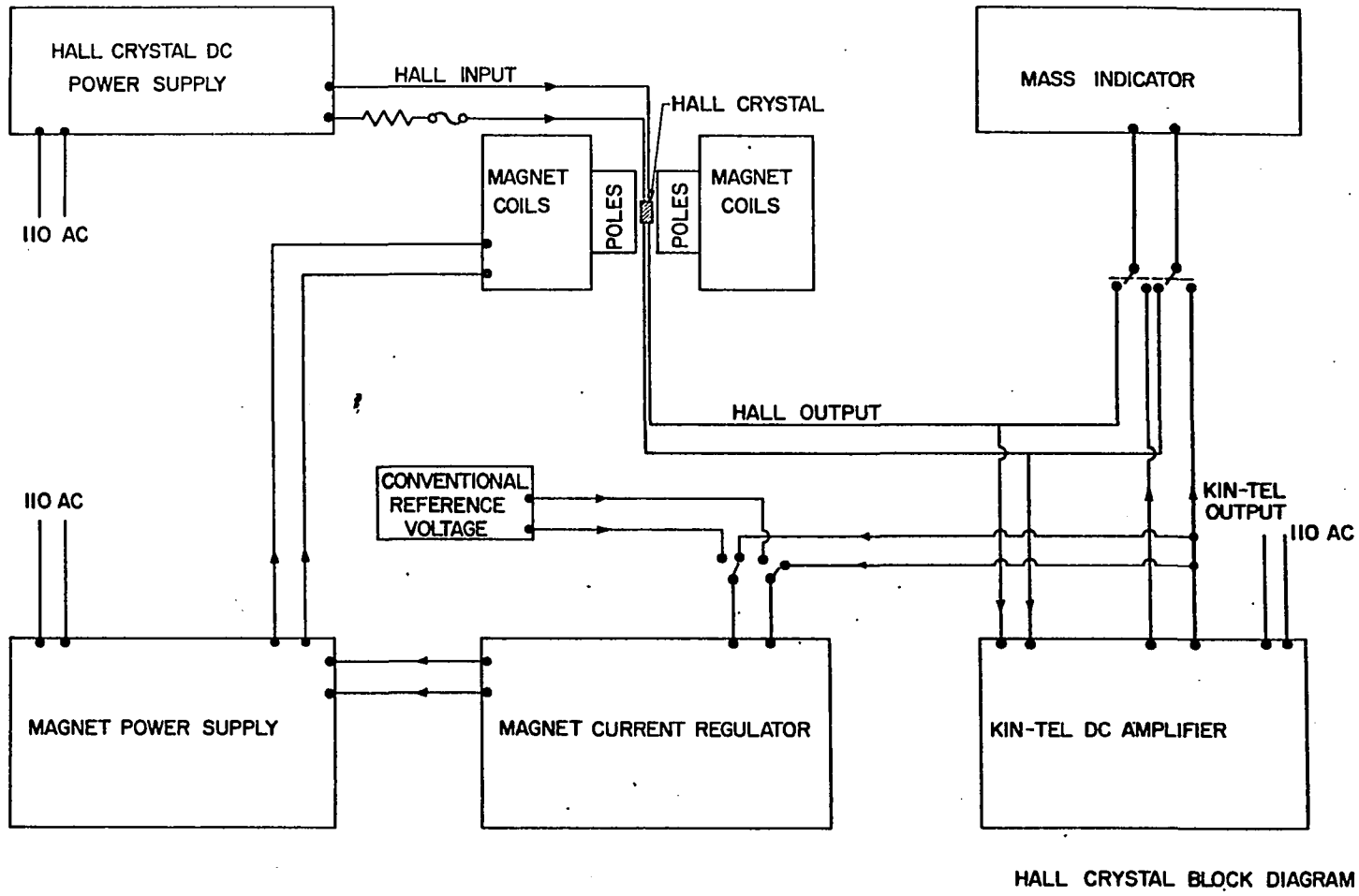

Fig. 29. Hall crystal block diagram.

strength by means of a Hall Crystal. An experimental curve is shown in Fig. 30 illustrating the nearly linear scan of magnetic field strength using this arrangement. Note that in this regulation mode, the mass dispersion of a magnetic mass spectrum scan is given by the inverse square root shown in Eq. 28. This is much more convenient than the complex mass dispersion function which results if the magnet coil current is regulated.

A magnetic mass spectral scan with a constant mass dispersion is desirable but, at present, methods for doing this have not been developed. Constant mass dispersion might be obtained by using the Hall crystal regulation of the magnetic field strength and a reference voltage which increases at a logarithmic rate. This would cause the magnetic field strength to increase at a logarithmic rate and thus,

$$\text{Log } H = Ct \tag{29}$$

$$\frac{dH}{dt} = HC. \tag{30}$$

For a constant time interval in Eq. 25

$$\frac{\Delta m}{\Delta t} = 2KH \frac{dH}{dt} \tag{31}$$

$$\frac{\Delta m}{\Delta m} = \frac{2KH^2C}{m} = \frac{2KmC}{mK} \tag{32}$$

leads to,

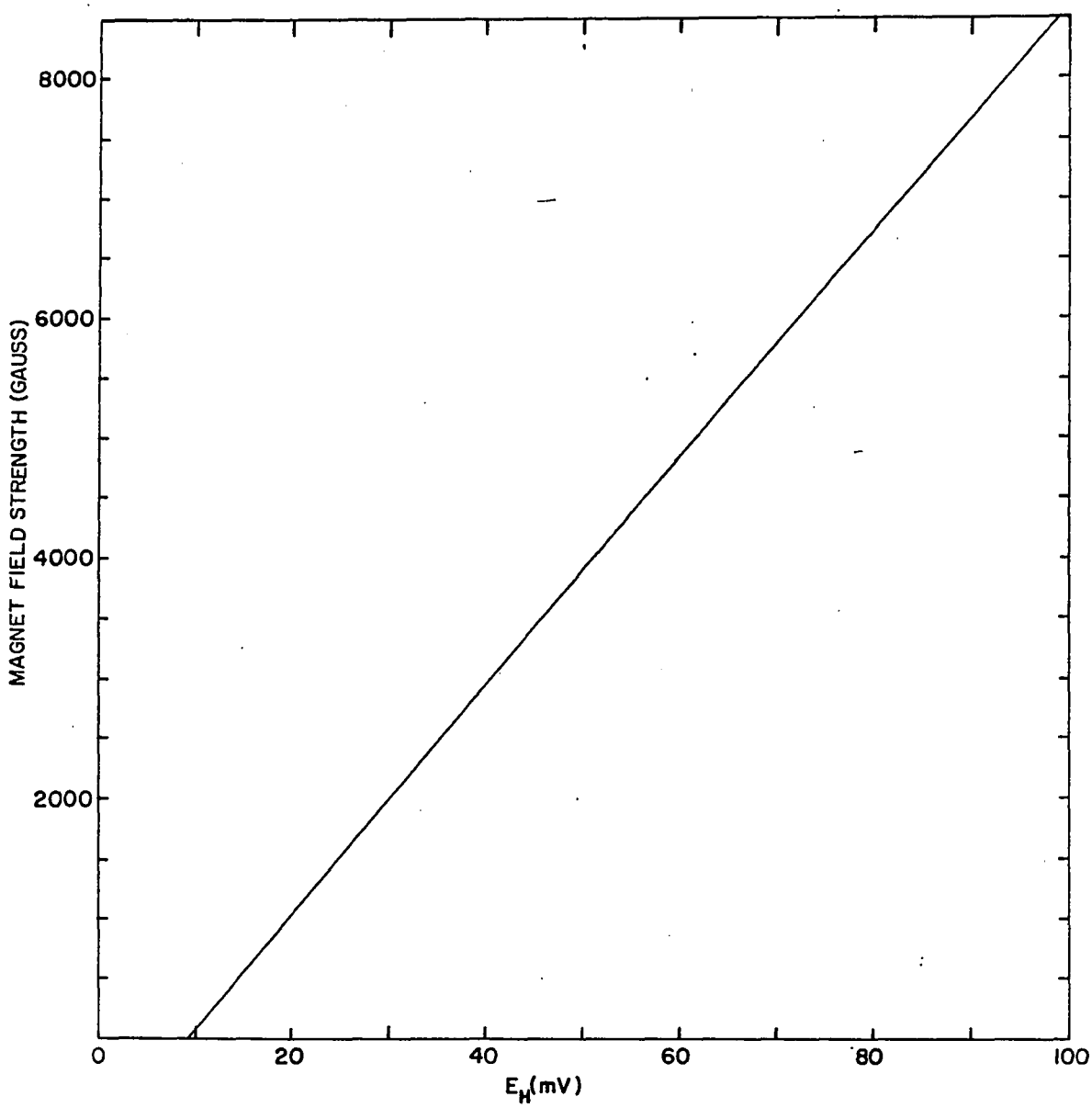

Fig. 30. Actual experimental magnetization curve using Hall crystal regulation.

$$\frac{\Delta m}{m} = 2C. \qquad 33$$

Thus a constant mass dispersion would be realized.

11. Ionization pumps and cold cathode ionization gauge

The high voltage power to the 11 l/s VacIon pump (Varian Associates, Palo Alto, California) is supplied and controlled by a standard Model 921-0011 Control Unit which is mounted in the main instrument cabinet. The pressure in the mass analyser is read from a meter which has a logarithmic scale and five-linear scales for full scale readings to indicate the pressure for a range of 1×10^{-5} to 1×10^{-9} Torr.

Another unit is mounted in the instrument panel to supply high voltage to the cold ionization gauge which is used to monitor the pressure in the ion source envelope. This pressure is read from a 0 - 1 milliammeter which has five positions for which the full scale readings can cover total pressure ranges of 1×10^{-3} to 1×10^{-7} Torr.

One modification has been made to this circuit. The circuit diagram of the original circuit can be found in Saalfeld (6a, 6b) work. A 5 watt, 50 Ω, 1 turn potentiometer is connected in series with the meter, and the three leads from this resistor are connected to a switch in the "pressure-protect" circuit.

12. Pressure protect circuit

The circuit diagram for this unit is shown in Fig. 31. The line power for the emission regulator and the high

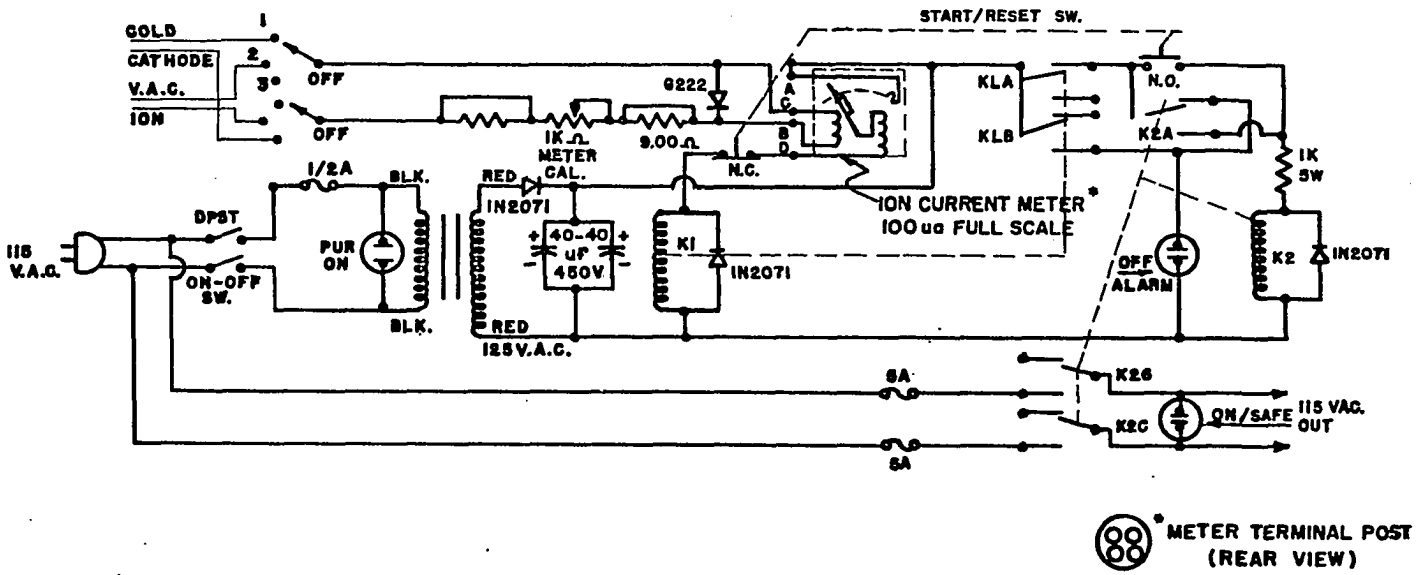

Fig. 31. Pressure protect circuit.

voltage supply is provided by this circuit. When the pressure in the mass spectrometer becomes excessively high, a relay is activated to turn off the ac power to the emission regulator and to the high voltage supply. A selector switch permits the selection of pressure protection from either the cold cathode unit or from the VacIon pump unit. The pressure at which the relay is activated, is controlled and indicated by a 0 - 100 microammeter in the pressure protect circuit.

13. Bakeout system

This circuit is mounted in the main instrument panel and serves the purpose of supplying, reading, and controlling the current to the mass analyzer bakeout heater, the inlet bakeout heater, and a high temperature furnace. A selector switch permits turning on any one of these heating elements or any combination of them. The furnace can be used to heat reaction mixtures to temperatures up to 1000°C.

V. EXPERIMENTAL PROCEDURE

The accuracy of the results obtained from ionization efficiency studies can often be directly influenced by the manner in which the data are obtained. To provide a better understanding and interpretation of the results from this work, the experimental procedure is explicitly described in detail.

Prior to making an ionization efficiency study, several preliminary steps are taken. First, the entire mass spectrum of the compound under investigation is scanned and analyzed, and the fragment ions are identified. Careful account is made of the background spectrum. This analysis is completed using a high sample pressure, a high trap current, a high electron accelerating voltage, a high repeller potential, and a moderate collector slit size, with the ion source in the conventional mode of operation. One ion current of a series of fragment ions for which the ionization efficiency curves are to be studied, is then focussed and the high voltage divider circuit is appropriately adjusted to establish the desired ion source mode of operation.

A. Pressure Conditions and Stabilization

The sample pressure is allowed to stabilize during an 8 to 10 hour period before the ionization efficiency studies are conducted. The pressure at which the sample is admitted, depends upon the intensity of the ion fragment which is to

be studied. Normally the sample gas pressure is 5×10^{-7} to 8×10^{-6} Torr during ionization efficiency studies of major fragments or at higher pressures for studies of minor fragments. Some workers adjust the pressure for each ionization efficiency study so that at one specific electron accelerating voltage, usually 50 volts, the ion intensity reads the same for both the calibrating gas and the ion fragment under investigation (50). From a theoretical viewpoint there is little reason to expect an improvement in results from this technique. Furthermore, one can certainly not speculate that the slopes, sensitivities, or any other physical characteristics are equalized for both specific ion processes of interest. Indeed, since the specific ionization process of importance occurs only within the first few volts above onset, any adjustments of ion current intensity based on readings as high as 50 volts may be superfluous. If the ion current intensities were equalized at electron accelerating potentials as low as 2 to 3 volts above their respective onsets, certain theoretical speculations might be acknowledged concerning the specific ionization processes, but improved accuracy would most likely be fortuitous. Empirically this technique might improve the <u>precision</u> for some specific studies but in general more <u>accurate</u> results will be obtained by using <u>optimum</u> sensitivity for the ion of concern. For this reason the sample pressure is only changed when necessary

in order to obtain sufficient ion current intensities to enable ionization efficiency studies of the less abundant ion fragments.

B. Emission Conditions

Next, the operating conditions for this specific ion source mode are adjusted using the differential voltmeter to monitor the potentials of the ion source electrodes. The electron accelerating voltage is decreased to a range within 10 to 15 volts above the anticipated threshold potential. If the adjacent ion beams are from the same fragment ion species, the variable collector slit is opened to its maximum width of 0.025 inch. The voltages of the electron collimating plates and the anode are adjusted to the selected values and the trap emission current is set as close to 15 microamperes as it is possible to maintain throughout the experiment. The emission regulator is set for trap current regulation. The repeller voltage is then decreased to a value which is dependent upon the ion current intensity. This potential is usually 1 to 5 volts or high enough such that the ion current intensity is sufficient to permit an ionization efficiency study.

C. Pulsing Conditions

When pulsing techniques are employed, the amplitudes of the anode and repeller pulses are adjusted by any one of the following methods.

Method 1. With the high voltage off, an oscilloscope is used to set the amplitude of the anode pulse equal to a

preset anode potential which is to be applied during the high voltage operating conditions. Likewise, the amplitude of the repeller pulse is also set equal to a preselected repeller potential. Both pulses are negative with respect to the normal voltages of these two electrodes.

Method 2. At the high voltage operating conditions, the amplitude of the anode pulse is increased until the trap emission current decreases to one half its initial value. This also reduces the ion current intensity; it is further reduced to 50 percent of the latter value by increasing the amplitude of the repeller pulse.

Method 3. The amplitude of the anode pulse is increased until the initial ion current intensity is reduced by 50 percent. The amplitude of the repeller pulse is then increased until the latter ion current density also reduced 50 percent.

D. Ion Beam Stability Check

After all ion source conditions are established, the shape of the ion beam is observed. If it is satisfactory, the ion beam is refocussed to its maximum and the ion current intensity is recorded for 20 to 30 minutes using the bucking attenuation mode. Usually during this period the ion current attains a constant value and satisfactory stability. If the ion current stabilizes but does not remain constant, compensation is made for the resulting drift that occurs during the ionization study. This is accomplished by comparing the ion current intensity reading

obtained for each value of the variable electron accelerating voltage to the ion current intensity reading obtained at a fixed reference electron accelerating voltage.

The vacuum system is baked out and pumped for two days between samples. The bakeout is normally left at about 80°C throughout the ionization efficiency studies.

E. Compilation of Data

All the data are recorded directly on IBM Computer Fortran Coding Forms in the following manner. The initial ion current intensity is read directly from the attenuation control dials and from the recorder. It is then recorded on the coding form. The initial electron accelerating voltage is accurately measured by means of the differential voltmeter and is recorded. The electron accelerating voltage is then reduced by small but arbitrary amounts (0.1 to 0.5 volts) and the ion current intensity and electron accelerating voltages are again read and recorded. From 50 to 100 such readings are made until the ion current is extremely small. Usually smaller electron accelerating voltage increments are used near the onset in order to obtain more experimental points in this region of the ionization efficiency curve.

If there is a drift in the ion current intensity throughout the initial stability check, compensation is made by comparing each of the above readings to readings of the ion current intensity at the reference electron accelerating voltage.

When the ion current becomes too small to detect, the following additional values are recorded:

1. The zero level of the ion readout system,
2. The potentials of the anode, repeller, electrodes D, E, and F,
3. The relative potential of the drawing out plate,
4. The filament current,
5. The ion source pressure, ion species, mass to charge ratio, compound investigated, and the calibration gas used,
6. The trap current,
7. The date, and miscellaneous comments.

The information on the IBM Coding Forms is then punched onto IBM Computer Cards by keypunch operators. The data are analyzed and plotted by various computer programs which are discussed later.

The use of a differential voltmeter and the technique described required less than an hour to read and record 70 to 80 points for an ionization efficiency curve. The use of the computer eliminates the time usually required to analyze and plot the data manually. Note that the ion current is read at <u>any</u> electron accelerating voltage intervals without introducing any excess work and without complicating the calculations. Furthermore, <u>numerical data</u> are obtained so that they can be conveniently treated and analyzed in many ways. This cannot be claimed for techniques which merely yield a graph.

VI. METHODS FOR INTERPRETING IONIZATION EFFICIENCY DATA

A. Introduction

Unfortunately, an overwhelming amount of confusion and disagreement exists concerning the appropriate or correct method of analyzing ionization efficiency data. In many instances one method might appear to give satisfactory results whereas another method does not. Perhaps the major cause for lack of a single consistent method of analysis arises because ionization efficiency processes are of such complexity that most workers are content to use empirical methods of analysis. A few attempts have been made to alleviate the problem of accuracy by using highly developed instrumental techniques; but, recently, there has been an increasing emphasis upon theoretical treatment of ionization efficiency data. Although it is not the intent of this work to provide a complete solution to eliminate the confusion, it is hoped that the theoretical analysis and viewpoints discussed in this report will help to create a better understanding of ionization efficiency studies.

Since some of the present methods of analyzing ionization efficiency data are pertinent to the following discussion, they are briefly described. Further explanation of these methods can be found in Field and Franklin (1), McDowell (2, 5), Reed (4), or in the original works of the various authors.

B. Empirical or Graphical Methods

The present methods of analysis are based primarily on graphical treatment of the data since ionization efficiency data are not ordinarily amenable to mathematical analysis. All these methods involve some assumption to justify using the technique. These assumptions may be valid for some specific ionizing processes but are often invalid for other processes. However, correct interpretation and understanding of their limitations can sometimes yield moderately accurate results.

1. Linear extrapolation

Linear extrapolation was one of the first techniques employed and it is probably the simplest to explain. The major assumption is that the near-linear portion of an ionization efficiency curve is caused by the ionization process of interest. The tail of this curve is attributed to extraneous effects such as electron thermal energy, potential gradients, and many of the other factors that were described earlier. The ionization process is assumed to conform to a linear threshold law, thus the near linear portion of the curve is extrapolated along a straight line to a point of zero ion current. This point is corrected by reference to a similar point from the ionization efficiency curve of a calibrating gas, (usually a rare gas) and the final value is assumed to be the appearance potential of the ion.

2. Initial onset or vanishing current method

When this method is used, an attempt is made to adjust the ionizing conditions for the particular ion of interest so that they are similar to the conditions of ionization for the calibrating gas. Two techniques are normally employed; the ion currents of the two ions are adjusted by pressure variation until they are both equal for an electron accelerating voltage of about 50v, or the ionization efficiency curves are plotted with different scales so that the two curves have equal slopes throughout their linear portions. From the ionization efficiency curve, the appearance potential is chosen as the electron accelerating voltage which corresponds to the initial formation of ions.

3. Extrapolated difference method

Warren (51) has proposed a modification of the Vanishing Current Method. The ionization efficiency curves due to the calibrating gas and the ion of interest are plotted on different scales such that their linear portions are parallel. The differences in electron accelerating voltage, ΔV, for various values of ion current, I, are plotted against ion current. This graph is extrapolated to obtain a value of ΔV at zero ion current, and this value is assumed to be the difference in appearance potentials between the ion of interest and the calibrating gas.

4. Critical slope method

Honig (7), as early as 1948, proposed one of the first methods of analyzing ionization efficiency curves without

using a completely empirical technique. He assumed that ionization near the threshold depended upon the square of the electron energy in excess of the critical energy, and he combined this assumption with the quasi-Maxwellian thermal energy function for electrons. He concluded that the critical energy, or appearance potential of the ion was the point at which the slope of the curve was 2/3KT for a semilog plot of ion current vs electron energy. Recently Wahrhaftig (52) used a similar procedure and determined that the critical slopes should be 1/2 KT for rare gas ions and 2/3 KT for the parent ion of a molecule.

5. Modification of critical slope method

Lossing (53) described a simple modification of the method described by Honig. He found that semilogarithmic plots of ion current intensity vs electron energy result in parallel linear regions near threshold if both the ion currents of the calibrating gas and sample gas are adjusted to be equal to 50V. The difference between the electron energies at 1 percent of the maximum ion current reading is taken to be the difference in appearance potentials. Dibeler (54) uses a method very similar to this.

Morrison (55a, 55b, 55c) proposed another slight adaptation of Honig's method of critical slopes. He assumed that the point at which a semilog plot departs from linearity is due to the tailing of the ionization efficiency curve caused by the exponential nature of the electron thermal energy

distribution. Thus this point is taken as the appearance potential.

C. Analytical Improvements

1. Removal of electron thermal energy

Several methods have already been discussed as to how electron thermal energy can be removed by assuming a Maxwellian thermal energy distribution (7, 56, 57, 58).

2. Differential method

Although the method of critical slopes and some of its modifications is based upon analytical treatment of ionization efficiency data, the results are still subject to some arbitrary or empirical assumptions.

Morrison (59) approached the problem of evaluating ionization efficiency data with a more sophisticated theoretical treatment of ionization processes. He assumed that ionization near threshold depends upon a polynomial function of the electron energy in excess of the critical voltage. This was combined with the electron thermal energy distribution to determine the function upon which the ion current depends. This treatment indicated that plots of the first and second differentials of ionization efficiency data permit the detection of much structural detail in curves plotted from the data (60a, 60b). He also describes an electronic method by which differential plots can be produced directly from the mass spectrometers.

3. Deconvolution

Morrison (60a, 60b) also described and used a method by which the ionization efficiency data is subjected to mathematical deconvolution to remove the effects of electron thermal energy and some instrumental effects. Basically a curve to be analyzed is compared to corresponding portions of a standard ionization efficiency curve of He.

D. Present Method

1. Introduction

None of the above methods of analysis of ionization efficiency data seemed satisfactory for this work. However, the method of linear extrapolation did appear to be the least arbitrary of the methods and it also seemed most adaptable for the theoretical modifications and computer techniques of interest in this work. The method of linear extrapolation was thus modified to accomodate computer techniques and then applied to the ionization efficiency data. The results of the analysis were studied in order to eliminate some of the inherent errors arising from this method of analysis. The emphasis is not placed on the result obtained from an extrapolation of one large linear portion of each curve but rather, the emphasis is on the linear extrapolation of various small linear segments and points of inflection throughout the curves. The original data can be handled by means of nonlinear functions of the

excess electron energy before the linear extrapolation is applied.

2. Initial treatment of data

Before the ionization efficiency data are analyzed, they are adjusted to compensate for several instrumental effects. First, the numerical order of the data is reversed so that the last datum point becomes the first point which is listed and treated by the computer. The zero reading of the amplifier and recorder system is then subtracted from each ion current intensity reading. The readings are also corrected for pressure drifts which might have occurred during the study. Correction for pressure drift is accomplished by assuming that the ion current intensity readings for the ionization efficiency curves change in the same ratio as do the ion current intensity readings for a reference electron accelerating voltage.

If a retarding potential difference study is made, two ion current intensities are read for each different electron accelerating voltage. The two readings correspond to the two retarding potentials used. The two sets of data are treated as above and the difference in the ion current intensity is also determined from each of the two readings.

The major advantage of this computer technique accrues from the versatility with which the data can be further treated before the plotting or analysis is executed. For example, the ionization efficiency data can be treated by

linear, square, power, exponential, or complex types of threshold laws merely by carrying out the appropriate mathematical operations on the ionization efficiency data.

3. Plotting subroutine

When no further data treatment is to be performed, the data points are plotted and a point-to-point line is drawn through them. Every third point on the plot is numbered to allow rapid identification of specific points. An example of such a plot is given in Fig. 1.

The plotting is generated in the computer program by the use of a CalComp subroutine plotting package (60c) (CalComp Digital Plotter Package, California Computer Products, Incorporated, Anaheim, California) which is incorporated into the computer system by the Computer Center at Iowa State University. This plotting routine automatically optimizes the plot size by determining convenient scales for the axes; draws, makes, and labels each axis; labels the graph; plots and numbers the points; and draws either a smooth line or a point to point line through the data. When modifications are desired, it is only necessary to change a few control parameters which are then read into the program with the data input.

The plot is generated onto magnetic tape by the use of the CalComp subroutine and the IBM-7074 computer, and it is then processed through an IBM 1401 computer. An IBM 1627 Model I digital incremental plotter is controlled by

the 1401 computer in the final, mechanical plotting operation. This plotter is capable of plotting 18,000 increments per minute, with a resolution of 0.01 inch. Plots can be 11 inches by 120 feet long but in this work they are usually 10 inches by 40 inches. The use of the CalComp plotting package is described in more detail in a bulletin from the computer service group (Computer Utilization Bulletin No. 20, Iowa State University).

4. Computer analysis by linear extrapolation

After the data are converted to the desired form, the main routine of this computer program subjects the ionization efficiency data to an extensive analysis involving linear extrapolation. The intimate details of the computer program are relevant in providing an understanding of the accuracy of the results, hence the computer technique is further described.

When linear extrapolation of ionization efficiency curves is performed with the unaided eye or with the use of a straight edge, several errors can result. When using these methods, one cannot readily detect small changes in slope or slight curvature, nor can this process produce accurate quantitative determinations of slopes, standard deviations, or points of intersection. Furthermore, if there is any scattering in the data points, the extrapolation is not usually the outcome of an optimum least squares line. Perhaps the greatest error is introduced by human judgement

which can bias the results. The use of a computer does not completely eliminate all of these inadequacies, but it does yield consistent results as well as unbiased and more accurate measures of slopes, standard deviations, error limits, points of intersection, elimination of computation errors, and more accurate plots.

The process of selecting and evaluating linear segments from the data is not easily executed using a computer. The process is based on two major error limits. The first error limit requires that the points must lie within a certain "scattering limit", ΔE, in order to be considered for extrapolation. This scattering limit, ΔE, is determined by an error that is allowed in the readings of electron accelerating voltage, ΔV. Initially this error, ΔV, is chosen as 0.25 volts.

Fig. 32 shows 5 points from a greatly enlarged section of data from an ionization efficiency curve. The scattering error limit, ΔE, is geometrically related to ΔV and is mathematically related to, m, the slope of the least squares line drawn through the points.

$$2\Delta E = \Delta V \sin \qquad 34$$

$$\Delta E = \frac{\Delta V M}{2\sqrt{1+m^2}} \qquad 35$$

It is indicated in Fig. 32 that although the points fit the scattering function, they can occur in such a way as to

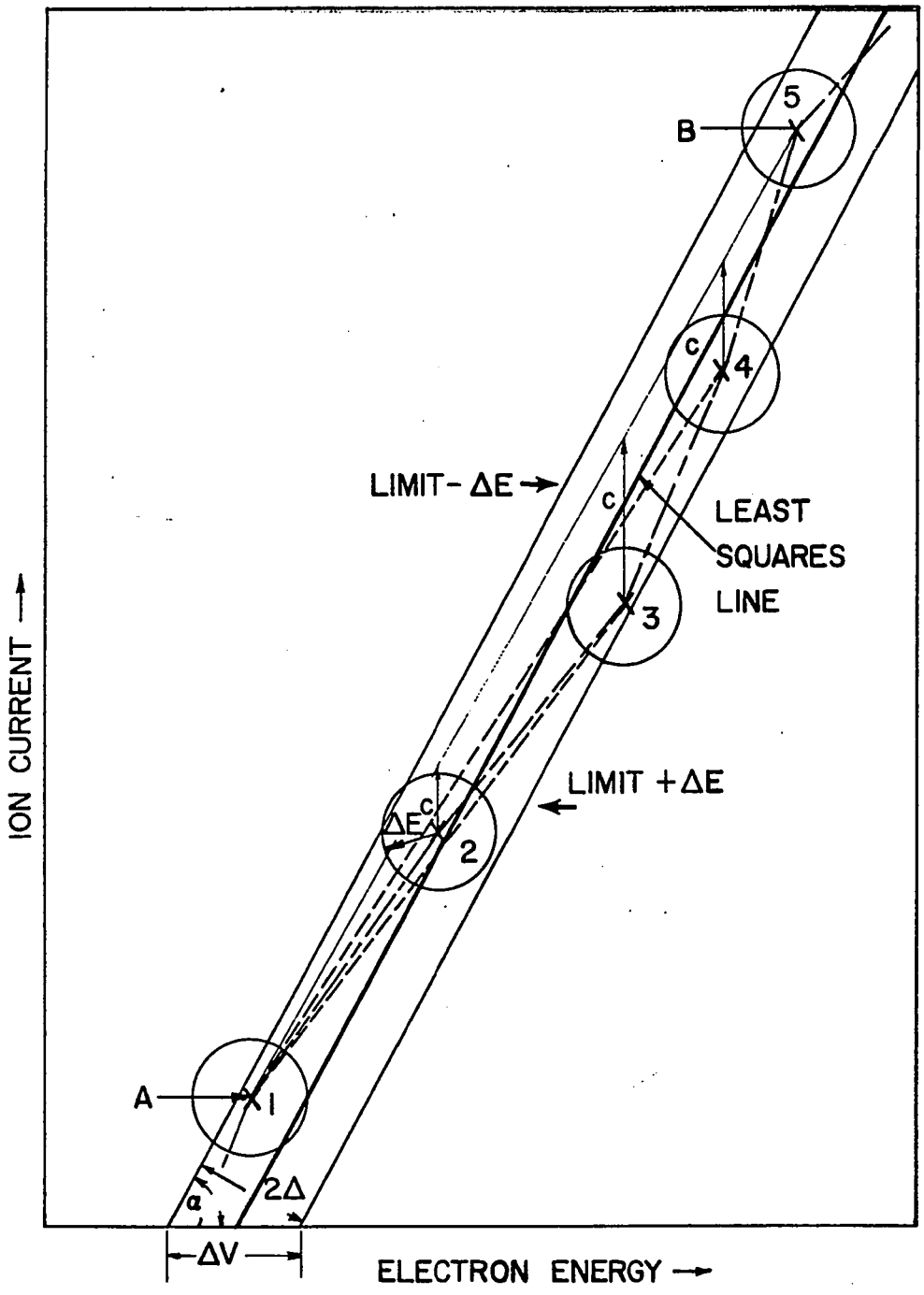

Fig. 32. Enlarged portion of ionization efficiency curve.

impart a general curvature to the ionization efficiency at that region.

A second error limit, ΔI, establishes the amount of general curvature that will be tolerated in the extrapolation. This "Curvature error limit", BEAM ERROR, is determined by the amount of error that will be allowed in the ion current intensity readings. In order to determine the curvature of the ionization efficiency curve in the region of these points, a line, AB, is drawn from the first point under consideration to the last point. The vertical distances, c, from each point to this line are calculated for all points between the two end points. The distances are weighted by a factor of I_i^2/I_N so that the smaller ion current readings receive less emphasis than do the larger ion current readings. For a series of N points starting at 1, the total error is:

$$\text{ERROR} = \sum_{i=2}^{N-1} \Delta I \, \frac{I_i^2}{I_N} . \qquad 36$$

ERROR, the sum of these distances, must be less than the allowable error, BEAM ERROR, which is determined by the chosen value assigned to ΔI. The initial ΔI is chosen as 2.4 percent of the ion current reading as the maximum tolerable ion current noise. BEAM ERROR is given by the sum of ΔI times the ion current intensity of each point between the end points.

$$\text{BEAM ERROR} = \sum_{i=2}^{N-1} \Delta I \; I_i \qquad 37$$

It is obvious that if the sum of these distances is significantly different than zero, most of the points are either below or above line AB. The representative geometrical values, V, E, and c are also indicated in Fig. 32.

The actual computer program operates according to the following scheme.

1. A linear least squares line is computed for the five points, N to N + 4. The first set begins at point 1.
2. The distance of each point from the least squares line is computed. If any of these distances are greater than the scattering limit, the first point (or base point) is rejected and the process is repeated for the next five points. When five points are found that lie within the scattering error tolerances, a linear least squares line is similarly computed for these five points plus the next point. Each time the set of points conforms to the scattering error, another point is included at the upper end and the cycle is repeated.
3. When all points are found that satisfy the scattering limit using point N as a base point, the entire procedure is repeated for point N + 1 as the base point. If more points fit the scattering limit

using N + 1 as the base point than for N, the procedure is repeated using N + 2 as the base point. The procedure continues until a base point is found for which a maximum number of points satisfy the scattering error limit.

4. The test for curvature is then applied. If the points indicate that the ionization efficiency curve has more curvature than is allowed by the curvature error limit, the highest point of this series of points is rejected and the curvature is redetermined using the remaining points. If the curvature is still too great, another point is rejected at the top of the series of points and a repetition of the procedure is completed.
5. If, after rejecting two upper points, the series of points still does not fit the curvature error, the upper two points are restored and the base point is rejected from the calculations. The entire cycle described in step 4 is then repeated using a new point as a base.
6. Steps 4 and 5 are repeated until less than five points remain to satisfy the scattering error limit or until a series of points is found that satisfies both error limits. The method of linear least squares analysis is then applied to this series of points to determine the equation of the line which

best fits them. Calculations are made to determine "Student" deviations of the electron accelerating voltage and the ion current intensity, slope, slope deviation, intercepts, and average ion current reading.

7. The point immediately below the highest point in the last series is then taken as a new base point. The entire procedure is repeated to determine a different linear portion of the ionization efficiency curve.
8. If another line is established, the deviations, slope, etc. are calculated for this line also. The points of intersection of this line, with the last line and with the axes are also calculated.
9. The entire data from the ionization efficiency curve are subjected to the above method of analysis and the calculated results are printed out for each line that is determined.
10. After all the data have been evaluated using the above process, the scattering error and curvature error limits are decreased by small increments and the entire process above is repeated. About twenty repetitions are completed until the error limits become very small.
11. An example of the output from a typical analysis of the data for the ionization efficiency curve of Xe^+ is shown in Chart 3a.

CURVE J=	NO.OF PTS. LL(J)	APPEARANCE POTENTIALS XO(J)	XX(J)	YY(J)	SLOPE S(J) AND SIGMA	B(J)	Y-INTERCEPT	INITIAL PT 1ST PT	LAST PT LP(J)	STANDARD DEVIATIONS YAVE	YSIG	XSIG
1	-0	-0.0000	-0.0000	-0.0000	0.0000	-0.0000	0.0000	-0	-0	-0.0000	-0.0000	-0.0000
2	41	9.2334	9.2334	0.0000	60.5076	0.0735	-558.6903	19	59	148.2951	0.5709	0.0094
3	9	7.8995	14.1081	294.9596	47.5080	0.4588	-375.2903	59	67	319.1000	0.5592	0.0118
4	20	6.9233	15.1414	344.0490	41.8645	0.1262	-289.8396	65	84	401.5250	0.5715	0.0137
5	6	9.6428	18.2534	474.3281	55.0866	0.4557	-531.1881	84	89	485.6333	0.3173	0.0058
6	4 154	4.1150	20.1217	577.2492	-4.3080	3.4594	663.9344	105	108	569.9500	1.0229	0.2374
			DAP(JJ)=	0.0400	ELECTRON VOLTS			SCATTERING	=-0.0189		BEAM ERROR	0.0130
2	23 21											

CURVE J=	NO.OF PTS. LL(J)	APPEARANCE POTENTIALS XO(J)	XX(J)	YY(J)	SLOPE S(J) AND SIGMA	B(J)	Y-INTERCEPT	INITIAL PT 1ST PT	LAST PT LP(J)	STANDARD DEVIATIONS YAVE	YSIG	XSIG
1	-0	-0.0000	-0.0000	-0.0000	0.0000	-0.0000	0.0000	-0	-0	-0.0000	-0.0000	-0.0000
2	16	9.2036	9.2036	0.0000	59.2001	0.3350	-544.8560	19	34	75.4438	0.4552	0.0077
3	20	9.2414	10.8579	97.9299	60.5842	0.1523	-559.8849	32	51	155.4300	0.4159	0.0069
4	12	9.2226	15.1037	355.1606	60.3902	0.2863	-556.9542	49	60	251.5417	0.4966	0.0082
5	7	8.2130	14.0251	290.0224	49.8998	0.8683	-409.8257	58	64	304.8857	0.7594	0.0152
6	15	7.1812	14.7482	326.1069	43.0958	0.2235	-309.4792	62	76	362.3467	0.6490	0.0151
7	12	6.7057	16.5136	402.1857	41.0066	0.2090	-274.9791	74	85	437.1500	0.4196	0.0102
8	6	9.6428	18.1966	471.2030	55.0866	0.4557	-531.1881	84	89	485.6333	0.3173	0.0058
9	4 154	4.1150	20.1217	577.2492	-4.3080	3.4594	663.9344	105	108	569.9500	1.0229	0.2374
			DAP(JJ)=	0.0350	ELECTRON VOLTS			SCATTERING	=-0.0165		BEAM ERROR	0.0119
3	31 27											

CURVE J=	NO.OF PTS. LL(J)	APPEARANCE POTENTIALS XO(J)	XX(J)	YY(J)	SLOPE S(J) AND SIGMA	B(J)	Y-INTERCEPT	INITIAL PT 1ST PT	LAST PT LP(J)	STANDARD DEVIATIONS YAVE	YSIG	XSIG
1	-0	-0.0000	-0.0000	-0.0000	0.0000	-0.0000	0.0000	-0	-0	-0.0000	-0.0000	-0.0000
2	16	9.2036	9.2036	0.0000	59.2001	0.3350	-544.8560	19	34	75.4438	0.4552	0.0077
3	14	9.2172	10.3211	66.1569	59.9276	0.2663	-552.3647	33	46	141.6929	0.3900	0.0065
4	17	9.2463	11.4473	133.6465	60.7197	0.1756	-561.4323	44	60	230.7235	0.5013	0.0083
5	6	8.3834	13.9987	288.5637	51.3887	0.6789	-430.8110	58	63	301.2167	0.4733	0.0092
6	14	7.2140	14.6192	320.4493	43.2736	0.2360	-312.1742	62	75	358.6714	0.6143	0.0142
7	13	6.7523	16.2979	393.0926	41.1804	0.1976	-278.0608	73	85	433.6538	0.4499	0.0109
8	6	9.6428	18.2025	471.5258	55.0866	0.4557	-531.1881	84	89	485.6333	0.3173	0.0058
9	4 154	4.1150	20.1217	577.2492	-4.3080	3.4594	663.9344	105	108	569.9500	1.0229	0.2374
			DAP(JJ)=	0.0300	ELECTRON VOLTS			SCATTERING	=-0.0142		BEAM ERROR	0.0108
1	16 14											

CURVE J=	NO.OF PTS. LL(J)	APPEARANCE POTENTIALS XO(J)	XX(J)	YY(J)	SLOPE S(J) AND SIGMA	B(J)	Y-INTERCEPT	INITIAL PT 1ST PT	LAST PT LP(J)	STANDARD DEVIATIONS YAVE	YSIG	XSIG
1	-0	-0.0000	-0.0000	-0.0000	0.0000	-0.0000	0.0000	-0	-0	-0.0000	-0.0000	-0.0000
2	13	9.1603	9.1603	0.0000	56.7860	0.3068	-520.1759	16	28	56.9769	0.2785	0.0049
3	11	9.2455	10.4314	72.1846	60.8658	0.4086	-562.7336	26	36	95.1909	0.3851	0.0063
4	10	9.1904	11.2077	119.4331	59.2047	0.3270	-544.1164	34	43	135.8400	0.2900	0.0049
5	20	9.2565	11.6055	142.9858	60.8707	0.1424	-563.4514	41	60	219.3550	0.4975	0.0082
6	6	8.3834	13.9887	288.0487	51.3887	0.6789	-430.8110	58	63	301.2167	0.4733	0.0092
7	11	7.3501	14.5741	318.1334	44.0386	0.2418	-323.6901	62	72	347.6727	0.4259	0.0097
8	12	6.8659	15.7986	372.0569	41.6511	0.1074	-285.9704	70	81	409.7083	0.2344	0.0056
9	6	6.4806	17.5062	443.1805	40.1958	0.6368	-260.4933	79	84	450.8833	0.4551	0.0113
10	6	9.6428	18.1786	470.2088	55.0866	0.4557	-531.1881	84	89	485.6333	0.3173	0.0058
			DAP(JJ)=	0.0250	ELECTRON VOLTS			SCATTERING	=-0.0118		BEAM ERROR	0.0097

Chart 3a. Typical linear extrapolation data.

J is the number of the curve or line; the first line is always the x-axis.

LL is the number of points that satisfied the extrapolation criteria.

XO and B are the intersection points of each line with the x-axis and y-axis respectively.

XX and YY are the coordinates for the intersection of two adjacent lines.

S and SIGMA represent the slope of the line and its standard deviation.

1st Pt and LP are the base point or first point and the last point of each line.

YAVE is the average ion current intensity reading for each series of points on a line.

YSIG and XSIG are the Student deviations in the ion current intensity readings and in the electron accelerating voltage.

DAP is the allowable error limit of the electron accelerating voltage; it determines the scattering limit.

BEAM ERROR is the percentage error allowed in the ion current reading; it determines the curvature limit.

Some of the advantages of computer applications are obvious. Note that the use of the computer plotting program eliminates the large amounts of manual analysis that

are otherwise necessary. The only manual labor required is reading the data and interpreting the results. The simplicity of conducting and analyzing ionization efficiency studies in this way, permits many more studies to be made in the same amount of time, yet, it yields numerical data which can be stored or treated in other ways. Furthermore, it removes most of the element of human judgement which can often produce biased, inaccurate results. It is also versatile since the data can be treated by several different mathematical methods and relationships.

5. Differential analysis

Whereas the method of linear extrapolation permits the determination of appearance potentials from large segments of an ionization efficiency curve, first and second differential plots magnify the details of such curves. This is quite obvious when the differentials at the point of intersection of two curves are compared to the differentials along the curves. Since only 70 to 100 data points are measured for each curve, simply taking the differences between points is not sufficient to produce smooth differential plots. For this purpose, a computer program was also written to determine the differentials of ionization efficiency curves from the numerical data. The data are read into an IBM 7074 computer and an interpolation subroutine (61a) is used to determine a total of 500 points spaced at intervals of 0.02 volts. The interpolation

procedure uses a preselected number of original data points and Legrangian interpolation. For this work 2 to 5 points are used. Note that two point interpolation is merely the same as a straight line interpolation between each two points.

A 5 point or a 7 point smoothing subroutine (61b) is also used to smooth the data either before or after the interpolation is completed. Normally the smoothing is completed only after interpolation so that the original data are not altered.

After the 500 points are generated, differentials are computed by taking the differences between each two readings or by taking an average of three of these differences. The final differentials are then plotted using a subroutine, GRAPH, (61c) and the IGM-1401, IBM-1627 Digital Plotting combination.

Variations of the above methods are used extensively, especially for double ions and fragment ions resulting from complex processes. With the exception of routine checks of the mathematical procedures and equations, all the calculations are carried out by means of an IBM 7074 computer.

VII. THEORETICAL DESCRIPTION OF IONIZATION EFFICIENCY CURVES

A. Introduction

The process of ionization is of such complexity that volumes have been written on the subject. For the ionization of very simple atoms and molecules some general methods of data treatment can be applied to yield significant accuracy. The necessary theoretical approximations can be made with adequate justification and only minor detrimental effects. The energy level schemes and transition rules are much simpler and better known for the inert gases than for most other gases. Also, more experimental and theoretical data are available for comparison and useage.

However, the ion source conditions, and the complexities of the molecules which most mass spectroscoptists are constrained to investigate, subject them to a more arduous task of interpreting and understanding the data. Wahrhaftig (52) presents a very commendable description of this plight.

Perhaps the most effective manner in which complex ionization processes can be interpreted and understood is to investigate first the basic processes and theories of ionization of simple compounds. This will help create better judgement of the feasibility and validity of assumptions which might be necessary to further improve the interpretation of ionization efficiency curves for more complex molecules.

The present work, attempts to provide a better understanding of both simple and complex ionization processes in a mass spectrometer by applying these basic principles to the ionization of Xe. Because a completely rigorous theoretical treatment of even this simple atomic ionization process is beyond the scope of this thesis, the treatment will be brief but pertinent to the development outlined below. It is hoped that the results of this detailed study of the ionization of Xe will provide a better basis for understanding complex ionization efficiency studies.

B. Ionization Processes

1. Atomic ions

As stated previously the ionization efficiency curves of the inert gases are the simplest, yet they entail much detail. The effects of the electron thermal energy distribution can be removed by mathematical (7, 56, 57, 58) or instrumental techniques (21, 29, 30); the effect of potential field penetrations can be eliminated by pulsing techniques; and the other effects which produce curvature of the ionization efficiency curve can be minimized. Never-the-less, the gas under study still may possess translational momentum and many excited electronic energy states.

The average translational energy of molecules within a gas is small, but its Maxwellian energy distribution is similar to the electron thermal energy distribution shown

in Fig. 2. The average electron thermal energy is only 0.2V, yet the total electron thermal energy imparts over a 0.5V tail to an ionization efficiency curve. It would appear then, that translational energy of a gas should also tend to limit the absolute resolution in ionization efficiency data. Even for an ideal study involving monoenergetic ionizing electrons and a linear threshold law, one would expect to observe a slight tail of length at least kT (approximately 0.02) for normal ion source conditions. There is a large uncertainty concerning the relationship between the temperature of the ion source and the average temperature of a gas molecule which is ionized in the electron beam. In this work it is assumed that the average molecular translational energy is due to a ion source temperature of 300°C. These translational energy distributions are seldom mentioned in ionization studies, however, workers who strive for high energy resolution should seriously consider this inherent energy distribution.

Recently, improved energy resolution and sensitivity of the mass spectrometer have enabled the investigation of electronic energy levels. The number of molecules or atoms, dN_N, in each electronic energy state, E_N, of degeneracy, g_N, is given by the Boltzman distribution,

$$dN_N = g_N \, e^{-E_N/kT} \qquad 34$$

for thermal population. Herzberg (62a, p. 160) states that in electrical discharges the population is approximately

equal to g_N. In a mass spectrometer where radiation from a hot filament or high electrical fields and a large amount of ionization within the electron beam exists, the population distribution is possibly between these two distributions. Nevertheless for normal mass spectrometer conditions the temperature is low enough and excited electronic energy states of neutral molecules and atoms are high enough above the ground state so that generally only the ground state is occupied. Oxygen, O_2, and nitrogen, N_2, are two exceptions (9, p. 104). Therefore, ionization can be considered as a transition from the ground state to some energy level at or above the ionization energy. If the neutral atom is excited to a discrete electronic energy level above the ionization potential, the process of pre-ionization or self-dissociation (often called autoionization) can occur (62a, p. 172). Morrison (62b, 62c) and Burns (63) have detected and explained many of these autoionization processes in their exemplary works on the ionization of Xe using mass spectrometers of high energy resolution.

Besides auto-ionization from excited states of the neutral atom or molecule, ionization can also result in the formation of excited states of the ion. The final result is that the ionization efficiency curve is a complex summation of ions resulting from all of these possible processes. Fig. 33 illustrates an ionization efficiency curve for Xe^+ with the $2p_{3/2}$ and the $2p_{1/2}$ excitation levels

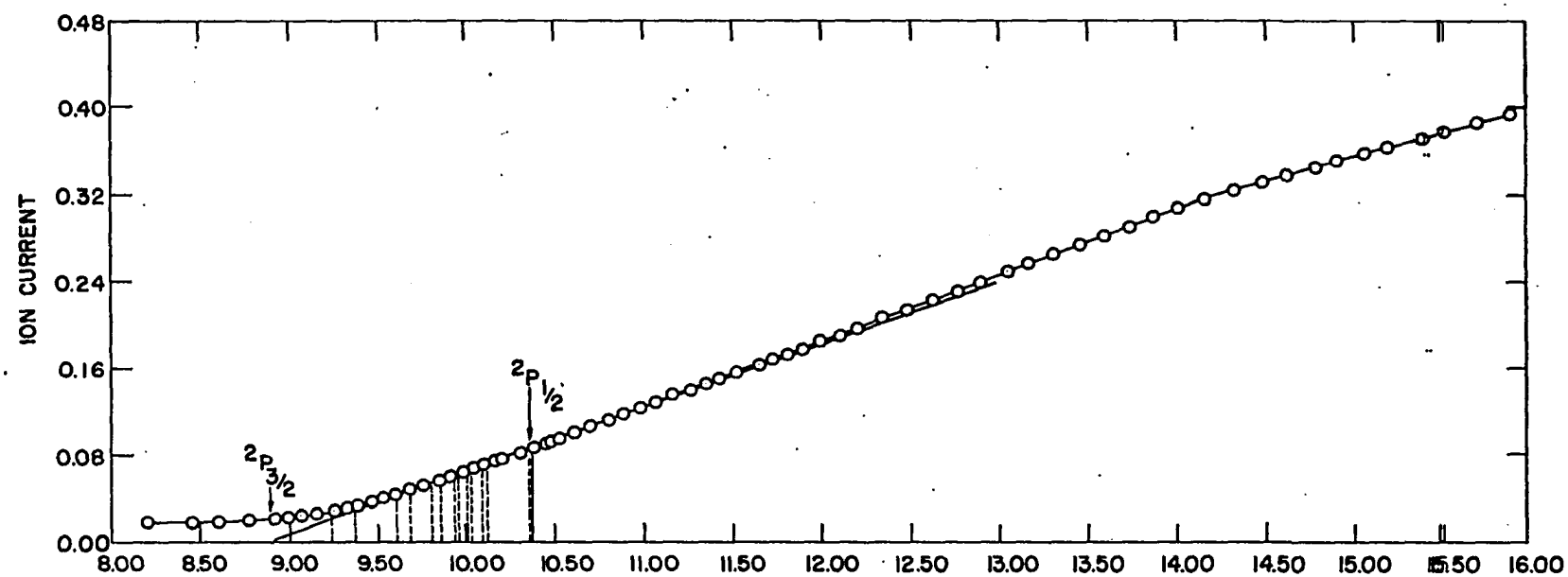

Fig. 33. Ionization efficiency curve for xenen.

indicated. The dotted lines indicate the excited states of the neutral atom from which autoionization can occur. The energies of these states were obtained from NBS Circular 467 (64).

2. Molecular parent ions

The ionization of molecules is a much more complicated process than is the ionization of inert gases. Diatomic molecules are the simplest, yet even these have complex vibrational and rotational energy levels in addition to the electronic states.

Furthermore, it is not valid to assure that all of the ionization takes place from the ground state when molecules are subject to the temperature of a typical ion source; especially if the vibrational energy states are closely spaced. For a single vibrational mode the population distribution of the vibrational energy levels is approximately (65)

$$\frac{N_i}{N_{tot}} = \left(\frac{1 - e^{-hv_i}}{kT} \right) - S_i \qquad 34$$

where $\frac{N_i}{N_{tot}}$ = fraction of molecules in the specified i.

v_i = vibrational frequency.

S_i = degeneracy.

It can be shown that when hv is significantly less than kT, many of the excited vibrational states are populated and the

process of ionization can occur from any one of them. For example, at 700°C only 89 percent of H_2O molecules are in their ground vibrational state and less than 32 percent of CO_2 molecules are in the ground state (65, 145)! Thus molecules which have many low lying vibrational energy levels may exhibit long tails in their ionization efficiency curves. It is especially apparent for complex molecules which have many vibrational modes. Recently, several papers have reported the observation of vibrational levels of simple molecules, although the studies on H_2^+ are perhaps the most widely known (66).

Just as ionization can arise <u>from</u> any occupied vibrational level of the molecule, it can proceed <u>to</u> any vibrational state of the ion. In general the final nuclear separation of the ionized molecule cannot be assumed to be the same as for the parent ion. This implies that the area of maximum overlap of the vibrational probability functions of the ground state and excited state potential energy curves <u>does not</u> occur at the same vibrational quantum number. In fact, there is a greater probability of forming the ion in an excited vibrational state than there is for forming it in the ground state.

Note that the ion or the original molecule may be in a ground electronic state and an excited vibrational state; in a ground vibrational state and an excited electronic state; or in either ground or excited states of both. These ionization processes are illustrated by the potential energy level

diagrams in Fig. 34. Potential energy Curve 1 is for the ground state of the molecule; Curve 2 for an excited electronic state of the molecule; Curve 3 for an excited state of the ion; and Curve 4 for an antibonding state of the molecule. The well-known Franck-Condon Principle involving δ -transition functions, and vertical transitions is generally applicable to ionization efficiency studies. This principle is adequately discussed in Field and Franklin (1). It must be stressed, however, that caution should be exercised in comparing appearance potential data to adiabatic values.

Most molecules also have higher rotational energy levels which are populated according to the following distribution function,

$$\frac{N_J}{N} = \frac{h(2J + 1)\ B}{kT}\ e^{-h(J + 1)B/kT} \qquad 35$$

where $B = \frac{h}{8\ ^2 I}$

I = the moment of inertia

J = rotational quantum number.

Whereas two adjacent rotational energy levels are very closely spaced, the total distribution may extend over a significantly wide energy range. For many molecules at normal temperatures, the energy of the most populous rotational level is approximately $\frac{kT}{2}$. Each rotational mode contributes this amount of energy to the molecule hence

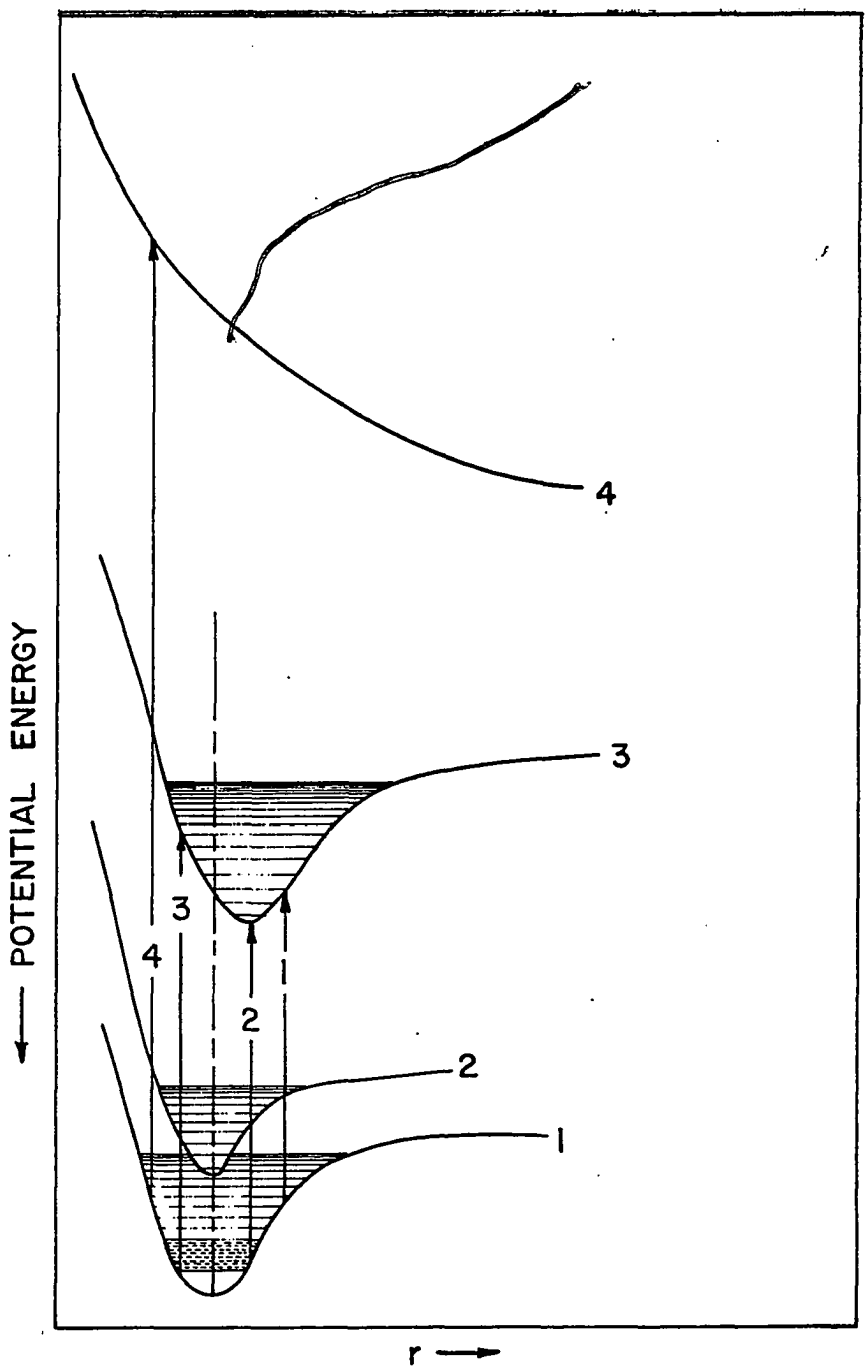

Fig. 34. Typical potential energy levels.

molecules having N rotational degrees of freedom would have an energy, $\frac{NkT}{2}$, above the ground state. Even at normal temperatures, where $\frac{kT}{2}$ is about 0.02 volts this can be significant.

It should be realized that the energy distributions which have been given above, express the minimum contribution from higher excited states. All of these energy distributions are also directly proportional to v, the radiation intensity encountered in the ion source. Further complexity is introduced because the wave functions for vibrational, rotational, and electronic energy states can interact to produce more energy levels, anharmonicity, and Fermi resonance.

3. Fragment ions

It is often difficult to distinguish the exact ionization process that corresponds to the observed appearance potential of a fragment ion. Some of the possible processes for the formation of fragment ion C^+ are indicated below.

a) $ABC \rightarrow ABC^{\neq} \rightarrow AB + C^+ + K.E.$

$\rightarrow \quad AB^{\neq} + C^+ + K.E.$

$\rightarrow \quad AB + C^{+\neq} + K.E.$

$\rightarrow \quad AB^{\neq} + C^{+\neq} + K.E.$

b) $ABC \rightarrow AB + C^+ + K.E.$

c) $ABC \rightarrow AB + C^+ + K.E.$

d) $ABC \rightarrow A + B + C^+ + K.E.$

Note that all of these processes can result in the various excited states, denoted by $\neq$, that are shown in (a). If the molecule is excited to a state above the appearance potential energy of the fragment ion, it can transfer excess kinetic energy, K.E., to the fragment ion when it dissociates. The resultant excess kinetic energy, K.E. can have values up to several volts. In addition to errors which arise due to electron thermal energy, excess kinetic energy, and excited electronic, vibrational and rotational energy levels, a large error can be introduced by a misinterpretation of the specific ionization process. Often, approximations of the relative energy of these different processes can be made and used to associate different breaks in ionization efficiency curves to the correct process. Threshold laws can also be observed over the entire curve in order to help distinguish the processes and determine if the process imparts excess kinetic energy to the fragment ion.

4. Multiply charges ions

The number of processes of formation and the number of occupied excited electronic, vibrational, and rotational states are even more numerous for the ionization of multiply charged ions than for singly charged ions.

$$
\begin{aligned}
AB + e^- &\rightarrow AB^{++} + 3e^- + K.E. \\
&\rightarrow AB^{+\neq} + 2e^- \rightarrow AB^{++} + 3e^- + K.E. \\
&\rightarrow AB^{\neq} + e^- \rightarrow AB^{++} + 3e^- + K.E. \\
&\rightarrow AB^{+\neq} + 2e^- \rightarrow AB^{++\neq} + 3e^- + K.E.
\end{aligned}
$$

$$\rightarrow A + B^{\neq} + e^{-} \qquad \rightarrow A + B^{++} + 3e^{-} + K.E.$$

$$\rightarrow AB^{+\neq} + 2e^{-} \qquad \rightarrow A + B^{++} + 3e^{-} + K.E.$$

$$\rightarrow A^{+} + B^{+\neq} + 2e^{-} \rightarrow A^{+} + B^{++} + 3e^{-} + K.E.$$

Several processes can result from successive collisions with electrons. Although the probability is small that already ionized or highly excited molecules undergo another electron collision, it may not be negligible. If double ionization occurs by a double collision process, then ions could be formed at electron energies approximately one half the second ionization potential. This type of process would be expected to result with a different threshold law than ionization by a single collision.

Whereas the probability is small for the occurrence of multiple collisions, the probability of forming multiple ions by other processes might also be small. In this case the ionization efficiency curve would tend to exhibit a long tail below the true ionization potential. Again, the investigation of threshold processes can sometimes divulge ample evidence to make possible a correct interpretation. Threshold laws are discussed in more detail later.

C. Previous Work

It has already been stated that initial workers assumed linear threshold laws for most ionization processes in appearance potential studies. The total number of ions, $N_i(V)$ formed at some electron energy, V, was expressed by,

$$N_i(V) = K(V - V_c) \qquad 36$$

where V_c is the appearance potential of the ion. Even when ionization efficiency curves exhibited long tails, a linear law was assumed and the tail was attributed to the electron thermal energy distribution. Honig (7) assumed that the number of ions formed at a given electron accelerating voltage, V_1 was the sum of ions formed in all electron energy states

$$E = U + V. \qquad 37$$

This implies that

$$N_i(V) = \int_0^\infty p(E)dN_e(U) \qquad 38$$

where $p(E)$ is the probability of ionization by an electron of energy, E, and $dN_e(U)$ is the Maxwellian thermal energy distribution of the electrons. He assumed that the threshold law was a function of the square of the energy in excess of the critical energy or appearance potential, V_c. Thus,

$$p(E) = 0 \qquad E \leq V_c \qquad 39$$
$$p(E) = C(E - V_c)^2 \qquad E \geq V_c$$

and

$$N_i(V) = \int_0^\infty C(E - V_c)^2 \frac{4\pi mAU}{h^3} Ue^{-\frac{\Phi+U}{kT}} dU. \qquad 40$$

Honig performed the integration to obtain the ion current as a function of the electron accelerating voltage,

$$N_i(V) = CT^2e^{-\Phi/kT}[6k^2T^2 + 4kT(V-V_c) + (V-V_c]^2. \qquad 41$$

taking logarithms and differentiating with respect to V, he obtained,

$$\frac{d(\ln N_i(V))}{dV} = \frac{-1}{(V_c-V) + 3kT} + \frac{1}{kT} \qquad 42$$

and for the appearance potential, $V = V_c$, he obtained the expression used for the critical slope method of interpreting ionization efficiency curves. Unfortunately this treatment is subject to three sources of error. First, the effects of potential gradients, space charge, excited states, and some of the other parameters mentioned earlier can affect the slope. Secondly, the assumption of a square threshold law is not theoretically or experimentally justified for all ionization processes. Third the law applies to the process of ionization within the ionization chamber, not at the collector.

Honig also found that a similar plot would give critical slopes at energies of $[n/(n+1)]kT$ for processes dependent upon the nth power of the excess energy of the electrons. Recently Barfield and Wahrhaftig (67) found that for complex parent ions the critical slope is more closely indicated by $\frac{n+1}{(n+2)kT}$ and for simple atoms and molecules, by $\frac{1}{2kT}$. Furthermore, they state that the activation energy for fragmentation processes makes it difficult to determine the appropriate critical slope since it may range from $\frac{0.67}{kT}$ to $\frac{0.85}{kT}$.

Morrison has given two analytical treatments (55a, 55b, 55c, 59). He assumes that ionization efficiency for a single process is given by

$$\rho(V) = \int P(E) e^{-(E-E_c)/E_c)^s} \; n(E-E_c)dE \qquad 43$$

where P(E) is the probability of energy transfer,

$$P(E) \alpha \int \cdots\cdots\cdots\cdots\cdots \int_{o}^{E} (E-E_c)dE^n. \qquad 44$$

The freedom factor, n, is proportional to the number of electrons leaving the collision process and the structural factor, s, is dependent upon the characteristics of the molecule being ionized. He further calculates, that the total ionization efficiency is,

$$N_i(V) = K_1\rho_1(V) + K_2\rho_2(V) + \cdots \qquad 45$$

for all of the processes. The coefficients, K_i, are the relative transition probabilities for ionization.

A second method used by Morrison (60a, 60b) consists of removing the electron thermal energy by a deconvoluting technique involving Fourier transforms. In this method the random scattering of data is essentially smoothed. The ionization of He^+ is assumed to follow a linear threshold law and its ionization efficiency curve is then used as an indication of electron thermal energy effects. This technique gives surprising improvements on energy resolution. Note that it includes a slightly different basis for subtracting out electron thermal energy since a Maxwellian

Run	Date	Pressure (Torr)	Trap Current	Anode Voltage	Retarding Voltage	Repeller Voltage	Observed Appearance Potential $^2P_{1/2}$	Correction
-	4/8/65	-	1.4	c	c	13.68	13.68	-0.237
-	5/4	-	10.3	c	c	13.73	13.73	-0.287
-	5/15	-	-	c	c	12.78	12.78	0.763
1	7/13	0.42	20.	4.885	-0.212	7.75	8.44	4.527
3	8/14	0.24	8.	4.862	-0.205	1.47	11.15	2.29
5	8/24	1.2	4.	5.248	-0.487	1.09	12.05	1.39
6	8/27	1.0	6.6	3.867	0.262	1.476	12.40	1.04
7	8/27	0.95	6.6	3.871	0.0125	1.393	-	0.93
8	8/27	0.95	6.6	3.849	-0.202	1.369	11.15	0.98
9	8/27	1.0	6.6	3.806	-0.405	1.273	12.13	1.31
10	8/27	0.9	6.6	3.760	-0.5993	1.259	12.19	1.37
11	8/27	0.95	6.6	3.706	-0.789	1.231	12.35	1.09
12	8/27	0.9	6.6	3.630	-1.008	1.219	12.28	1.16
13	1/21/66	0.63	0.8	7.997	8.033	4.897	-	9.863
14	11/8/65	0.6	12.2	3.036	-0.732	2.489	11.31	2.13
15	11/12	0.5	11.8	3.006	-0.0649	5.237	10.10	3.34
16	11/10	0.5	11.8	3.089	-0.0491	4.671	10.40	3.04
17	11/10	0.5	11.8	3.0125	-0.072	4.092	10.57	2.87
17a	11/10	0.5	11.7	3.008	-0.0299	3.510	10.80	2.64
18	11/10	0.6	11.7	3.000	-0.0699	2.994	10.80	2.64
19	11/10	0.6	11.7	2.973	-0.479	2.490	10.95	2.49
20	11/11	0.38	11.8	3.112	0.0205	2.008	11.45	1.99
21	11/11	0.38	11.7	3.111	0.0380	1.508	11.70	1.74
22	11/11	0.5	10.8	4.625	-0.2245	3.297	12.10	1.34
23	11/11	0.6	10.8	4.625	-0.2245	3.297	12.10	1.34
24b	11/30	0.9	10.0	5.488	-0.228	3.127	10.92	2.52
24a	12/14	1.1	7.9	6.060	-0.119	3.146	10.43	3.01

Chart 3b. Ionization efficiency data for Xe.

Run	Date	Pressure (Torr)	Trap Current	Anode Voltage	Retarding Voltage	Repeller Voltage	Observed Appearance Potential $^2P_{1/2}$	Correction
26-P	2/3	1.0	2.3	6.102	-0.121	4.009	11.9	1.54
27-P	2/3		2.3	6.587	-0.441	3.247	11.98	1.46
28-P	2/4	1.0	3.3	6.626	-0.494	2.49	12.45	0.99
29-P	2/4	1.0	5.0	6.847	-0.238	2.479	12.9	0.54
30-P	2/4	1.1	5.0	6.924	6.725	2.5023	12.33	
31-P	2/4	1.0	13.0	7.281	7.295	2.452	12.6	0.84
32	2/9	0.7	5.0	8.155	8.248	5.117	10.90	2.54
33	2/9	0.9	4.9	7.966	8.251	6.015	10.93	2.51

C = conventional

P = pulsed

Chart 3b. continued. Ionization efficiency data for Xe.

distribution is not necessarily assumed. Recently Hutchison (16) has measured electron thermal energy distributions and concluded that they are not Maxwellian. Furthermore, Marmet (17) has calculated from theoretical viewpoints that it is not Maxwellian. Both have also concluded that the electron thermal energy distribution changes as the electron accelerating voltage is changed.

D. Present Work

All of the previous methods either require a calibration curve to analytically correct the data, or they assume apriori knowledge of the true appearance potentials, and excited states before they are employed. The various ionization efficiency studies which were conducted and are discussed and treated throughout this thesis are listed in Chart 3b. In the present work a somewhat different technique is attempted. An analytical expression is derived for the ionization efficiency using both a linear threshold assumption and a general empirical cross section equation. For simplicity, a Maxwellian electron thermal energy distribution is used. Estimates of the absolute sensitivity of the mass spectrometer detection limit and the ion transmission coefficient are made and included in the calculations. Previous treatments by others use the experimental data per se without relating the ionization efficiency data directly to the actual conditions which exist in the ion source. Since the theory of concern is applicable to the ion source conditions,

the data in this work are corrected for instrument sensitivity and transmission in an attempt to relate the data to existing ion source conditions.

In the derived analytical expression for the ionization efficiency, two unknown terms are always present. Neither the actual critical voltage or appearance potential, V_c, nor the proportionality constant, C, are known,

$$N_i(V) = Cf(V, V_c, T, U) \qquad 46$$

This function is such that when the <u>true</u> appearance potential, V_c, is encountered in the calculations, C remains constant over a wide range of the data. The principle of this treatment is to apply the IBM 7074 computer and the following brute force method of solving a series of equations for two unknowns, C, and V_c, by a process of iteration.

1. The data points are all related to the actual absolute ion currents within the ion box.
2. The appearance potential, V_c, is estimated and the value C is computed for each datum point.
3. The value, V_c, is incremented by a small amount and the value of C is again calculated for each point.
4. The process of iteration is completed several times until V_c has been varied from slightly below the expected appearance potential to slightly above it. The values of C are calculated for the entire data set during each cycle.

5. The value of V_c for which C remains constant over a wide range of data points is taken as the true appearance potential.
6. The value of the constant, C, is useful as a direct approximation to the relative cross section of ionization.

Two different threshold laws are treated using this method. First, the linear threshold law is assumed and the ionization efficiency is calculated for the ion source region. A pseudo-Maxwellian thermal energy distribution is used,

$$dN_e = \frac{4\pi mUAe^{-(\ +U)/kT}}{h^3}\ dU. \qquad 47$$

Then from Eq. 45 the ionization efficiency is given by,

$$N_i(v) = \int_a^b (E)dN_e \qquad 48$$

where $\rho(E)$ is the probability of ionization. In this work, the data were often obtained using a retarding potential of energy, a, hence in the calculations the lower integration limit is a. The use of the retarding potential was found to give much better ionization efficiency data than did a conventional or Schiff method. Ionization efficiency curves were made under the various ion sources modes and conditions shown in Fig. 35. A straight line is drawn through the portion of each ionization efficiency curve that represents the $2p_{3/2}$ electronic state. It can be noted that less tailing occurs for large retarding potentials. The upper limit, b, is

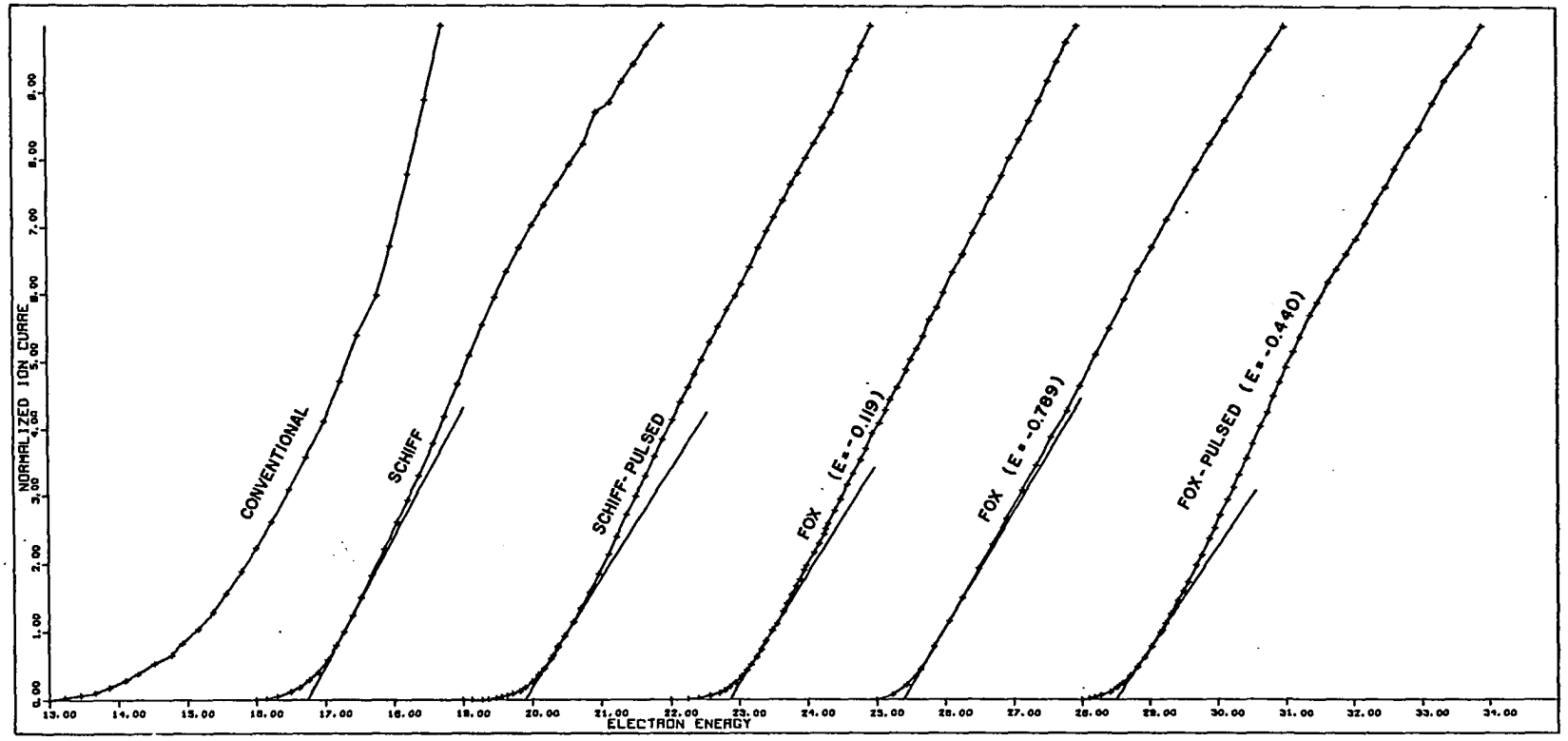

Fig. 35. Ionization efficiency of Xe^+ using various ion source modes.

normally very large for a Maxwellian distribution. In the computer program, Simpson's rule is used to evaluate some integrals, hence the iteration is completed to an upper integration, b, beyond which no further increase contributes significantly to the value of the integral. When a retarding potential difference method is used, b represents the upper limit of the second retarding potential. For a linear threshold law,

$$Q = C_1(E-E_c)$$

and

$$N_i(\ ) = C_1 \int_a^b \frac{4\pi mAU}{h^3} e^{-(\Phi+U)/kT} (E-E_c)dU \qquad 49$$

where the electron energy, E, is the sum of the electron thermal energy, U, and the electron accelerating voltage, V;

$$E = U + V$$

Thus

$$N_i = \frac{4\pi mA}{h^3} e^{-\Phi/kT} C_1 \int_a^b Ue^{-U/kT} (U+V-E_c)dU \qquad 50$$

and letting $K = \frac{4\pi mAe^{-\Phi/kT}}{h^3}$ 51

$$N_i = KC_1 \int_a^b (U^2 + UV - U) E_c e^{-U/kT} dU \qquad 52$$

or,

$$N_i = KC_1 \left[\int_a^b U^2 e^{-U/kT} dU + \int_a^b U(V-E_c)e^{-U/kT} dU \right] \qquad 53$$

Evaluating the two integrals and simplifying,

$$N_i = \int_a^b \left[KC_1(-kTU^2 e^{-U/kT} - 2(kT)^2 U e^{-U/kT} - 3(kT)^3 e^{-U/kT} \right.$$
$$\left. -(U(kT)^2 e^{-U/kT} - (kT)^3 e^{-U/kT})\ (V-E_c) \right] \qquad 54$$

and evaluating between the limits,

$$N_i = 4\pi mAe^{-\Phi/kT}\ kT \left[e^{-a/kT}(a^2 + 2kTa + 3(kT)^2 \right.$$
$$\left. (V-E_c) - e^{-b/kT}\ (b^2 + 2kTb + 3(kT)^2) \right]\ C_1 \qquad 55$$

This equation represents the theoretical ionization efficiency for ionization within the ion source assuming a linear threshold. It can be related to the actual ionization efficiency data observed at the collector by considering the ion transmission coefficient T_r, and the absolute sensitivity, S, of the instrument. The sensitivity, S, is composed of two terms, the vibrating reed minimum response, V_r, and the average noise level, N_o, of the instrument. A 100 percent efficiency is assumed for the amplifier and recorder system. From this,

$$S = V_r + N_o \qquad 56$$

The input of the vibrating reed is amplified by a factor of 10^8 and measured across a 5K ohm resistor. The minimum voltage that is readable during most ionization efficiency studies is approximately 0.1 millivolt. From this the vibrating reed sensitivity is calculated as,

$$V_r = \frac{1 \times 10^{-4}}{5 \times 10^3 \times 10^8} = 2 \times 10^{-16} \text{ amperes.}$$

Adding the average noise level of approximately 0.1 millivolt decreases the absolute sensitivity, S, to about 4×10^{-16} amperes. This sensitivity can be increased slightly by using the KinTel amplifier by increasing the signal-to-noise ratio. The coefficient for the transmission of ions from the ion box to the collector was not measured but rather it was estimated to be about one percent[1]. The measured ion current, N_m, is related to the actual ion current in the ion source, N_i, by the relationship,

$$N_m = T_r N_i - S \qquad 57$$

The values, N_m, are measured and used to compute the values, N_i,

$$N_i = \frac{N_m + S}{T_r} \qquad 58$$

Combining this equation with Eq. 55 and solving for the reciprocal of C_1, one gets,

$$C_1^{-1} = T_r \frac{4\pi mAkT}{h^3(N_m+S)} e^{-\frac{d}{}}[(a^2+2akT+3(kT)^2)\ e^{-a/kT}(V-E_c)$$

$$-(b^2+2bkT+3(kT)^2)\ e^{-b/kT}] \qquad 59$$

Note that calculating the value of C_1^{-1} instead of C_1 yields a number in units of cm^2 which is directly proportional to the actual cross section of ionization.

---

[1]Flesch, G. D. [Concluded from a private discussion]. Ames, Iowa, Ames Laboratory of Atomic Energy Commission. ca. 1965.

In order to use the measured values of ion current, N_m, for these calculations they are first converted to the actual number of ions formed in the source region. This is done by converting them to amperes, thence to the actual number of ions striking the collector. It is assumed that the ions striking the collector exhibit 100 percent charge transfer, to the vibrating reed input. For this conversion;

$$N_m = \frac{1 \times 10^{-3} V \times 6.281 \text{ esu}}{5 \times 10^3 \ \Omega \times 10^8 \times \text{amperes}} \qquad 60$$

after which Eq. 58 relates these values to N_i.

The assumption of a linear threshold law introduces some major disadvantages into the calculations. Note that the linear law predicts a monatomic increase of N_i with E, whereas a maximum is always observed in ionization efficiency curves. Secondly, the linear law is assumed for a large segment of the curve whereas often only a small part of it fits a linear law. These calculations were initially proposed for several reasons. One was to attempt to find an equation for ionization cross sections which would fit the data. Once an acceptable threshold law was found, it was hoped that contributions from lower excited states could be calculated and successively subtracted from the total ionization curve thereby breaking it down into its basic ionizing processes.

The second application of the computer involves using cross section equations rather than trying to propose

ionization threshold laws as previous workers have done. The specific equation used was that derived by Gsyzinski (68a, 68b, 68c, 69a, 69b) for simple atoms and molecules. The probability of ionization $\rho(E)$, in Eq. 48 is replaced by Gryzinski's equation,

$$Q = \rho(E) = N_e(\pi e^4/I^2)g_G(E_c/I) \qquad 61$$

where

$$g_G = \frac{1}{X}\left[\left(\frac{X-1}{X+1}\right)^{3/2}\left(1+\frac{2}{3}\left(1-\frac{1}{2X}\right)\ln\left(e+(X-1)^{1/2}\right)\right)\right] \qquad 62$$

and

$$X = E/I.$$

Making the substitution and including the electron thermal energy distribution, one obtains the complete expression

$$N_i = C_1 \int_a^b Tr \frac{4\pi mAe^{-\phi/kT}}{h^3(N_m+S)} N_e \frac{(\pi e^4)}{I^2} \frac{E}{I} g_G U e^{-U/kT} dU \qquad 64$$

where

$$g_G = \frac{I}{E}\left(\frac{E-I}{E+I}\right)^{3/2}\left(1+\frac{2}{3}\left(\frac{2E-I}{2E}\right)\ln\left(e+\left(\frac{E-I}{I}\right)^{1/2}\right)\right) \qquad 65$$

Inspection of this equation reveals two things. One, as E approaches I, N_i approaches zero <u>linearly</u> and two; if $E < I$, N_i is also less than zero. This latter result is not physically possible but analytically feasible due to ionization from excited states which may be populated. The second factor is eliminated by either of two ways. The probability of ionization for $E < I$ is assumed to be zero for simplicity, or Gryzinski's <u>general</u> equation is used to calculate the

probability of ionization from excited states when E < I. The latter method would also require calculating the probability of excitation within the ion source. For the case of Xe^+, only values of E ≥ I are considered. If one uses the relationships,

$$E = U + V$$

and

$$K = \frac{4\pi mAe^{-\Phi/kT}}{h^3} N_e \pi e^4$$

then N_i can be simplified to,

$$N_i = \frac{C_1 K}{I(N_m - S)} \int_a^b \left(\frac{E-I}{E+I} \right)^{3/2} U e^{-U/kT} dU + \frac{C_1 K}{I(N_m - S)} \frac{2}{3} \int_a^b \left(\frac{E-I}{E+I} \right)^{3/2} \left(\frac{2E-I}{2E} \right) U e^{-U/kT} \ln\left(e + \left(\frac{E-I}{I} \right)^{1/2}\right) dU \quad 66$$

The computer program as described is used with Eq. 57 and 66 to calculate the values of C_1 at each datum point for each value of V_c. The portion of data for which C_1 is constant throughout the greatest range of data points is considered as the best fit of the theoretical equation. The value of V_c from which these data resulted is taken to be the uncorrected appearance potential. It can be noted from Chart 4 that for an critical voltage of 8.95 volts, the value of C_1 is nearly constant for points 16 through 39. This corresponds with the data from the linear extrapolation program which lists 9.23 as the extrapolated appearance potential for points 18 to 57. Three factors would tend to give the lower calculated value.

METHOD TWL

CRITICAL VOLTAGE =	8.804300	8.954300	9.029300	9.104300	9.179300	9.254300	9.329300	9.404300
EAV = NO. IONS	82 VALUES FOR EACH OF ABOVE CRITICAL VOLTAGES USED.							
8.204300	0.000300-0.361 02E	C2-0.89452E	C2-0.88780E	C2-0.88112E	02-0.87421E	C2-0.86713E	C2-0.85969E	C2-0.85248E C2
8.453900	0.000700-0.905 70E	02-0.89931E	C2-0.89280E	02-0.88616E	02-0.87939E	02-0.87246E	C2-0.86528E	C2-0.85813E C2
8.600000	0.001100-0.90 82E	02-0.90356E	C2-0.89719E	02-0.89070E	02-0.88409E	02-0.87734E	C2-0.87044E	C2-0.86338E C2
8.779400	0.002100-0.90573E	02-0.90746E	C2-0.90117E	02-0.89482E	02-0.88833E	02-0.88171E	02-0.87455E	C2-0.86805E C2
8.912200	0.003400-0.90 3+0E	02-0.90165E	C2-0.90329E	C2-0.897C5E	02-0.89071E	02-0.88425E	02-0.87767E	02-0.87055E C2
8.995100	0.004500-0.90154E	02-0.89946E	C2-0.89729E	02-0.89933E	02-0.89307E	02-0.88671E	02-0.88023E	C2-0.87362E C2
9.067900	0.006000-0.89945E	02-0.89744E	C2-0.89536E	02-0.89319E	02-0.89573E	02-0.88947E	02-0.88311E	C2-0.87662E C2
9.182400	0.008000-0.89711E	02-0.89516E	C2-0.89314E	02-0.891C5E	02-0.89887E	02-0.88640E	02-0.88CC1E	C2-0.87359E C2
9.252000	0.010700-0.89553E	02-0.89364E	C2-0.89167E	02-0.88964E	02-0.88753E	02-0.88533E	02-0.88984E	C2-0.88254E C2
9.321900	0.013200-0.89426E	C2-0.89242E	C2-0.89051E	02-0.88854E	02-0.88650E	02-0.88437E	02-0.88216E	C2-0.88486E C2
9.381600	0.015800-0.89250E	02-0.89069E	C2-0.88882E	02-0.88688E	02-0.88488E	02-0.88279E	C2-0.88063E	C2-0.87837E C2
9.443100	0.019600-0.89202E	02-0.89029E	C2-0.88850E	02-0.88666E	02-0.88476E	02-0.88279E	C2-0.88074E	C2-0.87861E C2
9.528600	0.022600-0.89115E	02-0.88947E	C2-0.88774E	C2-0.88596E	02-0.88412E	02-0.88221E	02-0.88024E	C2-0.87819E C2
9.598300	0.026200-0.89014E	02-0.88851E	C2-0.88683E	C2-0.88510E	02-0.88331E	02-0.88147E	02-0.87957E	C2-0.87759E C2
9.684700	0.030700-0.88930E	02-0.88768E	C2-0.88602E	C2-0.88431E	C2-0.88255E	C2-0.88073E	02-0.87885E	C2-0.87691E C2
9.755200	0.033800-0.88922E	02-0.88663E	C2-0.88500E	C2-0.88332E	C2-0.88159E	C2-0.87981E	C2-0.87757E	C2-0.87606E C2
9.847700	0.039100-0.88793E	02-0.88639E	C2-0.88481E	C2-0.88319E	C2-0.88152E	C2-0.87980E	C2-0.87802E	C2-0.87619E C2
9.907200	0.042500-0.88767E	02-0.88617E	C2-0.88464E	02-0.88307E	02-0.88145E	C2-0.87979E	02-0.87808E	C2-0.87632E C2
9.981600	0.046500-0.88773E	02-0.88629E	C2-0.88481E	C2-0.88330E	C2-0.88175E	02-0.88016E	02-0.87852E	C2-0.87684E C2
10.042699	0.050100-0.88766E	02-0.88626E	C2-0.88482E	C2-0.88336E	02-0.88185E	02-0.88031E	C2-0.87872E	C2-0.87709E C2
10.099099	0.053300-0.88766E	02-0.88639E	C2-0.88492E	C2-0.88350E	02-0.88204E	C2-0.88056E	02-0.87903E	C2-0.87746E C2
10.161299	0.057000-0.88779E	02-0.88646E	C2-0.88510E	02-0.88372E	02-0.88230E	C2-0.88086E	C2-0.87937E	C2-0.87785E C2
10.199199	0.059200-0.88743E	02-0.88614E	C2-0.88482E	C2-0.88348E	02-0.88211E	02-0.88070E	C2-0.87927E	C2-0.87780E C2
10.306000	0.064700-0.88752E	02-0.88626E	C2-0.88498E	C2-0.88367E	C2-0.88234E	C2-0.88098E	C2-0.87959E	C2-0.87816E C2
10.378699	0.068800-0.88747E	C2-0.88624E	C2-0.88499E	C2-0.88371E	02-0.88241E	02-0.88109E	C2-0.87973E	C2-0.87835E C2
10.448599	0.072700-0.88754E	02-0.88634E	C2-0.88511E	C2-0.88386E	C2-0.88259E	02-0.88129E	02-0.87957E	C2-0.87862E C2
10.478000	0.075300-0.88782E	02-0.88664E	C2-0.88544E	C2-0.88423E	C2-0.88299E	C2-0.88173E	02-0.88044E	C2-0.87913E C2
10.522500	0.077700-0.88780E	C2-0.88665E	C2-0.88549E	C2-0.88431E	C2-0.88311E	C2-0.88189E	C2-0.88065E	C2-0.87939E C2
10.605599	0.083200-0.88760E	C2-0.88647E	C2-0.88533E	C2-0.88417E	02-0.88300E	02-0.88180E	02-0.88058E	C2-0.87934E C2
10.691699	0.088300-0.88738E	C2-0.88628E	C2-0.88516E	C2-0.884C2E	02-0.88287E	C2-0.88170E	C2-0.88050E	C2-0.87929E C2
10.800000	0.094400-0.88733E	C2-0.88625E	C2-0.88515E	C2-0.884C4E	02-0.88291E	02-0.88177E	02-0.88C60E	C2-0.87942E C2
10.882299	0.099400-0.88714E	C2-0.886C8E	C2-0.885C1E	C2-0.88352E	02-0.88282E	02-0.88170E	C2-0.88C56E	C2-0.87940E C2
10.985899	0.105800-0.88727E	02-0.88623E	C2-0.88513E	C2-0.88406E	02-0.88294E	02-0.88182E	02-0.88C84E	C2-0.87971E C2
11.065299	0.110700-0.88708E	C2-0.88607E	C2-0.885C4E	02-0.884C0E	02-0.88294E	02-0.88187E	C2-0.88078E	C2-0.87968E C2
11.162000	0.117400-0.88728E	C2-0.88629E	C2-0.88529E	C2-0.88427E	02-0.88324E	02-0.8822CE	02-0.88115E	C2-0.88CC8E C2
11.260399	0.122200-0.88743E	02-0.88646E	C2-0.88548E	C2-0.88449E	C2-0.88349E	C2-0.88248E	C2-0.88145E	C2-0.88041E C2
11.347500	0.127600-0.88769E	C2-0.88675E	C2-0.88580E	C2-0.88483E	02-0.88386E	02-0.88288E	C2-0.88189E	C2-0.88087E C2
11.423000	0.132300-0.88783E	C2-0.88691E	C2-0.88599E	C2-0.885C4E	02-0.88409E	02-0.88313E	02-0.88216E	C2-0.88118E C2
11.522599	0.137900-0.88776E	C2-0.88686E	C2-0.88595E	C2-0.885C3E	02-0.8841CE	02-0.88316E	02-0.88221E	C2-0.88125E C2
11.646399	0.145500-0.88804E	02-0.88716E	C2-0.88627E	C2-0.88537E	C2-0.88447E	C2-0.88355E	C2-0.88263E	C2-0.88169E C2
11.720399	0.149900-0.88811E	C2-0.88725E	C2-0.88637E	C2-0.88549E	C2-0.88460E	C2-0.88370E	C2-0.88280E	C2-0.88188E C2
11.805000	0.154900-0.88826E	C2-0.88741E	C2-0.88656E	C2-0.88569E	C2-0.88482E	C2-0.88394E	C2-0.883C6E	C2-0.88216E C2
11.896199	0.160100-0.88835E	C2-0.88752E	C2-0.88668E	C2-0.88583E	C2-0.88498E	C2-0.88412E	C2-0.88326E	C2-0.88238E C2
11.998500	0.167400-0.88847E	02-0.88765E	C2-0.88683E	C2-0.886C0E	C2-0.88516E	C2-0.88432E	C2-0.88347E	C2-0.88262E C2
12.106599	0.172800-0.88855E	C2-0.88774E	C2-0.88694E	C2-0.88612E	02-0.88530E	C2-0.88448E	C2-0.88365E	C2-0.88281E C2
12.203299	0.179300-0.88944E	02-0.88765E	C2-0.88685E	02-0.88605E	02-0.88525E	C2-0.88444E	C2-0.88362E	C2-0.88280E C2
12.342899	0.188200-0.88943E	02-0.88765E	C2-0.88687E	C2-0.886C8E	02-0.88529E	C2-0.88450E	02-0.88369E	C2-0.88289E C2
12.474500	0.196100-0.88945E	02-0.88768E	C2-0.88691E	C2-0.88613E	C2-0.88537E	C2-0.88458E	C2-0.88378E	C2-0.883C0E C2
12.630500	0.205600-0.88854E	C2-0.88780E	C2-0.88704E	C2-0.88620E	02-0.88552E	C2-0.88476E	C2-0.88359E	C2-0.88321E C2
12.770199	0.214000-0.88965E	02-0.88791E	C2-0.88717E	C2-0.88643E	02-0.88568E	C2-0.88493E	C2-0.88417E	C2-0.88341E C2
12.893699	0.221600-0.88964E	02-0.88791E	C2-0.88719E	C2-0.88645E	02-0.88571E	C2-0.88497E	02-0.88422E	C2-0.88347E C2
13.050399	0.231100-0.88892E	02-0.88810E	C2-0.88738E	C2-0.88666E	C2-0.88594E	C2-0.88521E	C2-0.88448E	C2-0.88375E C2
13.167299	0.238700-0.88880E	02-0.88808E	C2-0.88738E	C2-0.88667E	C2-0.88595E	C2-0.88524E	C2-0.88452E	C2-0.88379E C2
13.406399	0.247C00-0.88887E	02-0.88814E	C2-0.88748E	C2-0.88678E	02-0.88608E	C2-0.88537E	C2-0.884C6E	C2-0.88354E C2
13.457399	0.255400-0.88899E	02-0.88821E	C2-0.88752E	C2-0.88682E	C2-0.88613E	C2-0.88543E	C2-0.88473E	C2-0.884C3E C2

Chart 4. C_1 values.

First, the ionization efficiency curve was obtained without pulsing techniques, thus repeller gradients were present. Second, the retarding potential was only 0.119 volts. Third, the calculations relate the data to actual ion source conditions. All of these factors produce curvature at the lower end.

Whereas the analytical technique can compensate for this curvature, the linear extrapolation cannot. It is also possible that the lowest state, $2P_{3/2}$ was missed by one or both treatments.

The effect of repeller potential gradients upon the results could be determined by including a mathematical approximation of them in the calculations;

$$N_i = f(Q, E, V, T) + f(\Delta V_g) \qquad 67$$

where $f(\Delta V_g)$ represents the function due to potential gradients within the ionizing region of the ion source. The values of T_r, T, and S can also be varied in order to find a better fit for the experimental data or measurements could be made to determine them more precisely. It would be especially valuable to know the true ion transmission coefficient and instrument sensitivity, for then the actual cross sections of ionization could be computed using the values of C_1. Note that in order to relate C_1 to cross section, Q, it is necessary to know the absolute ion source pressure due to the specific isotopic species being studied, the electron beam

intensity, and the effect of ion source potential gradients upon the transmission coefficient and electron energy spread.

Although the analytical technique just described is mathematically complex, requires a computer, and does not actually improve the precision of results, several important conclusions are evident and further improvements could be made by extending the mathematical treatment.

1. This method illustrates that a purely analytical method can be used without a prior knowledge of the appearance potentials and without a calibrating gas.
2. It suggests that appearance potential results appear to be slightly lower in value when the appearance potential data are related to ion source conditions.
3. This method can also be used to investigate the theories of ionization and cross sections.
4. By including appropriate functions, one can investigate field gradients within the ion source, electron thermal energies, threshold laws, and the effects of excited energy levels.
5. It also illustrates the difficulty in determining true excited states and their cross sections. It appears that this method is very difficult to use in determining excited states unless the states are well separated in energy and the cross section equation is known and similar for each state. In Fig. 36 this problem is indicated very well. Curves

A through E represent some of the possible ionization efficiency curves for each of several processes having onset energies 1 through 5 respectively. Processes very similar to these could occur in an actual ion source. It must be realized that Fig. 36 is only a small enlarged portion of a possible ionization efficiency curve. The final observed ionization efficiency curve is indicated by the summation, A + B + C + D + E, of ions formed from all of these processes. It was stated that differential plots of ionization efficiency curves magnify detailed structure. Often an inflection point on a real curve may be so obscure that it is almost imperceptible to the eye whereas on a differential plot it is seen very easily. If Fig. 36 is reduced by a factor of 10, point C is difficult to see. Yet if the second differential is examined in the vicinity of point C, it can be seen that it goes from a negative value to a larger positive value and back to a negative value. It can also be shown that even using a Maxwellian electron energy distribution, processes of relatively close energy separations can still be detected. One of these ionization efficiency curves of Xe^+, expanded along the energy axis, is shown in Fig. 33 with the energy levels of XeI superimposed between the $2P_{3/2}$ and the $2P_{1/2}$ state of XeII. This curve was obtained using the ion source in the Fox mode with a retarding potential of 0.112 volts. A total of 108 points were taken during the run. Close observation of this curve reveals many small

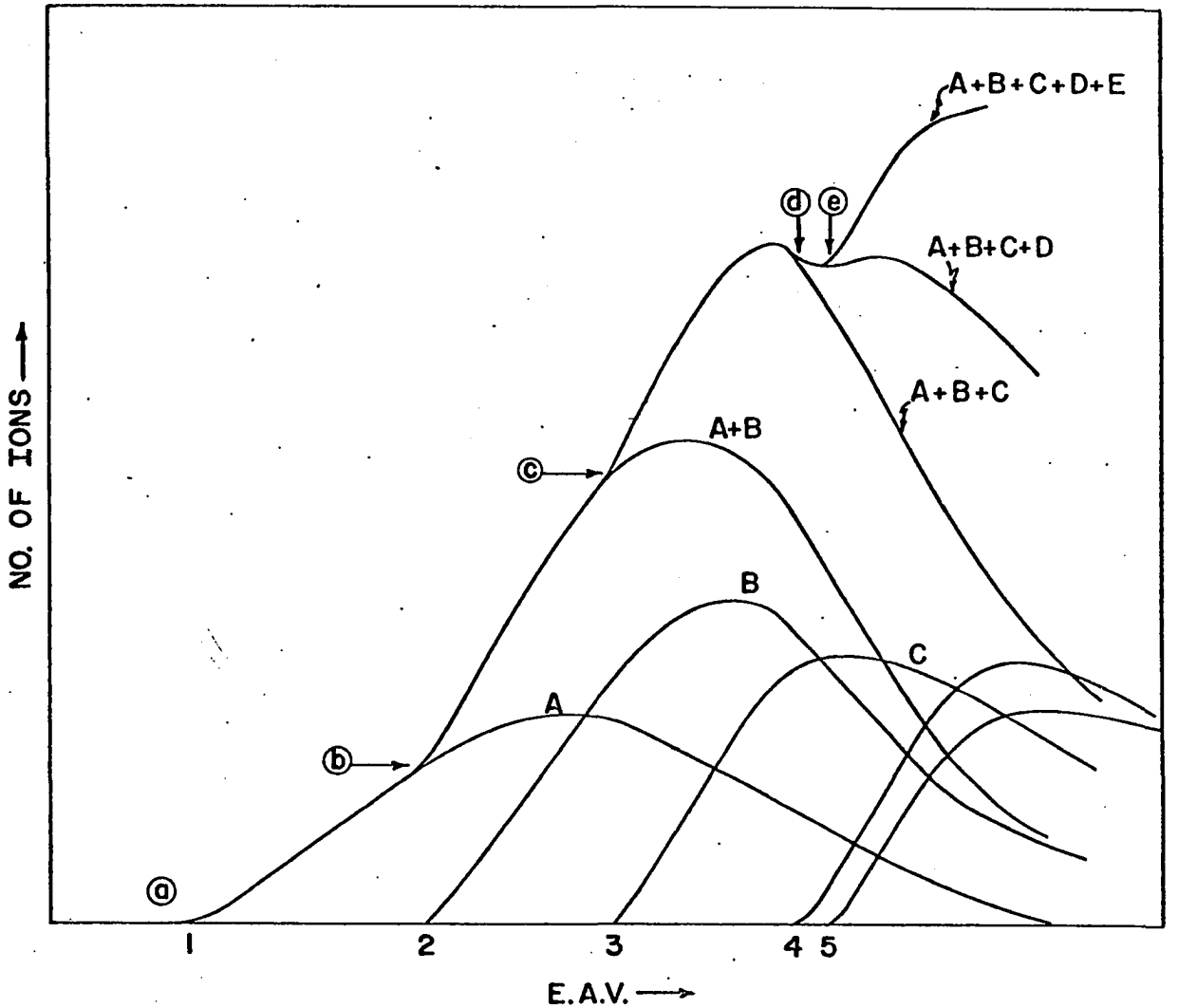

Fig. 36. Possible ionization efficiency curves of several processes.

humps and inflection points. It is assumed that instrumental conditions impart only general effects and not all of these small details. In spite of the general scattering of data points, several of these inflection points were reproducible in many different ionization efficiency curves of Xe^+. In order to facilitate a detailed analysis of the data between the $2P_{3/2}$ and the $2P_{1/2}$ states of Xe(II), the first and second differentials were plotted as shown in Figs. 37 and 38. These specific differential plots represent treatment of the original data without the use of smoothing routines. It is assumed that increases of slopes on the first differential plot and points of maximum curvature on the second differential plot are indicative of the onset of different processes. The $2P_{3/2}$ and the $2P_{1/2}$ states are illustrated on these plots by solid lines and the states from which autoionization can occur are indicated by the dotted lines.

This differential analysis was carried out on Xe^+, test 24, in a variety of ways; no data smoothing, 5 point smoothing, 7 point smoothing, 2, 3 or 5 point interpolations, etc. The results were always very similar in spite of the method of treatment.

Two further tests were examined to determine if these effects were reproducible. Test 31, Xe^+, was made using a Schiff ion source mode with the pulsing technique. Test 27, Xe^+, was made using a Fox ion source mode and a retarding potential of 0.441 volts with the pulsing method. The

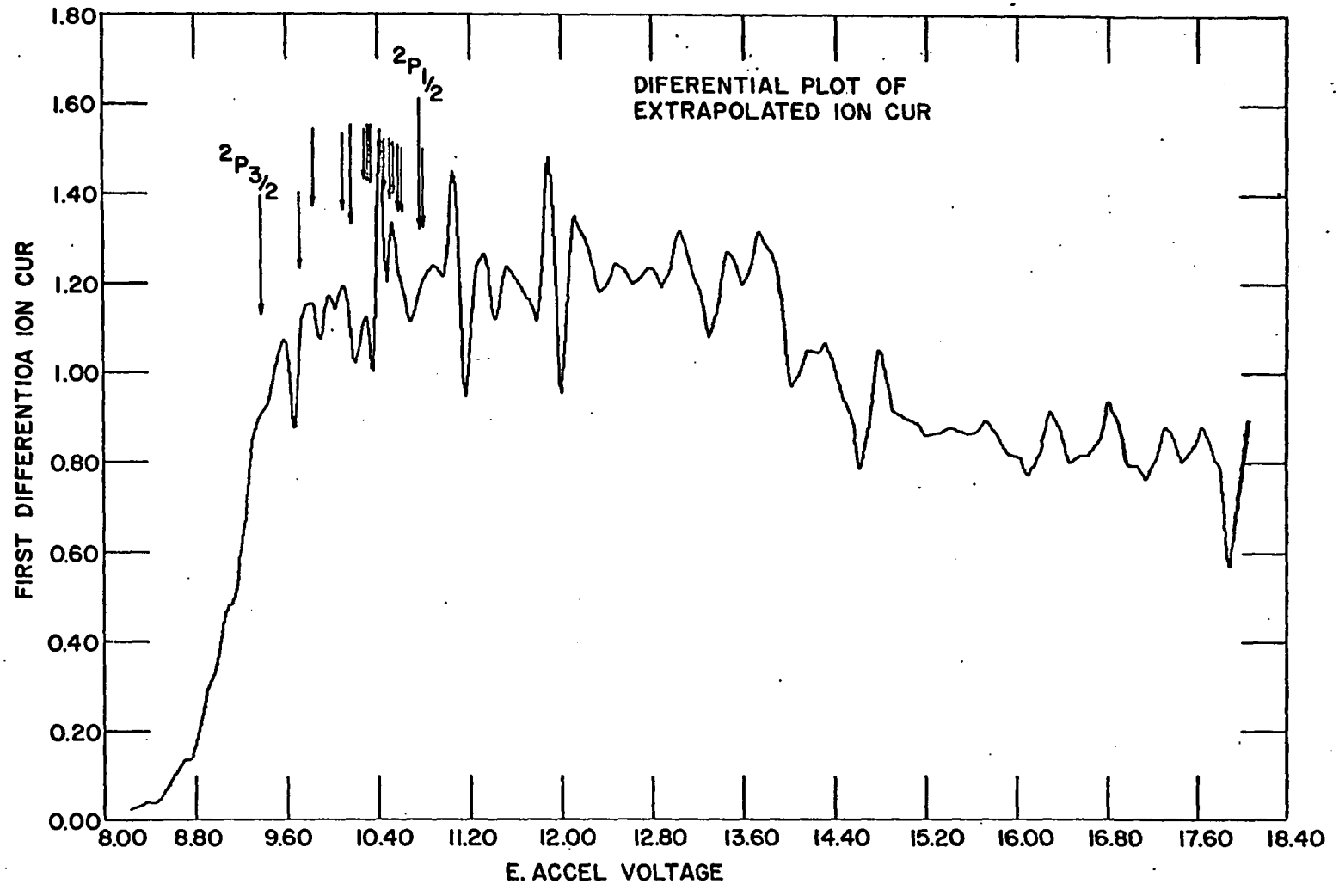

Fig. 37. First differential plot.

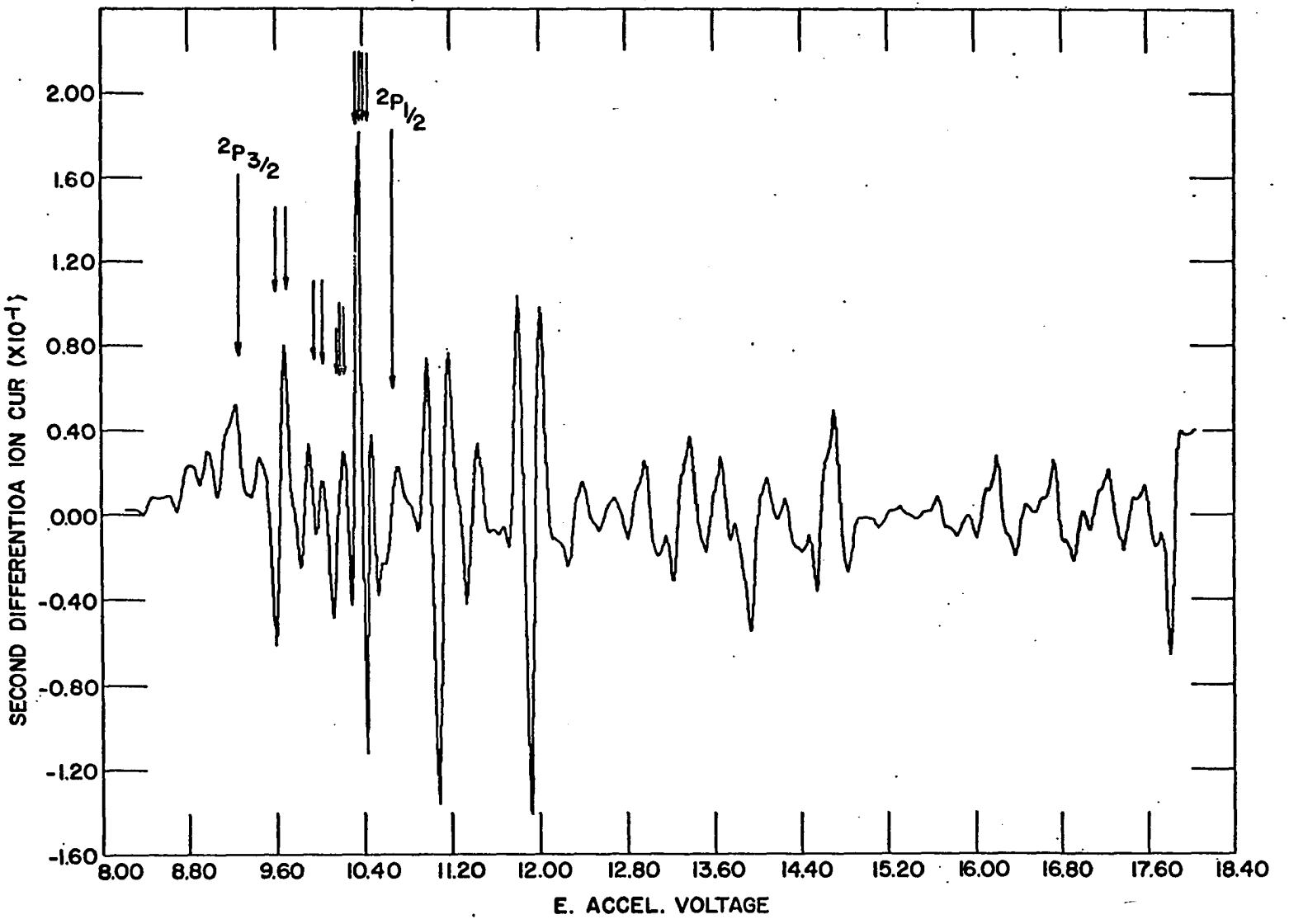

Fig. 38. Second differential plot.

pressures, repeller voltages and electron trap currents were different for all three samples. Yet each curve showed the same characteristics and correlations to the electronic energy states of Xe(I).

Another test for reproducibility involved comparing the details between the $2P_{3/2}$ and $2P_{1/2}$ limits for ten enlarged ionization efficiency curves for Xe^+. In most ionization efficiency curves obtained for Xe^+, the $2P_{1/2}$ limit was detected first by the computer linear extrapolation program. The first few volts above threshold were then plotted on a large scale (5 volts per inch) in order to determine the $2P_{1/2}$ limit more accurately. All of these curves were run using different mass spectrometer conditions, and over a period of a year. After the $2P_{1/2}$ limits were determined, the curves were normalized to read 100 for the ion current slightly above the $2P_{1/2}$ limit. All of the curves were then superimposed and all points were averaged to give an average plot of the data between the $2P_{3/2}$ and $2P_{1/2}$ limits. Illustrated in Figs. 39 and 40 are the final averaged results with the $2P_{3/2}$ and $2P_{1/2}$ energy levels of Xe^+(XeII) and the autoionization states of Xe(XeI) superimposed. The fact that such details can be observed without monoenergetic electrons is surprising considering the large thermal energy spread of the electron beam. Furthermore, note the reproducibility of the entire curves to 0.02 eV for studies made months apart at widely varying conditions! Also proposed and used

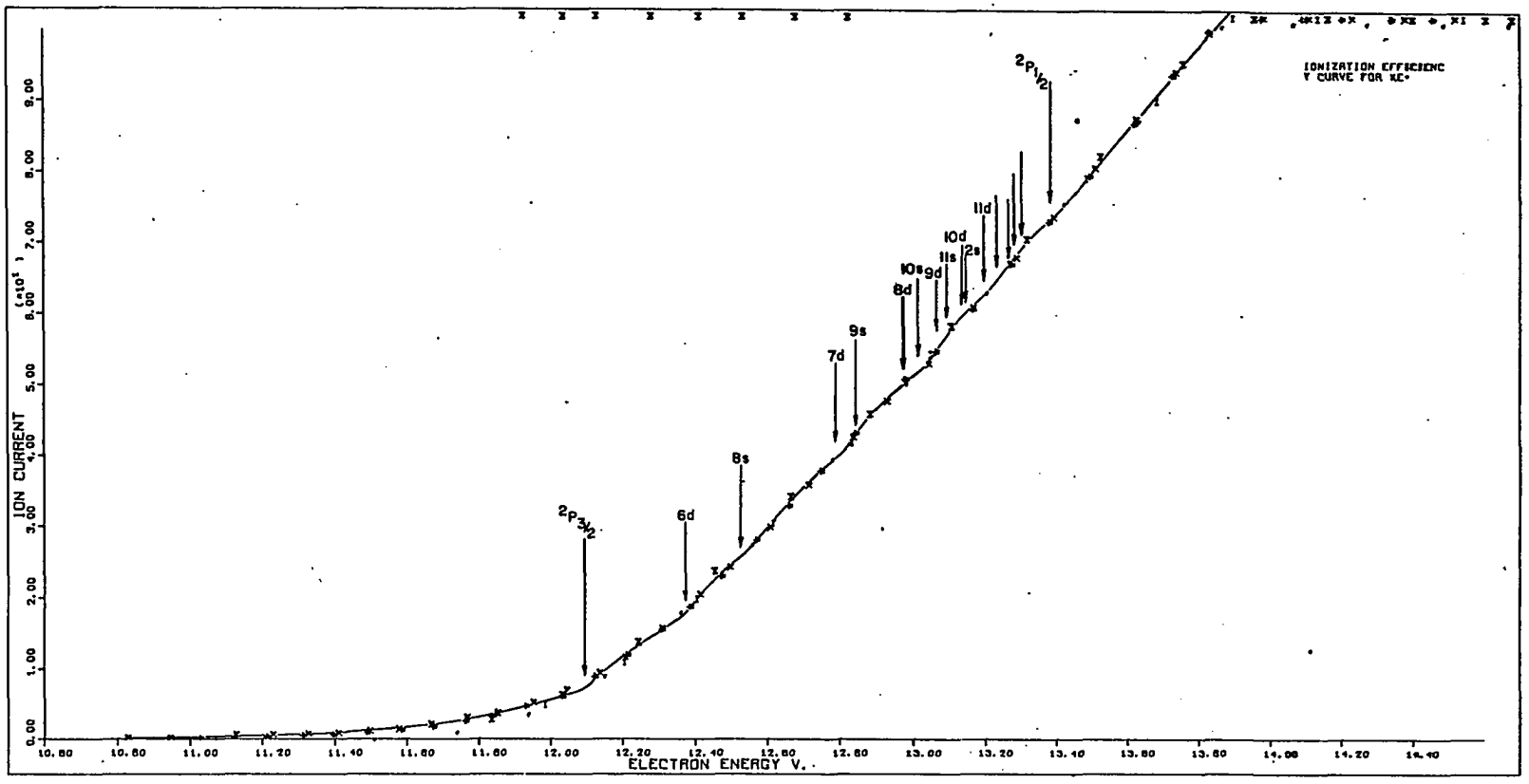

Fig. 39. Expanded, superimposed ionization efficiency curves of xenon.

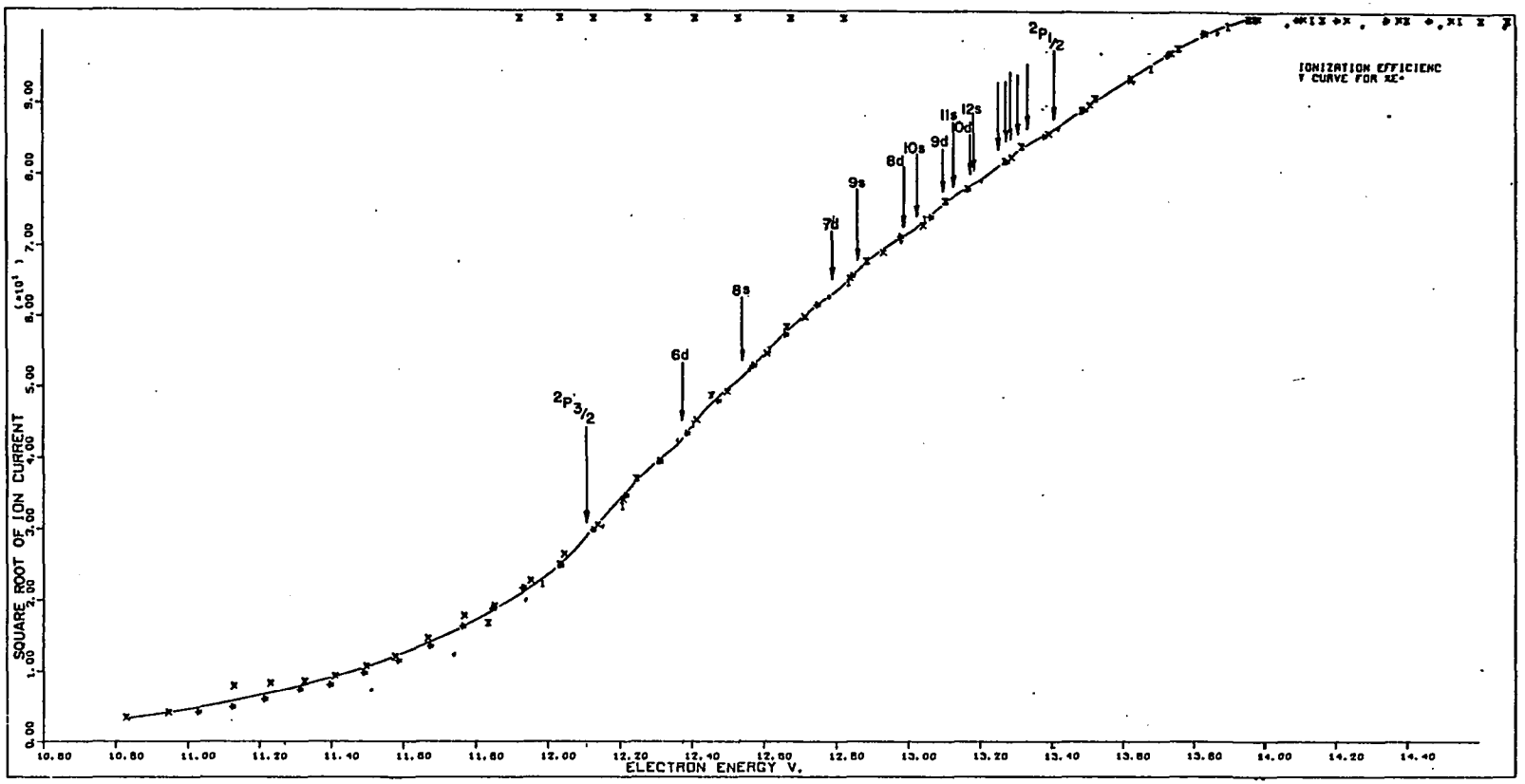

Fig. 40. Superpositioned plots of square-root of ion current vs energy.

extensively is a new method of evaluating and determining appearance potentials. The usual linear plot produces a long positive curvature for both the effects due to electron thermal energy and the ionization process. A semilogarithmic plot produces a negative curvature for both effects. Using either of these methods it is difficult to determine the transition point on the curve between the effects of electron thermal energy and the effects of the ionization process. If the electron thermal energy is close to a pseudo-Maxwellian distribution, it should produce an exponentially increasing tail on the ionization efficiency curve. In contrast to this, the ionization threshold process is usually between a linear and a square function of the electron energy in excess of the appearance potential. It is expected, then, that a plot of the square root of the ion current vs the electron energy will result in an initial positive curvature, due to electron thermal energy,

$$\frac{d^2N_i}{dE^2} \alpha \quad e^{E/kT} \tag{68}$$

and a negative curvature due to the ionization process,

$$N_i \alpha [(E - V_c)^n]^{1/2} \tag{69}$$

where the curvature is derived from;

$$\frac{dN_i}{dE} \alpha \quad (n-2)\frac{n}{4}(E - V_c)^{(n-4)/2} \tag{70}$$

Since $n-2 < 0$ for $n < 2$ then $\frac{d^2N_i}{dE^2}$ is negative. The result, which is as expected, is illustrated in Fig. 40. The point at which the curvature exhibits a transition from negative to positive is easily determined and taken as the actual appearance potential. The ten curves mentioned above were also analyzed by this square root technique, normalized, averaged, and plotted. Fig. 40 illustrates these results with the energy levels of Xe again superimposed. The dotted line is drawn merely as an aid to distinguish the details. Although it is difficult to observe the details on the plot, shown in this figure, they are more easily visible on enlarged plots. Furthermore, if any two of the plots are superimposed, all of the details occur at precisely the same positions. From the several methods of analysis discussed above it appears that the differential curves shown in Figs. 37 and 38 exhibit a strong, reproducible correlation with the actual electronic states of Xe from which autoionization occurs.

E. Threshold Laws

The validity of assumptions concerning the characteristic dependency of ionization upon the excess electron energy near onset has been debated for some time. Wigner (69c) proposed that the electron collision results in a collision complex which dissociates into two electrons and an ion. From this concept, Wannier (70) and Geltman (71) predicted that the

ion current would be proportional to the 1.127 power of the excess energy. Theoretical treatments usually assume that when the collision complex dissociates, the electrons carry off all of the excess energy. The final derived expressions relate the ion efficiency to excess energy near the threshold and for ionization from one electron state to only one other state. With a slight simplification and extension, the same theory predicts threshold laws which are dependent upon the nth power of the excess energy for the nth ionization potential respectively (72).

At present, much disagreement exists in the literature concerning the correct threshold laws for ionization. Many authors have published experimental results to support a linear threshold law for single ionization (34, 73, 74, 75, 76) and a square law for double ionization (34, 72). Some papers (34, 77, 78) support an nth law for n-fold ionization and at least one paper (79) indicates that a linear law holds even for these processes. Most of these publications refer to work on the insert gases and simple molecules. It is generally accepted that threshold laws for ionization of complex molecules and fragment ions are not linear.

When all of these apparent discrepancies are examined and compared in detail, it appears that most of the treatments and data are actually correct in certain respects. The disagreements stem primarily from different interpretations as to the range of the ionization efficiency curve to which the

threshold law is applicable. This results in two entirely different interpretations of the terms "threshold". Literature concerning threshold laws reflects this, since some workers consider threshold laws valid for ionization from one specified state to only one other state. Other workers merely evaluate the entire ionization curve over a relatively large energy range. Thus, an ionization efficiency curve might appear to follow a nonlinear threshold law in general, whereas each single transition might follow a linear threshold law! The contrast of these two methods of evaluating is well illustrated by comparing the work on the multiple ionization of Xenon by Fox (79), who proposes a linear threshold law, and by several others (34, 74, 77, 78) who propose the nonlinear law of ionization. Fox used high energy resolution, and high sensitivity for examining a single specific transition, and the others used convential instruments for examining the entire ionization efficiency curve in general. It is obvious that when different energy states are closely spaced, it requires extremely high ion collector sensitivity and fine electron energy discrimination to investigate the threshold law over a range applicable to a single transition. Unfortunately very few atoms have widely separated electronic states and few instruments fulfill the necessary requirements. Perhaps the strongest support of a linear threshold law is the work on the ionization of He especially that by Hutchison (75), and that by

Fox et al. on Xe^{+N} (79). Both of these studies were made using monoenergetic electrons. Hutchison used an electron energy selector and emphasized that the estimated precision was sufficient to show that ionization to the first electronic state of He^+, mass 3, followed a 1.00 threshold law rather than the 1.127 law predicted theoretically.

Workers should be cautious when examining threshold laws unless their interpretation of the term "threshold" is clearly defined. It would seem from most experimental results, that the word "threshold" should be reserved for reference to single ionization transitions of only simple atoms or molecules studied with high sensitivity and high energy resolution. Even then, there are several reasons to suspect that it is fortuitous when a threshold law is exactly 1.00.

1. It is relatively easy to fit a straight line to data, even when there is slight curvature. This was illustrated in the computer linear extrapolation program described earlier in this thesis. (Refer to Fig. 32). Often a large range of points appear linear to the unaided eye whereas the computer indicates slight curvature.
2. Few workers, other than Hutchison have investigated ionization of a single transition with high precision. Only his work on He^+ is precise enough to speculate on the difference between a 1.00 or a

1.127 threshold law, but He^+ is also the simplest atom available for ionization studies.

3. The theoretical threshold law is based upon simple assumptions for two body collisions. The electrons are assumed to carry off all of the excess energy and during this separation, only long range electrostatic interactions are considered. It is also assumed that the ionization proceeds to single states with no interacting states present. Thus the ionization probability is given as

$$\rho(V) = f(E - V_c)^{kn} \qquad 71$$

where n is the charge on the ion. It would seem that for more complex atoms and molecules, one should consider the nature of the transition, the total electronic configuration of the collision complex, the chemical nature of the molecular bonding orbitals, the velocity vectors before the collision, close lying energy levels, the probability of excitation of the complex, the initial state of the molecule, and half-life of the collision complex. From all of these considerations it is unlikely that the threshold laws for two processes will be exactly equal for even a small energy range above onset.

4. When ionization efficiency curves are obtained under closely controlled conditions and are greatly enlarged, the effects of atomic electronic energy states are shown by the processes of autionization. Autoionization occurs via a different process than direct ionization hence these states can influence the apparent threshold law. In fact Burns (63) emphasizes that autoionization states may even make it impractical to attempt discriminating between a 1.00 and a 1.127 threshold law.

It is much more practical in most ionization efficiency studies, to investigate the dependency on the excess electron energy over a range of 2 to 5 volts rather than to attempt to resolve the ionization process between single states. Furthermore, for the sake of clarity, the term "threshold" should not be applied to investigations in which the states of the atom and molecule are not single or specified. Other investigations should use the general term ionization efficiency law to prevent confusion.

In view of the above considerations, it is assumed that each ionization efficiency curve follows a different "ionization efficiency law" and that these differences are sometimes quite distinct. In fact, different portions of the same ionization efficiency curve can also exhibit different ionization efficiency laws which may indicate the occurence of different processes. This is already reflected by the

discussion of the different threshold laws for autoionization and direct ionization. The following method is used to determine the appearance potentials of complex and multiple ions. It is assumed that ionization efficiency laws are power functions of the excess energy,

$$N_i = (E - V_c)^K \qquad 72$$

The ionization efficiency data are plotted after first taking the nth root of N_i using the computer. Several plots are made for ionization efficiency laws with values of 1/k ranging from 1.0 to 0.5. These plots are then observed to determine what power function is most applicable for each process. For example, if the curvature of a specific portion of a curve goes from positive to negative for values plotted with k = 1.11 and 1.25 respectively, then the actual ionization efficiency law is assumed to lie between 1.11 and 1.25. Instrumental conditions affect the general curvature slightly but this is not appreciable and it is not detrimental to appearance potential results. One of the many studies made using this technique is illustrated in Fig. 41. Each curve is normalized so that all of the curves are of the same height, and each curve is displaced 3 volts along the energy axis. The power dependency, 1/k, is indicated for each curve. The difference between two portions of the curves are indicated by the two lines.

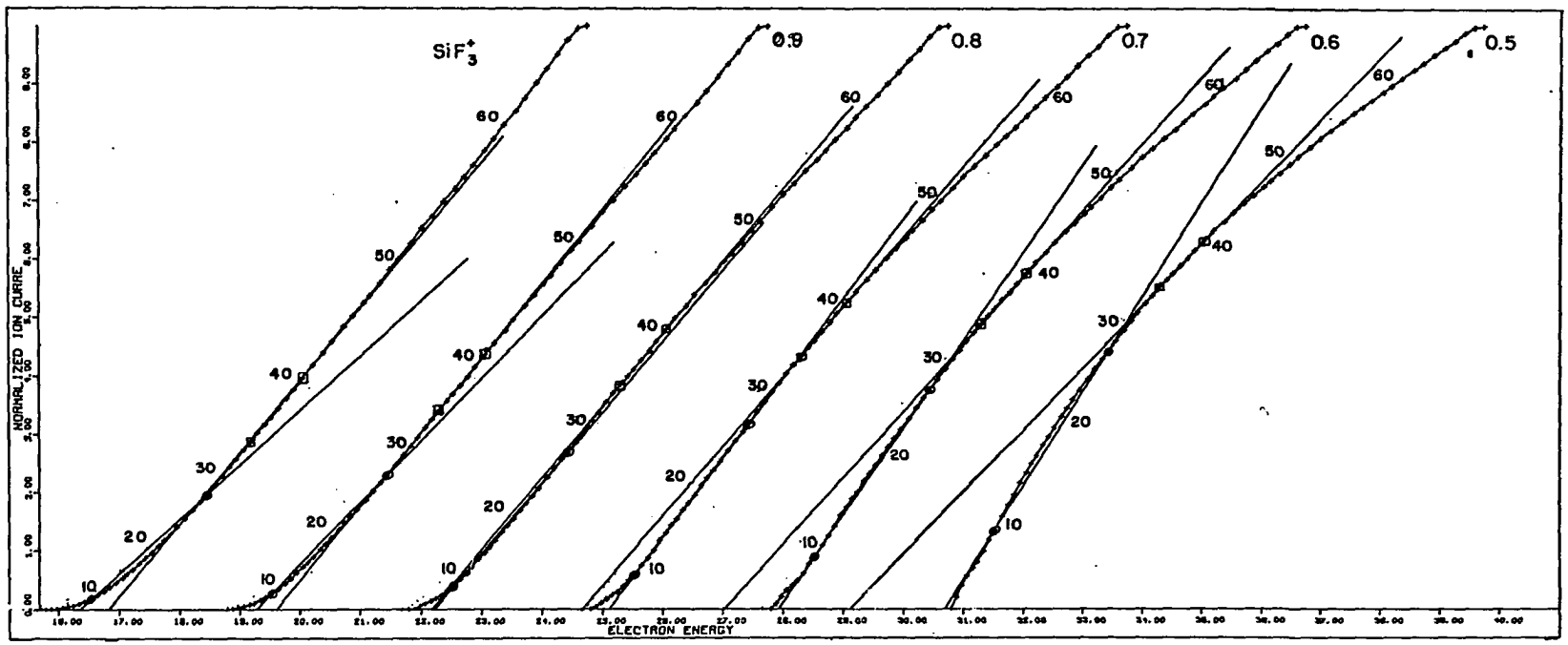

Fig. 41. Typical plots of an ionization efficiency curve at various powers.

Ionization efficiency curves for several different ions are shown in Fig. 42; an inert gas single ion, Xe^+; two parent ions, SiF_4^+, $SiCl_4^+$; two fragment ions, SiF_3^+, SiF_2^+; two double ions SiF_2^{++}, and the double ion Xe^{++}. The energy scale is not corrected and each curve is displaced 3 volts along the energy axis. Instrumental conditions were similar for all of these studies and the value of k is 1.0 for each curve. Although these curves represent only a limited sample of the many curves that were studied, the comparison illustrates significant differences in the ionization efficiency laws for the several processes. Furthermore, it was found that the ionization efficiency law differs for a series of parent ions; a series of fragment ions; or a series of double ions. As an example, from Fig. 42 it is easily seen that SiF_4^+ and $SiCl_4^+$ fit the 1.0 law better than do SiF_3^+ and SiF_2^+ respectively.

The critical slope and the initial onset methods might give reproducible values; and even good precision for these studies. However, such methods depend entirely upon arbitrary empirical bases which necessitate constant instrument conditions, sensitivity, etc. Often an ion current is so small that it becomes impractical to even attempt to equalize the sensitivities of the sample gas and calibrating gas.

The linear extrapolation method has been extensively criticized because only a few simple ionization processes do

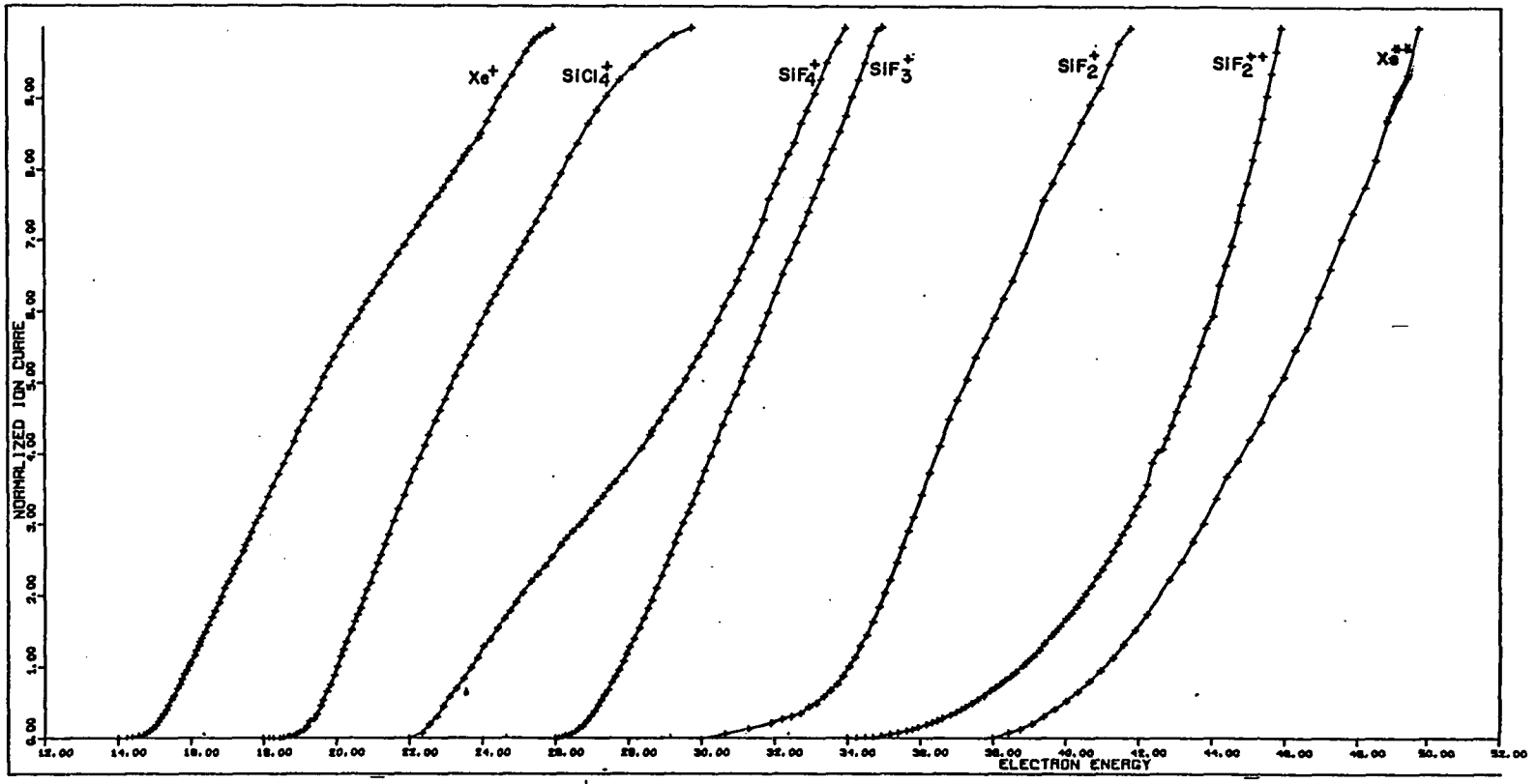

Fig. 42. Comparison of ionization efficiency curves for different ionic species.

not exhibit long tails. It is very obvious that without high sensitivity and high resolution, and/or, with closely spaced energy levels it is unfeasible to attempt linear extrapolation. However, Figs. 41 and 42 clearly indicate that when an ionization efficiency curve is plotted according to the correct power, k, a linear plot is obtained. This can then be extrapolated to obtain the appearance potential. Many examples could be cited but only the results from Xe^{+2} are given. The general ionization efficiency curve for Xe^{+2} has a long tail which must be neglected if linear extrapolation is used for k = 1 (see Fig. 42). The corrected results are 36.2 volts and 33.4 volts for values of k = 1.0 and k = 1.8 respectively. The spectroscopic value is 33.33 volts.

The advantages of this method are evident. The method is applicable to any ionization process; a specific point is not chosen arbitrarily; the relative sensitivities of a calibrating gas and the sample gas do not have to be equalized; monoenergetic electrons are unnecessary; high sensitivity is not necessary; and much more information is obtained.

VIII. MEASUREMENTS OF APPEARANCE POTENTIALS WITHOUT USE OF CALIBRATING GASES

A. Experimental Procedure

Normally the observed values of an appearance potential must be corrected by reference to the observed appearance potential of a known calibrating gas, usually an inert gas. The calibrating gas is admitted into the ion source simultaneously with the sample gas, and both appearance potentials are obtained using the same instrument conditions. The observed appearance potential of the unknown ion is corrected by appropriately adding or subtracting the difference between the observed appearance potential of the calibrating gas and its spectroscopic value. This necessitates scrupulous adjustments of many instrumental conditions and gas pressures, demands low drift of these instrumental parameters, and requires performing a new calibration each time the instrument conditions are changed; this is usually very often.

It was found during this work that if all the effects of major instrumental parameters upon appearance potentials are carefully analyzed, many correlations can be precisely estaablished. These correlations can then be used to relate an observed appearance potential to the true appearance potential without directly using a calibrating gas, and for widely variable instrument conditions. This procedure obviously offers many very desirable advantages.

The explicit dependency of the observed appearance potential on some of these instrumental parameters was established after 40 ionization efficiency studies of Xe^+ were carefully examined. These studies were made at widely differing trap currents, retarding voltages, ion detection sensitivities, anode voltages, and repeller voltages, throughout an ion gun pressure range of 2×10^{-6} to 2.0×10^{-5} Torr. Some of these studies were made while various other substances (SiF_4, $SiCl_4$, $SiBr_4$, Ar, N_2) were simultaneously being introduced into the ion source and some were made using only pure Xe^+. The tests were conducted over a period of a year, during which time the ion source was twice disassembled and modified. Many times the filament was replaced or repositioned. Frequently, some of the circuit diagrams were grossly modified or repaired. All of these tests were conducted primarily as preliminary steps to evaluate the instrument capabilities and performance during its development. The attempt to establish correlations from the recorded data and to use these correlations for calculating absolute appearance potentials was conceived and conducted after all the tests had been completed and analyzed with the aid of the linear extrapolation computer program. This eliminated the possibility of a biased operating procedure and yielded measurements which are, therefore, not results of attempts to accurately control the instrumental conditions. Rather emphasis was placed upon accurately

recording the instrumental conditions immediately after an ionization study. In some respects, this certainly did not result in ideal, or complete data, yet, the results are relatively precise.

The true appearance potential, A.P., is assumed to be a function of the parameters,

$$A.P. = f(A.P._{obs}, R_v, E_v, A_v, U_A, I_c, P) + f(C) \qquad 73$$

where

$A.P._{obs}$ = observed appearance potential

R_v = repeller voltage

E_v = retarding plate voltage

A_v = anode voltage

U_A = average electron thermal energy

I_c = trap current

P = total pressure

c = constant.

The function, f(c), is assumed to be a function of the contact and surface potentials, the voltage drop across the filament, and miscellaneous effects. It has been assumed by many others that contact and surface potentials create many large indeterminate errors in appearance potential measurements and that these effects are not constant. This is the major reason why nearly all workers resort to employing calibrating gases. It is shown below that the function, f(c), which includes indeterminate contact potentials, is

constant within the standard deviation of the calibration of the instrument under the widely varied studies already mentioned.

The values, $A.P._{obs}$ are determined using the computer linear extrapolation program. The lowest values resulting from extrapolation of the $2P_{3/2}$ electronic state of Xe^+ are used. Using this technique, the actual ionization efficiency plots are not even referred to, except for qualitative information.

The energy corrections that are evaluated and applied to the observed appearance potentials are illustrated in Fig. 43. Normally the electron energy is measured from filament to the retarding electrode, plate E, however, when there is no retarding voltage, it is measured from filament to shield. It is obvious that the true energy of the electrons in the ionizing electron beam is actually greater than the measured value by the amounts, x, and y (see Fig. 44). This is because of gradients due to the repeller potential, and gradients due to the increased average electron thermal energy caused by retarding the lower energy electrons. A slight decrease, z, also results from the effect of the anode potential gradient upon the space charge and potentials near the filament. The factor, z, thus represents a change in the energy of the entire electron distribution but not a change in the distribution itself. Hence this is not effective when a retarding potential is used since the

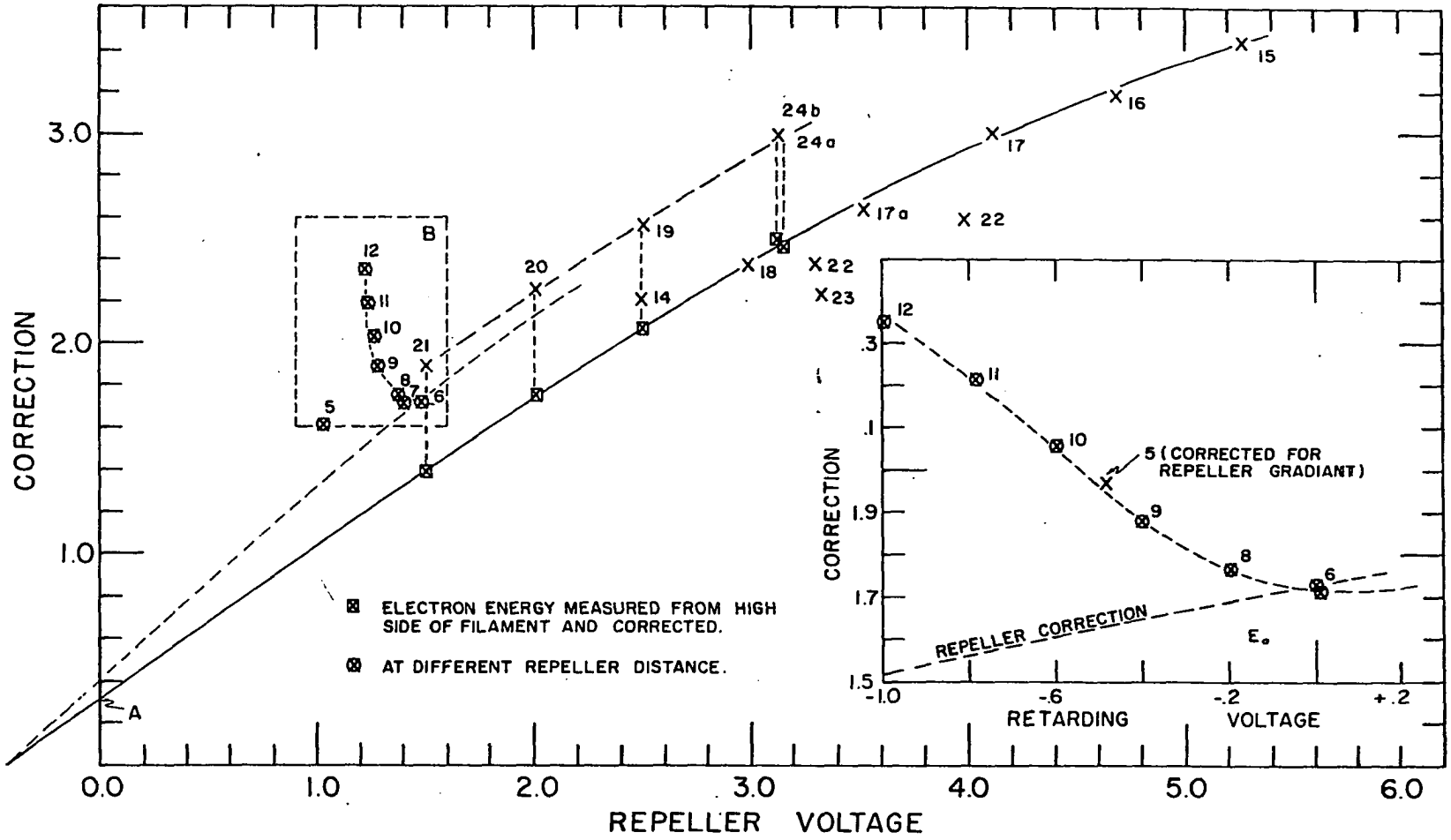

Fig. 43. Appearance potential corrections.

electron energy is measured from plate E to shield when a retarding potential is used and factors which affect the total energy of the electron beam before they reach the retarding plate do not influence the thermal energy distribution significantly. Thus the energy distribution of electrons which pass plate E is relatively independent of the anode voltage. In the Schiff mode of source operation this is not true.

B. Initial Correction Due to Repeller Gradient

The largest error in determining appearance potentials is caused by the effect of the repeller potential on the voltage gradients in the ionizing region of the source. The differences between the spectroscopic ionization potential of Xe^+ and the observed values as calculated using the computer technique are plotted as ordinate against the respective repeller voltages as shown in Fig. 43. Several things should be clarified concerning this graph. The numbers refer to the specific test from which the appearance potentials were obtained. Refer to Table 3a. Insufficient readings were obtained at the lower electron energies near onset for tests 2, 3, 22, and 23, so that the computer extrapolation results were not used for these tests. Furthermore, test 25 was a retarding potential difference study, and tests 26 through 31 involved pulsing techniques hence they were not used either. Tests 1 through 12 were run

during a 6 month period although tests 6 through 12 were completed during only a 2 day interval. Test 1 is used in the calculations although it is off scale on the plot of Fig. 43. The voltage applied to plate E was the only condition that was intentionally varied in tests 6 to 12, and it was observed that the repeller and anode voltages also varied slightly with the retarding voltage. The enlargement of area B, shown at the right in Fig. 43, illustrates that further correction is necessary depending upon the value of the retarding potential, although the electron energy was measured from the retarding plate to the shield.

After performing test 12, the ion source was partly disassembled, the repeller plate was moved 0.065 inches further from the electron path, and the ion source was reassembled. After running tests 15 through 18, the leads supplying power to the filament were changed and then tests 19 through 24b were completed. It is apparent that the differences in the corrections for tests 15 through 18, and 19 through 24b are most likely due to the voltage drop across the filament. The average of the distance from points 24a and 24b to the extrapolated line through points 15 to 18 is assumed to be a constant correction due to this filament voltage drop. The value of this correction is 0.44 volts and it is subtracted from the corrections of each of tests 19 through 24b.

In order to evaluate the corrections x, y and z indicated in Fig. 43, Eq. 73 is rewritten,

$$A.P. = AP_{obs} + C_R + C_E + C_A + C \qquad 74$$

where C_R, C_E, C_A, and C are the corrections due to the repeller gradient, retarding potential, anode potential, and miscellaneous effects. Note, all of the instrumental variables are treated as being independent of one another. Although this may not represent the true state of affairs, it yields consistent and accurate results when the following procedure is applied. This procedure is discussed in detail below.

From the data shown in Fig. 43, tests 15 through 24b are used to establish a first order correlation of the repeller potential with the correction, x. This is done by using a computer program for applying the method of least squares to data for linear, simple parabolic, and general gradiatic equations. If it is assumed that the correction due to the repeller gradient increases approximately as the square of the applied repeller voltage, then one would expect the measured repeller potential to be proportional to the square of the correction due to this gradient. This is, indeed, the case since it is found that the data fit a quadratic function very well. Some of the tests were not performed at the same retarding potential hence this first least squares result is considered only as a first order approximation of the magnitude of this correction.

C. Correction for Electron Thermal Energy

The data from the above results are used as a first approximation to normalize the correction factors of tests 5 through 12 to the same repeller gradient. These normalized corrections are plotted vs the voltage of plate E as shown in the enlarged portion of Fig. 43. The correction, y, in addition to the correction, x, is also indicated in Fig. 44. Since the total electron energy is measured from the retarding plate to the shield, the correction factor, y, indicates that the true electron energy is still greater than the measured energy plus the repeller gradient correction. This extra correction, y, is assumed to be caused by the average thermal energy of the electrons which reach the ion box. It might also be the result of smaller effects such as focussing, or voltage drops between plates.

The curves in Fig. 44 illustrate the electron thermal energy distributions for temperatures 2140 to 2320°K, and the average thermal energies of each entire distribution. In tests 5 through 12, electron trap regulation was used with trap current of 6.6 microamperes for each test. Thus, if a retarding potential prevents some electrons from reaching the electron trap, indicated by Area A, then the filament temperature must increase to increase the number of emitted electrons. For example, when the retarding potential is increased from 0.40 volts to 0.80 volts, the electrons

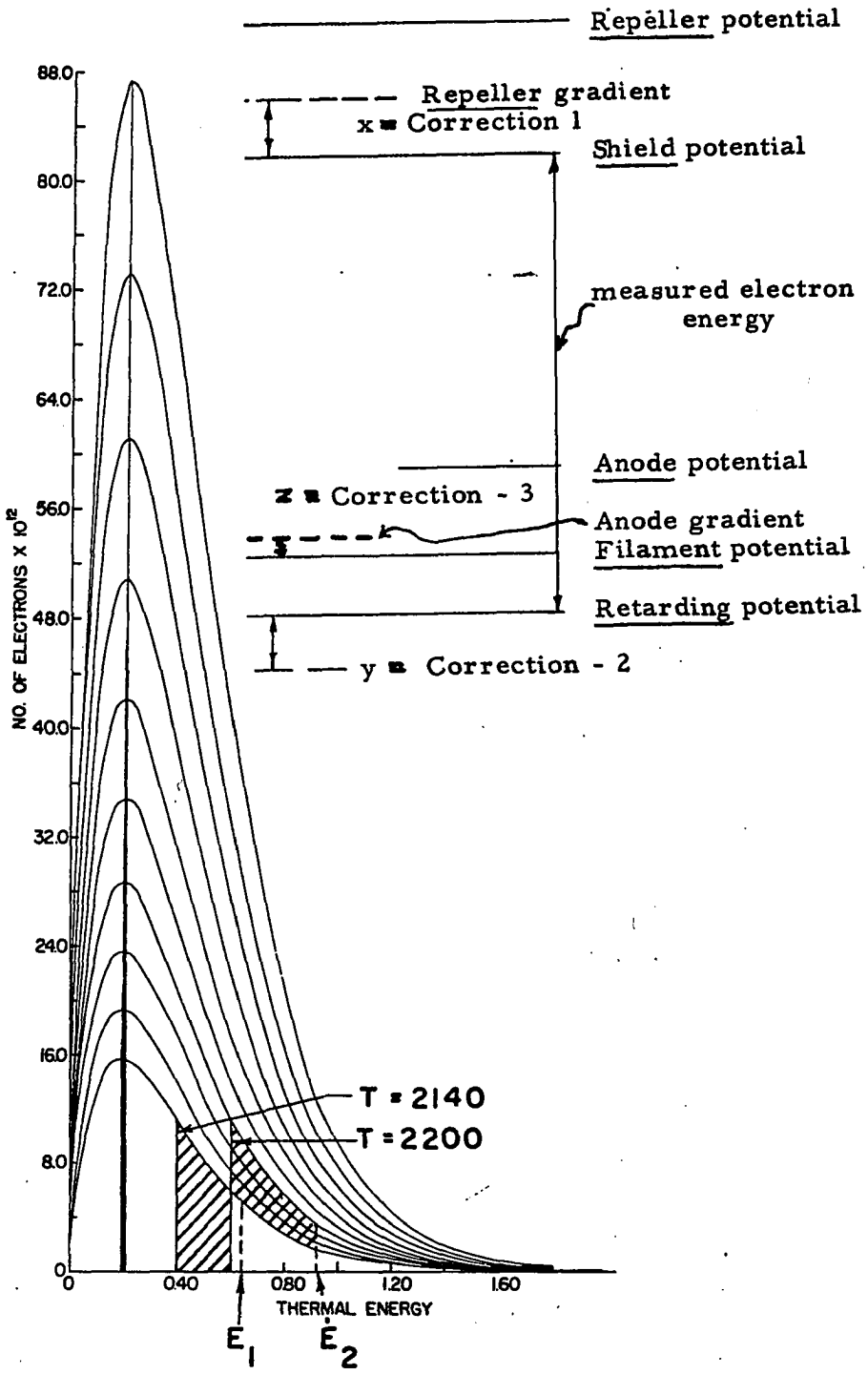

Fig. 44. Representation of corrections to appearance potential measurements.

represented in area A are also retarded. Thus the filament temperature must increase so that the number of electrons with thermal energy above 0.8 volts increases by the same number. This is represented by area B. If the trap current is to remain constant then the total number of electrons emitted with thermal energies greater than 0.4 volts is equal to the total number of electrons emitted with thermal energies greater than 0.8 volts for these respective retarding voltages. Earlier, Eq. 5 expressed the number of electrons emitted at a temperature, T_i, thus

$$N_i = \frac{4\pi mAu}{h^3} e^{\frac{-\phi+u}{kT_1}} du \qquad 75$$

and

$$N_2 = \frac{4\pi mAu}{h^3} e^{\frac{-\phi+u}{kT_2}} du \qquad 76$$

Although experimental (16) and theoretical (17) evidence have already been presented to suggest non-Maxwellian electron thermal energy distributions, it is assumed here for simplicity that the pseudo-Maxwellian distribution represents the thermal energy of the electrons which do reach the retarding slit. Then the limits a_1, and a_2 are assumed to be related to the measured values of the voltages applied to the retarding electrode, plate E. Using Eqs. 75 and 76, the measured voltage of plate E, and the known total current, N_T the approximate temperature, T_i, is calculated. Then, since,

$$N_1 = N_2, \tag{77}$$

$$\int_{a_1}^{\infty} \frac{4\pi mAUe}{h^3} \frac{-\Phi+U}{kT_1} \, dU = \int_{a_2}^{\infty} \frac{4\pi mAU}{h^3} e \frac{-\Phi+U}{kT_{2dU}} \tag{78}$$

or simplifying,

$$\int_{a_1}^{\infty} Ue^{-U/kT_1} \, dU = \int_{a_2}^{\infty} ue^{-U/kT_2} \, dU. \tag{79}$$

It is further assumed that the focussing effects of the retarding plate do not influence the coefficient of transmission of electrons from plate E to the trap. The relationship expresses in Eq. 79 is then used to calculate the new temperature, T_2. The initial temperature, T_1, is associated with a retarding potential of zero. Hence completing the integrations and solving for T_1, one obtains the expression,

$$T_i = \frac{-a_i + [a_i^2 + 4(kT_1)^2 e^{a_i/kT_i}]^{1/2}}{2k} \tag{80}$$

The final numerical solution of this equation is calculated by employing 10 cycles of Newton's Method of Approximation using the IBM 7074 computer program that was also used for calculating electron energy distributions. After T_i has been calculated, it is possible to determine the average energy of the electrons which reach the electron trap. This is done by applying the relationship,

$$U_{iave} = \int_{a_i}^{\infty} U_i dN_i / N_{itot} \tag{81}$$

where dN_i is the number of electrons emitted with thermal energies U_i. Thus,

$$U_{iave} = \int_{a_i}^{\infty} \frac{4\pi mAU^2 e}{h^3} \frac{-\phi+U}{kT_i} \, dU \Big/ \int_{a_i}^{\infty} \frac{4\pi mAUe}{h^3} \frac{-\phi+U}{kT_i} \, dU \qquad 82$$

or simplifying,

$$U_{iave} = \int_{a_i}^{\infty} U^2 e^{-U/kT_i} \, dU \Big/ \int_{a_i}^{\infty} e^{-U/kT} \, dU \qquad 83$$

The resulting solution gives the average thermal energy of the electrons entering the ionizing region as a function of the retarding potential, a_i, and the filament temperature, T_i,

$$U_{iave} = a_i = 2kT_i + \frac{2(kT_i)^2}{a_i} . \qquad 84$$

The temperature, T_i, is determined first by Eq. 80. The computer program discussed earlier for calculating electron emission characteristics was used to calculate the average thermal energies of electron distributions that result after passing through various retarding potentials, a_i. This was done for several initial emitting temperatures as illustrated in Fig. . ., although Chart 5 lists the results for only one initial temperature, 2280°K. In this table, the columns from left to right represent, the minimum kinetic or thermal energy of the distribution established by the retarding potential, a_i, the new temperature, T_1, the average electron thermal energy, U_{iAve}, the total electron emission from the

filament, the constant trap current, the percent of electrons retarded, and the percent total electron transmission increase based on the initial total emission.

If the entire observed correction, y, due to the effects of the voltage applied to plate E is assumed to be caused by the difference of U_{oAve} and U_{iAve}, then Chart 5 can be used to relate y to the true retarding potential barrier that is actually defined by plate E. The initial average thermal energy, U_{oAve}, is for a zero retarding potential. This is done for tests 5 through 12 using the calculated electron emitting temperatures for each of the respective retarding potentials. The retarding potential is assumed initially to be equal to the measured voltage, E_v, applied to plate E. Chart 5 is then used to determine the average thermal energy, U_{iAve}, of the resulting trap current. If the applied voltage is initially assumed to be 100 percent efficient in defining the retarding potential, the observed correction due to y at the measured voltage, E_V, should equal the difference between U_{iAve} and U_{oAve}, where

$$C_i = U_{iAve} - U_{oAve}. \qquad 85$$

The example underlined in Chart 5 illustrates the procedure for an applied retarding potential, E_v, of -0.206 volts shown in the first column. In an experiment using -0.206 volts as the retarding potential the observed correction, C_i (or y),

11-10-65

KINETIC E	NEW TEMP	AVER.E	TOTAL	HIGH E.ELECTRONS	PERCENT RETARDED	C/C INCREASE
0.00000	2280.000	0.19640	0.25312E 00	0.25312E 00	0.00000	0.00
0.01875	2288.700	0.21590	0.27838E 00	0.25312E 00	9.07210	9.98
0.03750	2297.398	0.23540	0.30593E 00	0.25312E 00	17.26160	20.86
0.05625	2306.093	0.25490	0.33597E 00	0.25312E 00	24.65992	32.73
0.07500	2314.786	0.27440	0.36871E 00	0.25312E 00	31.34843	45.66
0.09375	2323.476	0.29390	0.40435E 00	0.25312E 00	37.39965	59.74
0.11250	2332.163	0.31340	0.44313E 00	0.25312E 00	42.87826	75.06
0.13125	2340.848	→ 0.33290	0.48530E 00	0.25312E 00	47.84199	91.73
0.15000	2349.530	0.35239	0.53113E 00	0.25312E 00	52.34241	109.83
0.16875	2358.210	0.37189	0.58090E 00	0.25312E 00	56.42561	129.49
0.18750	2366.887	0.39139	0.63492E 00	0.25312E 00	60.13282	150.83
0.20625	2375.561	0.41089	0.69351E 00	0.25312E 00	63.50098	173.98
0.22500	2384.233	0.43038	0.75702E 00	0.25312E 00	66.56314	199.07
0.24375	2392.903	0.44988	0.82582E 00	0.25312E 00	69.34858	226.25
0.26250	2401.570	0.46938	0.90031E 00	0.25312E 00	71.88510	255.68
0.28125	2410.234	0.48887	0.98092E 00	0.25312E 00	74.19538	287.53
0.30000	2418.896	0.50837	0.10681E 01	0.25312E 00	76.30131	321.96
0.31875	2427.556	0.52787	0.11623E 01	0.25312E 00	78.22217	359.18
0.33750	2436.213	0.54736	0.12641E 01	0.25312E 00	79.97534	399.38
0.35625	2444.867	0.56686	0.13739E 01	0.25312E 00	81.57646	442.78
0.37500	2453.520	0.58635	0.14924E 01	0.25312E 00	83.03963	489.61
0.39375	2462.170	0.60585	0.16203E 01	0.25312E 00	84.37754	540.10
0.41250	2470.817	0.62534	0.17580E 01	0.25312E 00	85.60165	594.52
0.43125	2479.462	0.64484	0.19064E 01	0.25312E 00	86.72232	653.14
0.45000	2488.105	0.66433	0.20661E 01	0.25312E 00	87.74889	716.25
0.46875	2496.745	0.68383	0.22380E 01	0.25312E 00	88.68982	784.16
0.48750	2505.382	0.70332	0.24229E 01	0.25312E 00	89.55274	857.19
0.50625	2514.018	0.72281	0.26216E 01	0.25312E 00	90.34458	935.69
0.52500	2522.651	0.74231	0.28350E 01	0.25312E 00	91.07162	1020.02
0.54375	2531.282	0.76180	0.30643E 01	0.25312E 00	91.73951	1110.56
0.56250	2539.910	0.78129	0.33103E 01	0.25312E 00	92.35342	1207.77
0.58125	2548.536	0.80079	0.35742E 01	0.25312E 00	92.91802	1312.03
0.60000	2557.160	0.82028	0.38572E 01	0.25312E 00	93.43756	1423.82
0.61875	2565.782	0.83977	0.41604E 01	0.25312E 00	93.91588	1543.62
0.63750	2574.401	0.85926	0.44852E 01	0.25312E 00	94.35649	1671.99
0.65625	2583.018	0.87876	0.48330E 01	0.25312E 00	94.76258	1809.34
0.67500	2591.632	0.89825	0.52051E 01	0.25312E 00	95.13705	1956.36
0.69375	2600.245	0.91774	0.56032E 01	0.25312E 00	95.48253	2113.63
0.71250	2608.855	0.93723	0.60288E 01	0.25312E 00	95.80144	2281.77
0.73125	2617.463	0.95672	0.64836E 01	0.25312E 00	96.09597	2461.46
0.75000	2626.069	0.97622	0.69695E 01	0.25312E 00	96.36811	2653.39
0.76875	2634.672	0.99571	0.74882E 01	0.25312E 00	96.61970	2858.32
0.78750	2643.273	1.01520	0.80418E 01	0.25312E 00	96.85240	3077.03
0.80625	2651.872	1.03469	0.86323E 01	0.25312E 00	97.06773	3310.33
0.82500	2660.469	1.05418	0.92621E 01	0.25312E 00	97.26709	3559.11
0.84375	2669.063	1.07367	0.99332E 01	0.25312E 00	97.45175	3824.26
0.86250	2677.656	1.09316	0.10648E 02	0.25312E 00	97.62287	4106.74
0.88125	2686.246	1.11265	0.11410E 02	0.25312E 00	97.78151	4407.59
0.90000	2694.834	1.13214	0.12220E 02	0.25312E 00	97.92866	4727.82
0.91875	2703.420	1.15163	0.13083E 02	0.25312E 00	98.06522	5068.57
0.93750	2712.004	1.17112	0.14000E 02	0.25312E 00	98.19200	5430.99
0.95625	2720.586	1.19061	0.14976E 02	0.25312E 00	98.30976	5816.34
0.97500	2729.165	1.21010	0.16012E 02	0.25312E 00	98.41918	6225.85
0.99375	2737.742	1.22959	0.17113E 02	0.25312E 00	98.52090	6660.90
1.01250	2746.317	1.24907	0.18283E 02	0.25312E 00	98.61551	7122.88
1.03125	2754.890	1.26856	0.19524E 02	0.25312E 00	98.70354	7613.28
1.05000	2763.461	1.28805	0.20841E 02	0.25312E 00	98.78547	8133.66
1.06875	2772.030	1.30754	0.22238E 02	0.25312E 00	98.86177	8685.63

Chart 5. Electron thermal energies.

was 0.137 volts. The correction calculated from Eq. 85 (see column 3) is,

$$C_{calc} = 0.411 - 0.196$$
$$= 0.215 \text{ volts},$$

assuming 100 percent definition occurs at the retarding slit. If the experimental correction, 0.137 volts, is entirely due to electron thermal energy but 100 percent definition does not occur, then the actual thermal energy involved in this example is given by Eq. 85,

$$U_{iAve} = C_i + U_{oAve}$$
$$= 0.137 + 0.196$$
$$= 0.333 \text{ volts}.$$

It is found in Chart 5 that this corresponds to a retarding potential 0.131 which is nearly equal to the observed correction of 0.137. It is therefore assumed that the observed corrections are approximately equal to the "effective" retarding potential established by the measured voltages applied to plate E. If it is further assumed that the effective retarding potential is established by the potential gradient in the center of the slit in plate E, then the observed corrections, which also represent these gradients, should depend upon the square of the voltage applied to plate E. (See discussion concerning the repeller correction on p. 167). The observed corrections are based upon a zero correction for a zero retarding potential. This is not true

since the correction, y, is always equal to at least the average thermal energy of the total electron distribution. For a zero retarding potential this is shown to be 0.196 volts, hence this amount should be added to all the observed y corrections. The application of the method of least squares calculations for a general parabolic equation indicates that the above assumptions are surprisingly accurate. The relationship between retarding potential and this correction is

$$E_v = + 0.380 - 1.866\ C_E + 0.559\ C_E^2. \qquad 86$$

The standard deviation of the correction is $\pm$ 0.042 volts for the 8 appearance potentials observed in tests 5 through 12. Eq. 85 can be used to calculate the retarding potential necessary to cause a correction of 0.196v, just equal to the theoretical average electron thermal energy for zero retarding potential. This calculated result is 0.29v which is greater than the theoretical value of zero. This indicates that perhaps the measured voltages at plate E are too high.

The above procedure required several assumptions,

1. It was assumed that the total electron thermal energy distribution was Maxwellian and independent of the ion source conditions.
2. It was assumed that the correction, C_E was equal to the average thermal energy of the trap electrons.

Actually it would be better to assume that C_E is equal to the average energy of <u>electrons which cause ionization</u> since the probability of ionization is proportional to the energy of the electrons. This would mean that the calculated correction would be slightly higher than the average energies indicated.

3. Focus effects of Plate E were ignored.
4. It was assumed that the <u>entire</u> correction was due to the effect of the electron thermal energy.
5. The initial temperature was approximated.

In spite of these rough approximations, it is evident that there is a strong correlation between the observed corrections and the measured retarding voltages or the average electron thermal energies calculated from these measured voltages.

D. Second Order Correction for the Repeller Gradient

After the corrections due to the effects of the retarding potentials have been determined they are subtracted from the <u>total</u> corrections observed. It is then assumed that the resulting corrections, C_R, are due only to the repeller gradients. These final corrections obtained after subtracting C_E, as shown in Fig. 45, are again subjected to analysis by the method of least squares for a general quadratic equation. Note that 10 tests, 1 through 12 were obtained with a different repeller-to-electron beam distance than

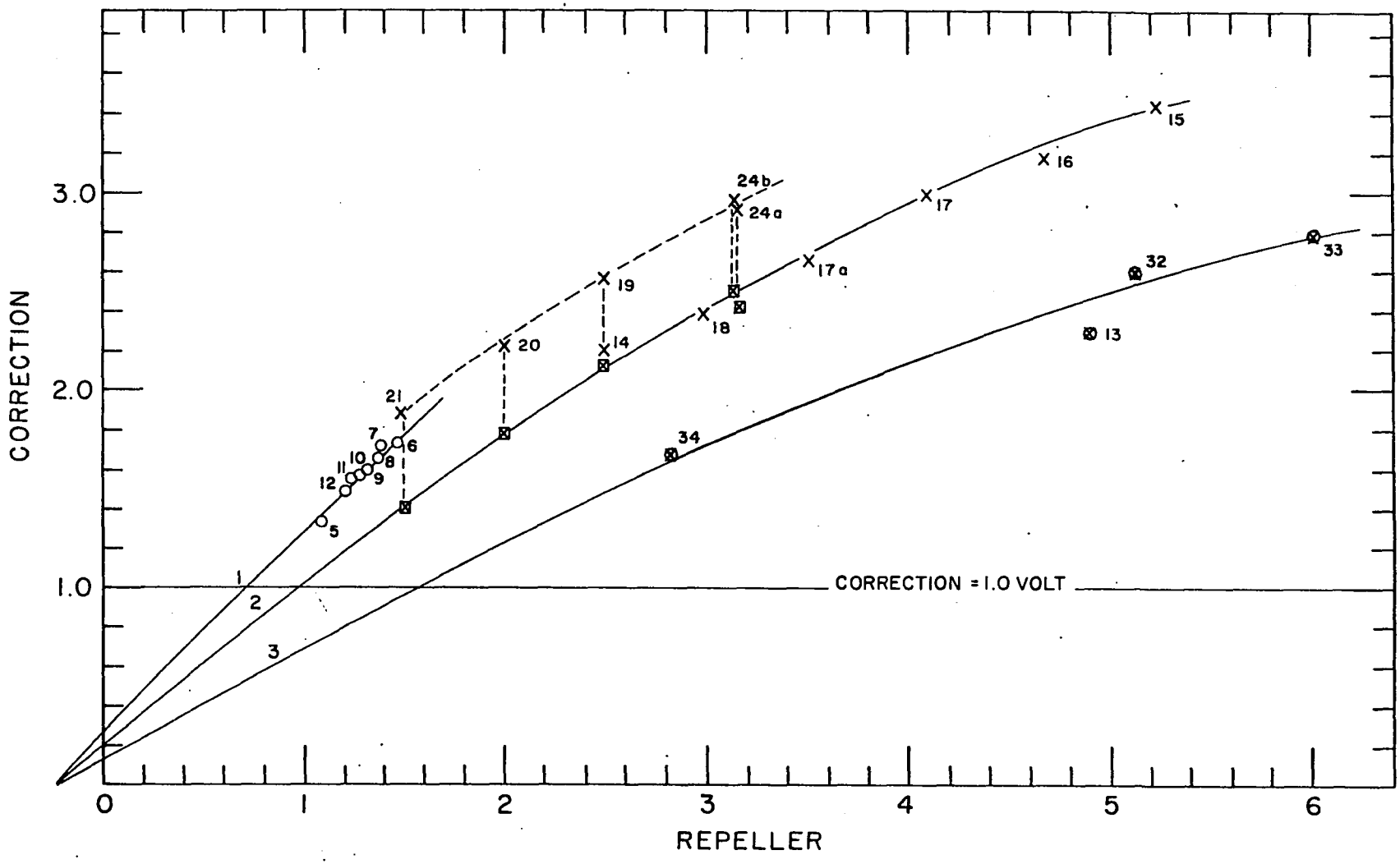

Fig. 45. Appearance potential corrections after a first order correction.

were the 13 tests, 14 through 24b. For this reason a least squares analysis was made for each set of data. Eqs. 87 and 88 represent the final results respectively,

$$R_V = 0.480 + 0.400C_R^2 \qquad 87$$

$$C_R = \pm 0.063 \text{ volts}$$

$$R_V = 0.541 + 0.385C_R + 0.330C_R^2 \qquad 88$$

$$C_R = \pm 0.050 \text{ volts.}$$

Note that the slope, $\frac{dC_R}{dR_V}$, is greater for tests 1 through 10 than for tests 14 through 24b because the repeller plate was closer to the ionizing region during these tests. Furthermore, the calculated correction is zero for a repeller voltages of 0.480 and 0.541 volts respectively. Whereas this is only slightly greater than the expected result of zero, it indicates two possible effects; the measured repeller voltage is not the true repeller voltage, or there is another, nearly constant potential gradient that exists in the ionizing region. Obviously the above results could be used to make a second order correction in C_E which, in turn, could be used to make a third order correction in C_R, etc. The standard deviation of the measured corrections for Eqs. 87 and 88 are surprisingly good considering the many assumptions to which the entire data were subjected. It should be stressed that these standard deviations also include the standard deviations of the corrections, C_E and $A.P._{obs}$.

E. Correction Due to Space Charge Around the Filament

It was stated earlier that the anode potential can influence the space charge in the region of the filament. This can effect the energy of the emitted electron beam and its total energy distribution. It was shown that these effects do not influence appearance potential measurements for the Fox mode of operation but for a Schiff mode the correction factor, z, can be significant. In Fig. 15 tests 13, 32, 33 and 34 were run using the Schiff mode. The fact that the observed corrections for these tests are significantly lower than the other results indicates that z, or C_A is negative. This is precisely what one would expect since, due to the anode potential gradient, the emitted electrons are accelerated from a potential that is above the filament potential. These corrections, C_A, range from 0.58 to 0.95 volts but unfortunately the four tests were insufficient to determine the explicit dependency of C_A upon the anode voltage.

Tests 1 through 24b were performed over a range of anode voltages of 2.2 to 6.1 volts. All of the tests were performed in the Fox mode, and thus it was found that within 0.05 volts the anode voltage had no detectable effect upon the corrections.

F. Other Effects

Previously, it has been stated that pressure, other gases, surface potentials, contact potentials, ion detection sensitivities, and electron currents affect the accuracy of appearance potential measurements. It is quite probable that some of these factors affect the curvature of an ion efficiency curve for specific instruments or conditions, but by careful analysis the effects are of small significance to the appearance potential measurement. In this work no correlations could be found between the observed corrections and any of these variables. The ranges of these variables are listed below,

ion sensitivity at 17.5 volts electron energy
= 11.2 millivolts to 4.323 volts,
pressure = 2×10^{-6} to 2×10^{-5} Torr,
electron current = 0.8 to 20 μa.

Since the above variables were investigated after making the corrections due to the repeller and retarding potentials one cannot eliminate the possibility that the effects of some of these factors depends upon the retarding or repeller voltages.

IX. SUMMARY AND CONCLUSIONS

A. Instrumental

In mass spectroscopy, mass spectra may be obtained using magnetic field scanning. Direct recordings of this magnetic field vs time were shown to be complex analytical functions when the magnet coil current is linearly increased. A method has been described whereby crystals which exhibit the Hall effect due to a magnetic flux passing through them were used in an electronic circuit to produce a linear magnetic field response. Comparisons of the calculated magnet field strength vs magnet coil current and the measured field strength vs magnet coil current were in good agreement. A further modification of the method was discussed in which constant mass dispersion could be obtained throughout the entire mass spectral scan. Such a modification also involves the use of the Hall crystal as a circuit element and a reference voltage which increases at a logarithmic rate.

Many present day mass spectrometers do not have adequate or convenient methods for accurately determining the mass of an ion in focus. A circuit which employs a Hall crystal which is capable of being used as a mass indicator has been described in detail. The reproducibility, stability, and accuracy are sufficient for normal mass spectrometric work; the cost is moderate; and the method is easily and generally

adaptable to mass spectrometers. With slight modifications and careful application, this mass indicator could be improved to obtain a mass indication to 1 part in 2000 to 3000 or better. Thus it is capable of distinguishing multiply-charged species, metastable ions, and singly-charged ions when uncertainty arises in mass spectral work.

The major instrumental improvement in mass spectrometer design during the work described in this thesis is evident by the versatility of the electron-ionizing system. It is emphasized that the voltages applied to all of the ion source electrodes are independently and externally variable over wide ranges. This allows complete control of the electron beam and the fields in the ionizing region to permit Fox, Schiff, conventional or other types of ion source operating modes for use in ionizing efficiency studies. Either the normal or the retarding potential difference technique can be used with or without square-wave pulsing of the repeller and the electron current. The design, construction, and characteristics of this ion source are described in detail. An adapter to aid in aligning the ion source slits and the collector slits is also described.

The technique described for measuring and recording ionization efficiency data using a differential voltmeter affords faster and more precise measurements, yields numerical data, and eliminates the necessity of employing constant accelerating voltage intervals. Although direct

recording of an ionization efficiency curve or its first differential by means of an X-Y recording potentiometer is faster, the resulting plots must be further interpreted if a rigorous and accurate analysis is to be made. It has already been shown in this work and others, especially in that of Morrison (60b), that optimum results are obtained from ionization, efficiency studies when analytical treatments are applied to numerical data. Recently this laboratory has acquired equipment which could improve numerical data acquisition considerably. This would involve simultaneous print-out of the electron accelerating voltage and ion current intensity while the electron accelerating voltage is increased at a slow constant rate. The print-out can be accomplished through the use of two voltage-to-frequency converters, digital voltmeter, and a two-channel printer capable of printing 5 measurements per second. In this manner accurate numerical data could be acquired in a very short time and subjected to further computer analysis.

B. Experimental

The ionization efficiency data are obtained in a unique way using the instrument described. It involves one of the first attempts to illustrate the effects of various types of ion source designs and operating conditions upon ionization efficiency data using the same mass spectrometer and without physically changing the ion source. The results

shown in Figs. 41 and 42 indicate these comparisons between the conventional, Schiff, Schiff pulsed, Fox and Fox pulsed modes using various retarding potentials. Two conclusions are emphasized. The data are significantly improved in changing from the conventional to the Fox mode, from non-pulsed to pulsed technique, and from low to high retarding potentials. These results indicate that the Fox mode of operation offers better control over the electron beam. The reduced tailing observed in the ionization efficiency curves for higher retarding potentials suggests that the electron beam entering the ionizing region does not have a true Maxwellian distribution. It can be seen from Fig. 41 that at higher retarding potentials the energy spread is increased for a Maxwellian energy distribution. Thus one would actually expect more tailing as the retarding potential is increased. From the work of Cloutier (20) and from the basic physics of motion of charged particles in a magnetic field, it can be shown that electrons of high energy do not pass through the series of electron collimating plates. Hence the electron energy distribution does not necessarily extend to infinity but rather, it has some finite maximum energy. This is suggested by workers who use the vanishing current method. A maximum electron thermal energy would certainly make such results easier to reproduce than would a long tail as given by a Maxwellian distribution. The

observations of this work are in close agreement with the work of Hutchison (16) and Marmet (17).

It was shown that the energy scale of a mass spectrometer can be precisely calibrated and that it will remain so for widely varying instrumental conditions. This is advantageous for obtaining faster, more precise appearance potential measurements using various ion source conditions without performing frequent calibration ionization efficiency curves. It was shown that effects of the repeller potential, retarding potential, potential drop across the filament, and filament space charge can be established and applied in a manner which corrects observed appearance potential measurements without the use of a calibrating gas.

Perhaps of prime importance is the observation that so called "contact potentials" or "surface potentials" are constant, or precisely compensated for in other corrections. Previously it has been speculated that such factors contribute large errors to measurements. In this work, any error introduced by variations of contact or surface potentials was found to be less than 0.05 volts for a wide range of conditions.

The use of purely analytical treatments which do not rely upon plotting methods have been illustrated also. The results of such treatments suggest that many of the actual ion source conditions, threshold behaviours, cross sections,

and general theories of ionization can be deducted by similar analytical methods.

The Fox ion source has already been recognized as one which yields excellent ionization efficiency data when it is used with the retarding potential difference method. In this difference method, the differences in two large ion currents certainly can be no more precise than either of the large ion current readings themselves. Each of these two series of ion current measurements establishes an ionization efficiency curve similar to the one established by the differences. Thus it is quite apparent that the difference method does not yield more data; it merely renders it more obvious in graphical analysis. In this thesis the observation of the autoionization states of Xe^+ shows that the retarding potential difference method is not necessary to distinguish many of the details present in ionization efficiency data. Although the difference method usually makes details more obvious it has several disadvantages. The difference of two large numbers can be relatively inaccurate. Obtaining such measurements certainly requires more time and better instrument stability. Since the ion source conditions must be changed repeatedly it is desirable to have an ion source and circuitry that attain equilibrium rapidly without enduring memory effects. However one cannot assume that the resulting data are analytically representative of the actual ionization

efficiency data, hence speculations on threshold or ionization efficiency laws must be made with caution.

One other important point that became apparent during this work is that each ionization efficiency curve should be carefully analyzed. Several methods were proposed, discussed, and applied in this thesis. The linear extrapolation of data by means of a computer eliminates possible human bias, provides more accurate and reproducible results; requires less time; and furnishes quantitative measurements of the error limits, slopes, and standard deviations, that are otherwise not ordinarily obtained by manual methods. These quantitative additional data are very useful for further analysis of the experiments. For example, it is noted that the slope of ionization efficiency curves of the Xe^+ $^2P_{1/2}$ and the $^2P_{3/2}$ states are in a ratio of about 2:1. This might be interpreted as an indication of the relative cross sections of ionization for the two processes.

The linear extrapolation program can be used also after treating the data by means of different analytical functions. It has been shown that ionization efficiency data for different ions and different processes do not behave the same when they are subjected to such analytical treatments indicating that the mechanisms for forming the various types of ions are different.

The primary point that should be emphasized is that careful analysis of each ionization efficiency curve is

necessary in order to obtain optimum accuracy and results from the data. It was shown in this thesis that even the ionization efficiency data of Xe^+, a simple atomic ion, contain a surprising amount of detail within the first few volts above onset. Very recent work by others, especially that by Winters (80a, 80b) also exemplifies the increasing importance of careful analytical evaluation of ionization efficiency data. Presently it is apparent that the development of methods of mathematical analysis of ionization efficiency data are far behind the present instrumental sophistication in mass spectrometers. Future improvements in mass spectrometry will no doubt be in the area of better treatment of data which will make use of the technique for obtaining more reliable values for thermochemical properties.

X. BIBLIOGRAPHY

1. Field, F. D. and Franklin, J. L. Electron impact phenomena and the properties of gaseous ions. 2nd ed. New York, N.Y., Academic Press, Inc. 1951.

2. McDowell, Charles A., ed. Mass spectrometry. New York, N.Y., McGraw-Hill Book Co. 1963.

3. Waldron, J. D., ed. Advanced in mass spectrometry. New York, N.Y., Pergamon Press. 1959.

4. Reed, R. I., ed. Mass spectrometry. New York, N.Y., Academic Press, Inc. 1965.

5. McDowell, Charles A., ed. Atomic collision processes. New York, N.Y., John Wiley and Sons, Inc. 1964.

6a. Saalfeld, Fred Eric. The mass spectra of some volatile hydrides. Unpublished Ph.D. thesis. Ames, Iowa, Library, Iowa State University of Science and Technology. 1961.

6b. Saalfeld, Fred Eric and Svec, Harry J. "The mass spectra of some volatile hydrides". U.S. Atomic Energy Commission Report IS-386 [Iowa State University of Science and Technology, Ames. Inst. for Atomic Research]. 1961.

7. Honig, R. E. Ionization potentials of some hydrocarbon series. J. Chem. Phys. 16:105. 1948.

8. Richardson, O. W. The emission of electricity from hot bodies. 2nd ed. New York, N.Y., Longmans, Green and Co. 1921.

9. Fowler, Ralph and Guggenheim, E. A. Statistical thermodynamics. 2nd ed. Cambridge, England, University Press. 1960.

10. Rieman, A. L. Thermonic emission. New York, N.Y., John Wiley and Sons, Inc. 1934.

11a. Dushman, S. "Electron emission from metals as a function of temperature". Phys. Rev. 21:625. 1923.

11b. Dushman, S. "Thermionic emission". Rev. Mod. Phys. 2:381. 1930.

12. Harman, Willis W. Fundamentals of electronic motion. New York, N.Y., McGraw-Hill Book Co., Inc. 1953.

13. Ryder, John D. Electronic fundamentals and applications. New York, N.Y., Prentice-Hall, Inc. 1950.

14. Heemstra, Frank William. Thermionic work functions of some rare earth borides. Unpublished Ph.D. thesis. Ames, Iowa, Library, Iowa State University of Science and Technology. 1953.

15. Becker, J. A. "Thermionic emission and adsorption". Rev. Mod. Phys. 7:95. 1935.

16. Hutchison, Dwight A. "Effects of electron energy distributions on ion appearance potential measurements". An. Conf. on Mass Spectrometry and Allied Topics. 12:134. 1964.

17. Marmet, P. "An effect of electronic space charge on ionization curves probability". An. Conf. on Mass Spectrometry and Allied Topics 12:140. 1964.

18. Flesch, G. D. and Svec, H. J. "A more efficient electron gun for sector mass spectrometers". [To be published in Fourteenth An. Conf. on Mass Spectrometry and Allied Topics, Dallas, Texas, May 1966, ca. 1966].

19. Barnard, G. P. Modern mass spectrometry. London, England, The Institute of Physics. 1953.

20. Cloutier, Gilles G. A monoenergetic electron source for mass spectrometers and its application to the electron impact study of nitric oxide. Unpublished Ph.D. thesis. Montreal, Quebec, Library, McGill University. 1959.

21. Fox, R. E., Hickam, W. M., Kjeldass, T., Jr., and Grove, D. J. "Ionization in a mass spectrometer by monoenergetic electrons". Nat. Bur. Standards Circ. No. 522:211. 1953.

22. Pierce, J. R. Theory and design of electron beams. New York, N.Y., D. Van Nostrand Co., Inc. 1949.

23. Taubert, R. "Kinetic energy of fragment ions". In Waldron, J. D., ed. Advanced in mass spectrometry. pp. 489-503. New York, N.Y., Pergamon Press. 1959.

24. Elbert, Stephen. [Experimental potential gradients in a model retarding potential mass spectrometer ion source]. Unpublished work performed in Ames Laboratory of the Atomic Energy Commission, Ames, Iowa. Ames, Iowa, Dept. of Chem., Iowa State University of Science and Technology. ca. 1965.

25. Robertson, A. J. B., Mass spectrometry. New York, N.Y., John Wiley and Sons. 1954.

26. Klemperer, O. Electron optics. 2nd ed. Cambridge, England, University Press. 1953.

27. Nottingham, W. B. "Ionization and excitation in mercury vapor produced by electron bombardment". Phys. Rev. 55:203. 1939.

28. Fox, R. E., Hickam, W. M., Grove, D. J., and Kjeldaus, T. "Ionization in a mass spectrometer by monoenergetic electrons". Rev. Sci. Instr. 26:1101. 1955.

29. Cloutier, G. G. and Schiff, H. I. "Electron impact study of nitric oxide using a modified retarding potential difference method". J. Chem. Phys. 31:793. 1959.

30. Marmet, Paul and Kerwin, Larkin. "An improved electrostatic electron selector". Can. J. Phys. 38:787. 1960.

31. Kerwin, L., Marmet, P., and Clarke, E. M. "Recent work with the electrostatic electron selector". Symposium on Mass Spectrometry 1961:8. 1961.

32. Hutchison, D. A. "An electrostatic parallel-plate electron-energy selector for determinations of critical ionization potentials by electron impact". Symposium on Mass Specrrometry. 1961:116. 1961.

33. Kerwin, Larkin,and Marmet, Paul. "Recent appearance potential measurements using an electrostatic electron selector". J. Appl. Phys. 31:2071. 1960.

34. Clarke, E. M. "Ionization probability curves using an electron energy selector: results on N_2^+, N^+, Xe^{++}". Can. J. Phys. 32:764. 1954.

35. Weissler, G. L., Sampson, J. A. R., Ogawa, M., and Cook, G. R. "Photoionization analysis by mass spectroscopy". J. Opt. Soc. Am. 49:338. 1959.

36. Morrison, J. D. and Stanton, H. E. "Fragmentation of methane by electron impact and the latent heat of sublimation of carbon". J. Chem. Phys. 28:9. 1958.

37. Svec, H. J. Mass spectrometry. Unpublished Ph.D. thesis. Ames, Iowa, Library, Iowa State University of Science and Technology. 1950.

38. Conzemius, Robert J. and Svec, Harry J. "Improvement of the ion transmission in a typical mass spectrometer ion source". J. Appl. Phys. 34:2486. 1963.

39. Flesch, G. Simple electromagnetic circuits. Unpublished mimeographed paper. Ames, Iowa, Ames Laboratory of the Atomic Energy Commission. ca. 1961.

40. Weber, Robert L., White, Marsh W., and Manning, Kenneth V. Physics for science and engineering. New York, N.Y. McGraw-Hill Book Co., Inc. 1957.

41. Dushman, Saul. Scientific foundations of vacuum techniques. 2nd ed. New York, N.Y., John Wiley and Sons, Inc. 1962.

42. Caldecourt, V. J. and Adler, S. E. "A mass indicator using a vibrating coil magnetometer". Rev. Sci. Inst. 25:10. 1954.

43. Finley, Hugh O. and Hemmer, Ralph J. "The measurement of M/e positions for a mass spectrometer using a rotating coil gaussmeter". U.S. Atomic Energy Commission Report TLD-4500 (19th ed.) 194 [Division of Technical Information Extension, AEC]. ca. 1960.

44. Germain, C. "Bibliographic review of the methods of measuring magnetic fields". Nucl. Inst. Methods. 21:17. 1963.

45. Voeikov, D. D. "A compensation magnetometer with a thermostat-controlled Hall data transmitter". Instruments and Experimental Techniques. 4:616. 1959.

46. Aleksandru, G. and Vasilevskaya, D. P. "A magnetometer based on the Hall effect and operating on alternating current". Instruments and Experimental Techniques. 2:289. 1960.

47. Vasilevskaya, O. P. and Denisov, YU. N. "A magnetometer based on the Hall effect". Instruments and Experimental Techniques. 3:492. 1959.

48. Harasty, G. A. Investigation of the problem of using Hall generator devices for regulation and measurement of magnetic fields in experimental magnets fot the 26.5. Argonne Nat. Lab., Argonne, Ill. TID-17610. ca. 1960.

49. Rubin, S. and Rogers, G. J. "Sensitivity indices for Hall generators". Natl. Bur. Standards Tech. Note 233. 1964.

50. Lossing, F. P., Tickner, A. W., and Bryce, W. A. "The ionization potentials of the deuterated methanes". J. Chem. Phys. 19:1254. 1951.

51. Warren, J. W. "Measurement of appearance potentials of ions produced by electron impact using a mass spectrometer". Nature 165:810. 1950.

52. Wahrhaftig, Austin L. "The theory of mass spectra and the interpretation of ionization efficiency curves". In Reed, R. I. ed. Mass spectrometry. pp. 137-152. New York, N.Y., Academic Press. 1965.

53. Lossing, F. P., Ingold, K. U., and Henderson, I. H. S., "Free radicatls by mass spectrometry. VI. The bond dissociation energies of some methyl, allyl and benzyl compounds by electron impact". J. Chem. Phys. 22:1489. 1954.

54. Dibeler, V. H. and Reese, R. M. "Selected positive and negative ions in the mass spectra of the monohalo-methanes". J. Res. Natl. Bur. Standards 54:127. 1955.

55a. Morrison, J. D. "Studies of ionization efficiency. I. The determination of molecular appearance potentials using the mass spectrometer". J. Chem. Phys. 19:1-500 1305. 1951.

55b. Morrison, J. D. "Studies of ionization efficiency. Part III. The detection and interpretation of fine structure". J. Chem. Phys. 22:1219. 1954.

55c. Morrison, J. D. "Studies of ionization efficiency. Part IV. The electron spectra of some simple molecules". J. Chem. Phys. 22:1219. 1954.

56. Foner, S. N. and Hudson, R. L. "Ionization potential of the free HO_2 radical and the H-O_2 bond dissociation energy". J. Chem. Phys. 23:1364. 1955.

57. Robertson, A. J. B. "Mass spectrometry". London, England, Institute of Petroleum. 1952.

58. Stevenson, D. P. and Hipple, J. A. "Ionization of argon and neon by electron impact". Phys. Rev. 62: 237. 1942.

59. Morrison, J. D. "Application of the mass spectrometer to the study of the upper energy states of molecules". J. Appl. Phys. 28:1409. 1957.

60a. Morrison, J. D. "Some recent developments in the study of ionization processes". An. Conf. on Mass Spectrometry and Allied Topics. 12:32. 1964.

60b. Morrison, J. D. "On the optimum use of ionization-efficiency data". J. Chem. Phys. 39:200. 1963.

60c. Johnson, Thomas R. "Use of Calcomp digital incremental plotter system". Unpublished mimeographed paper: Computer Utilization Bulletin Number 20. Ames, Iowa, Computer Service Dept., Iowa State University of Science and Technology. ca. 1964.

61a. Erbeck, D. H. ["Instructions for using subroutine INTERP"]. Unpublished mimeographed paper: Library Program Submitted 70740864130074. Ames, Iowa, Computer Service Dept., Iowa State University of Science and Technology. 1964.

61b. Erbeck, D. H. ["Subroutine SMOOTH"]. Unpublished card-punched Fortran computer deck. Ames, Iowa, Computer Service Dept., Iowa State University of Science and Technology. ca. 1965.

61c. Scranton, Donald G. ["Instructions for using computer subroutine GRAPH"]. Unpublished mimeographed paper: Computer Utilization Bulletin Number 22. Ames, Iowa, Computer Service Dept., Iowa State University of Science and Technology. Mar. 1966.

62a. Herzberg, Gerhard. Atomic spectra and atomic structure. New York, N.Y., Dover Publications. 1944.

62b. Morrison, J. D. Threshold laws for processes of autoionization. J. Chem. Phys. 40:2488. 1964.

62c. Dorman, F. H. and Morrison, J. D. "Determination of relative electronic transitions probabilities by impact methods". J. Chem. Phys. 34:578. 1961.

63. Burns, J. F. "Auto-ionization and the ionization efficiency curves for krypton and xenon". In McDowell, M. R. C., ed. Atomic collision processes. pp. 451-460. New York, N.Y., John Wiley and Sons, Inc. 1963.

64. Moore, Charlotte E. Atomic energy levels. Natl. Bur. Standards Circ. 467. 1958.

65. Brand, J. C. D. and Speakman, J. C. Molecular structure the physical approach. London, England, Edward Arnold, Ltd. 1961.

66. Weingartshofer, A. and Clarke, E. M. "Cross sections for the ion-molecule reaction $H_2 + H_2^{+*} = H_3^+$ as a function of the vibrational state of the H_2^+ ion". An. Conf. on Mass Spectrometry and Allied Topics. 12:166. 1964.

67. Barfield, Ariel F. and Wahrhaftig, A. L. "Determination of appearance potentials by the critical slope method". J. Chem. Phys. 41:2947. 1964.

68a. Gryzinski, M. "Classical theory of electronic and ionic inelastic collisions". Phys. Rev. 115:374. 1959.

68b. Gryzinski, M. "Two particle collisions. Part I. Phys. Rev. 138:A305. 1965.

68c. Gryzinski, M. "Two particle collisions". Part II. Phys. Rev. 138:A322. 1965.

69a. Gryzinski, M. "Two particle collision. Part III. Phys. Rev. 138:A336. 1965.

69b. Baur, Ernest and Bartky, Charlotte Decker. "Calculation of inelastic electron-molecule collision cross sections by classical methods". J. Chem. Phys. 43:2466. 1965.

69c. Wigner, E. P. "On the behavior of cross sections near thresholds". Phys. Rev. 73:1002. 1948.

70. Wannier, G. H. "The threshold law for single ionization of atoms or ions by electrons". Phys. Rev. 90: 817. 1953.

71. Geltman, S. "Theory of ionization probability near threshold". Phys. Rev. 102:171. 1956.

72. Morrison, J. D. "Electron-molecule and photon-molecule collisions". In Stoops, R., ed. Energy transfer in gases. pp. 397-466. New York, N.Y. Interscience Publishers. 1962.

73. Hickam, W. M., Fox, R. E., and Kjeldaas, T., Jr. "Probability curves near threshold for the formation of He^+, Ne^{++}, A^{++}, Kr^{++}, and Xe^{++} by electron impact". Phys. Rev. 96:63. 1954.

74. Morrison, J. D., Hurzeler, H., and Inghram, Mark G. "Threshold law for the probability of excitation of molecules by photon impact: a study of the photo-ionization efficiencies of Br_2, I_2, HI, and CH_3I". J. Chem. Phys. 33:821. 1960.

75. Hutchison, Dwight A. "Experimental threshold laws for ionization in the rare gases". In McDowell, M. R. C., ed. Atomic collision processes. pp. 443-450. New York, N.Y., John Wiley and Sons, Inc. 1964.

76. Hickam, W. M., Fox, R. E., and Kjeldaa, T. "Ionization probability near threshold for the formation of Xe^{++}, Kr^{++}, A^{++}, and Ne^{++}". Phys. Rev. 90:386. 1953.

77. Dorman, F. H., Morrison, J. D., and Nicholson, A. J. C. "Probability of multiple ionization by electron impact". J. Chem. Phys. 35:575. 1961.

78. Dorman, F. H. and Morrison, J. D. "Double and triple ionization in molecules induced by electron impact". J. Chem. Phys. 35:575. 1961.

79. Fox, R. E. "Study of multiple ionization in helium and xenon by electron impact". In Waldron, J. D., ed. Advanced in mass spectrometry. pp. 397-412. New York, N.Y., Pergamon Press. 1959.

80a. Winters, Robert E., Collins, J. H., and Courchene, W. L. "Resolution of fine structure in ionization efficiency curves". [To be published in An. Conf. on Mass Spectrometry and Allied Topics, Dallas, Texas, May, 1966. ca. 1966].

80b. Winters, Robert E., Collins, J. H., and Courchene, W. L. "Resolution of fine structure in ionization efficiency curves". [Mimeographed reprint accepted for publication in J. Chem. Phys. ca. 1966].

XI. ACKNOWLEDGEMENTS

The author wishes to acknowledge his grateful appreciation to Dr. Harry J. Svec for his patience and guidance, for his timely encouragement, and for his many helpful suggestions throughout all of the work, particularly during the entire writing of the manuscript.

The author also expresses his sincere appreciation to Messrs. Gerald Flesch, Gregor Junk, Robert Conzemius, Arthur Anderson, Harold Belsheim (who also critically reviewed most of the manuscript), and to all the other members of Dr. Svec's research group for their technical assistance and advice, and for their many stimulating and productive discussions and comments which made much of the work possible; to the personnel of the chemistry shop and the glass shop for the construction and repair of numerous items which were necessary to complete and run the instrument; to the personnel of the electronics shop for their frequent aid in constructing, "trouble shooting", and repairing the electronic components, especially Mr. Dean VanZuuk who designed the emission regulator and aided in designing the square-wave filter circuitry; to the computer services group, especially to Mr. Donald G. Scranton and Mr. David H. Erbeck for their frequent assistance in the computer programming; to Dr. Robert S. Hansen who aided greatly in deriving the expression for the electron

thermal energy distribution; to Mrs. Paula Toms for accepting the difficulties of preparing and typing the rough draft of the manuscript; to Mrs. Mary Reynolds for typing the finished manuscript; to the Ames Laboratory drafting service for their excellent work in reproducing the many illustrations, and to other innumerable friends for their cooperation and help in making the work as interesting and pleasant as possible. The author is also indebted to Miss Judy Sandstrom, his future wife, for her continual help and encouragement during the many hours spent writing the manuscript.

XII. APPENDIX: DERIVATION OF MAXWELLIAN ELECTRON THERMAL ENERGY DISTRIBUTION

The study of the emission of electrons from hot bodies dates back to the early works of Richardson (8) and Rieman (10). In deriving a quantitative expression for this emission the assumptions listed on p. 11 are made and statistical thermodynamics theory is applied. It is assumed that the reader has some understanding of thermodynamics and the relationship between it and statistical thermodynamics. Refer to Fowler and Guggenheim (9) for a more detailed discussion concerning basic statistical thermodynamics and the theory of electron gases (p. 454). First it is assumed that the emission of electrons from a hot body obeys the theory of a vapor in equilibrium with a metal. The density of the electron vapor is assumed to be so small that although electrons obey strictly Fermi-Dirac statistics, the equation for the absolute activity of the electrons in the gas phase (denoted by subscript "g") is given according to classical statistical thermodynamics as

$$\lambda_g = \left(\frac{N_g}{V_g} \right) \frac{h^3}{2(2\pi mkT)^{3/2}} = e^{\mu g/kT} \qquad 89$$

This assumes that the electron vapor behaves as an ideal gas. The electron at rest in the vapor is assumed to have zero energy.

Next the absolute activity of the electrons in the metal, λ_m, must be evaluated with reference to the same zero energy. Defining as the average energy required to remove an electron from within the metal, also termed the thermionic work function to a position at rest outside the metal, the chemical potential of the electrons within the metal is given to a good approximation by

$$\mu_m = -\chi. \tag{90}$$

From this, the absolute activity is given as

$$\lambda_m = e^{-\chi/kT}. \tag{91}$$

In order to establish an equilibrium between the electron vapor and the metal, the condition

$$\lambda_g = \lambda_m \tag{92}$$

must be satisfied. Substituting the appropriate values of λ_g and λ_m,

$$\left(\frac{N_g}{V_g}\right) \frac{h^3}{2(2\pi mkT)^{3/2}} = e^{-\chi/kT}. \tag{93}$$

For an ideal gas

$$P = \left(\frac{N_g}{V_g}\right)kT, \tag{94}$$

hence from Eq. 93 the equilibrium vapor pressure of the electron gas is given by

$$P = e^{-\chi/kT} \frac{2kT(2\pi mkT)^{3/2}}{h^3}, \qquad 95$$

or rewriting,

$$P = 2kT \left(\frac{2\pi mkT}{h^2} \right)^{3/2} e^{-\chi/kT}$$

Since the momentum of the electrons in the gas follow a Maxwellian-Boltzman distribution, the equation

$$d\left(\frac{N_g}{V_g} \right) = Ce^{-p^2/2mkT} \sin \theta p^2 dp \, d\theta \, d\varphi \qquad 96$$

gives the total number of electrons per unit volume with momentum between p and p + dp, directed between θ, $\theta + d\theta$ and φ, $\varphi + d\varphi$. The number of electrons, dn, striking a unit area of the surface in a direction between θ, and $\theta + d\theta$, and φ and, $\varphi + d\varphi$ is given as the product of the number of electrons per unit volume in the gas phase and the velocity increment normal to the surface,

$$dn = C \frac{p \cos \theta}{m} d\left(\frac{N_g}{V_g} \right), \qquad 97a$$

thus

$$dn = C \frac{p \cos \theta}{m} e^{-p^2/2mkT} \sin \theta \, p^2 dp \, d\theta \, d\varphi \qquad 97b$$

In order to evaluate the constant, C, Eq. 96 is solved. Thus,

$$\left(\frac{N_g}{V_g} \right) = \int d\left(\frac{N_g}{V_g} \right) = \int_0^{\infty} \int_0^{\pi} \int_0^{2\pi} Ce^{-p^2/2mkT} p^3 dp \sin \theta \, d\theta \, d\varphi \qquad 98$$

$$= 2\pi C \int_0^{\infty} \int_0^{\pi} e^{-p^2/2mkT}\, p^3 dp \sin\theta\, d\theta$$

$$= 2\pi C \int_0^{\infty} e^{-p^2/2mkT}\, p^3 dp$$

$$\left(\frac{N_g}{V_g}\right) = C(2\pi mkT)^{3/2}.$$

Solving for C,

$$C = \frac{\left(N_g/V_g\right)}{(2\pi mkT)^{3/2}}. \qquad 99$$

Replacing C in Eq. 97b results in the expression,

$$dn = \frac{\left(N_g/V_g\right) p \cos\theta\, e^{-p^2/2mkT}}{(2\,mkT)^{3/2}\, m}\, p^2 \sin\theta$$

$$\cos\theta\, dp\, d\theta\, d\varphi \qquad 100$$

In order to solve this expression explicitly, (N_g/V_g) can be replaced by its equivalent taken from Eq. 93.

$$dn = \frac{2(2\pi mkT)^{3/2}\, e^{-\chi/kT}}{m(2\pi mkT)^{3/2}\, h^3}\, p \cos\theta\, e^{-p^2/2mkT}$$

$$p^2 \sin\theta\, dp\, d\theta\, d\varphi \qquad 101a$$

$$= \frac{2e^{-\chi/kT}\, e^{-p^2/2mkT}}{mh^3}\, p^3 \sin\theta \cos\theta\, dp\, d\theta\, d\varphi \qquad 101b$$

$$= \frac{2}{mh^3}\, e^{-(\chi + \frac{p^2}{2m})/kT}\, p^3 \sin\theta \cos\theta \qquad 101c$$

$$dp\, d\theta\, d\varphi$$

It is now assumed that the number of electrons striking the surface is equal to the number of electrons emitted minus the fraction, r, of electrons that are reflected into the metal. In order to calculate the total emission from a hot filament of surface area, A, for electrons with momentum between p and p + dp in <u>any</u> direction, the integration is performed from $\theta = 0$ to π and $\varphi = 0$ to 2π.

Thus

$$dn = \frac{(1-r)\ 2\pi A}{mh^3}\ e^{-(\chi\ +\ \frac{p^2}{2m}\ )/kT}\ \ p^3dp \qquad 102$$

Furthermore since,

$$p = mv \qquad 103$$

and

$$U = \frac{mv^2}{2}\ ,$$

where U is the energy of the electron, the relationships between momentum, p, and energy can be expressed as,

$$p = (2mU)^{1/2},$$

or $\quad p^2 = 2mU,$

from which $\qquad 104$

$$2pdp = 2mU,$$

or $\quad pdp = mdU,$

and $\quad p^3dp = 2m^2UdU.$

In the relationships expressed in Eqs. 104, the electron momentum distribution can be converted to the electron energy distribution, by

$$dn = (1-r)\,\frac{2\pi A}{mh^3}\,e^{-(\chi + U)/kT}\,2m^2 U dU$$

or

$$dn = \frac{(1-r)\,4\pi mAUe^{-(\chi + U)/kT}}{h^3}\,dU. \qquad 105$$

For most electron impact work the fraction of electrons, r, reflected into the metal is assumed to be negligible with respect to unity. Hence the total number of electrons emitted per unit volume, dN_e, over an area A is expressed by

$$dN_e = \frac{4\pi mAUe^{-(\chi + U)/kT}}{h^3}\,dU. \qquad 106$$

Strictly speaking, in a mass spectrometer only those electrons passing through the volume defined by the collimating slits are effective in ionization. However these electrons still possess the same thermal energy distribution given in Eq. 106. Note that Φ is often used in place of χ as the thermionic work function of the metal.